Data on Internal Rarefied Gas Flows

Felix Sharipov[a)]
Departamento de Física, Universidade Federal do Paraná, 81531-990 Curitiba, Brazil

Vladimir Seleznev[b)]
Department of Molecular Physics, Faculty of Physics and Technology, Urals State Polytechnical University, 620002 Yekaterinburg, Russia

Received May 5, 1997; revised manuscript received January 7, 1998

The present review, containing 178 references, is dedicated to one of the largest and most important branches of the rarefied gas dynamics, namely internal flows. A critical analysis of the corresponding numerical data and analytical results available in the literature was made. The most reliable data were selected and tabulated. The review will be useful as a reference for mathematicians, physicists and aerodynamicists interested in rarefied gas flows. In this paper the complete ranges of the main parameters, determining rarefied gas flows through a capillary, are covered. The capillary length varies from zero, when the capillary degenerates into a thin orifice, to infinity when the end effects can be neglected. The Knudsen number, characterizing the gas rarefaction, varies from zero when the gas is considered as a continuous medium to infinity when the intermolecular collisions can be discounted. The pressure and temperature drops on the capillary ends vary from the small values when the linear theory is valid to the large values when the nonlinear equations must be applied. The influence of the gas–surface interaction is considered. © *1998 American Institute of Physics and American Chemical Society.* [S0047-2689(98)00103-2]

Key words: critical review; data compilation; evaluated recommended data; heat flux; kinetic coefficients; mass flow rate; mechanocaloric effect; rarefied gases; slip coefficients; thermocreep; thermomolecular pressure difference; transport.

Contents

[a)]Electronic mail: sharipov@fisica.ufpr.br
[b)]Electronic mail: seleznev@kmf.rcupi.e-burg.su

List of Tables

List of Figures

List of Symbols

a	across size of capillary (tube radius/channel height)
A_P	viscous slip coefficient, (3.69)
A_T	thermal slip coefficient, (3.69)
$\mathscr{A}_{ij}$	matrix of the algebraic systems (3.53)
$\hat{A}$	linearized scattering operator, (2.70)
b	width of channel
$\mathscr{B}_{im}$	free terms of the algebraic systems (3.53)
$\mathbf{c}$	reduced molecular velocity, (3.11)
c_i	constants of the trial functions, Secs. 2.12.2., 2.12.4. and 3.3.4.
d	molecular diameter
$\hat{D}$	differential operator, (2.54)
$\tilde{\hat{D}}$	reduced differential operator, (3.14)
$E(x)$	complete elliptic integral, (3.57)
$\dot{E}$	heat flux, (1.3), (1.9), (1.11)
$f(t,\mathbf{r},\mathbf{v})$	velocity distribution function, Sec. 2.2.
f^M_{loc}	local Maxwellian, (2.30)
f^M_0	absolute Maxwellian, (2.52)
G	reduced flow rate, (3.25), (3.26), (3.102), (5.12)
$\mathscr{G}$	reduced flow rate, (4.9)
$h(t,\mathbf{r},\mathbf{v})$	perturbation function, (2.51)
h_w	perturbation of the surface Maxwellian, (2.69)
$H(x)$	Heaviside step function, (2.19)
$H^{(N)}_{\alpha_1 \ldots \alpha_N}$	Hermite polynomials, (2.31)
I_n	special transcendental functions, (3.42)
J_0	modified Bessel function, (2.25)
J_P, J_T	thermodynamic fluxes, Sec. 2.10.
$J(\tilde{h})$	functional, (2.97)
k_B	Boltzmann constant, $k_B = 1.380658 \times 10^{-23}$ J/K
$\mathscr{K}_{ij}$	kernels of the integral equations, Sec. 3.3.
Kn	Knudsen number, (2.1)
l	length of capillary
L	dimensionless length of capillary, $L = l/a$
$\hat{L}$	linearized collision operator, (2.55)
$\tilde{\hat{L}}$	reduced linearized collision operator, (3.14)
$\mathscr{L}$	linear operator, (2.95)
m	molecular mass
$\dot{M}$	mass flow rate, (1.3), (1.8), (1.10)
$M^{(N)}_{\alpha_1 \ldots \alpha_N}(t,\mathbf{r})$	moments of the distribution function, (2.26)
$\mathscr{M}^{(N)}_{\alpha_1 \ldots \alpha_N}(t,\mathbf{r})$	moments of the distribution function (2.27)
n	number density of gas, (2.4)
P	pressure of gas, (2.6)
P_{av}	average pressure, (3.8)
P_{ij}	stress tensor, (2.7)
$\mathscr{P}$	reduced pressure, (3.103)
$\mathbf{q}$	heat flow vector, (2.9)
$\tilde{\mathbf{q}}$	reduced heat flow vector, (3.11)
Q	reduced heat flux, (3.25),(3.26)
$Q(ff_*)$	collision integral, (2.13)
$\mathbf{r}$	position vector
$\tilde{\mathbf{r}}$	reduced position vector, $\tilde{\mathbf{r}} = \mathbf{r}/a$
$\tilde{\mathbf{r}}_-$	two-dimensional reduced position vector
$R(\mathbf{r},\mathbf{v}' \to \mathbf{v})$	scattering kernel, Sec. 2.3.
$\mathscr{S}_{1m}, \mathscr{S}_{2m}$	free terms of the integral equations, Sec. 3.3.
S_{ij}	rate of shear tensor, (2.38)

t	time
T	temperature of gas, (2.8)
T_{av}	average temperature, (3.8)
$\mathscr{T}$	reduced temperature, (3.103)
T_w	temperature of capillary wall
$\hat{T}$	time reversal operator, (2.56)
$\mathbf{u}$	hydrodynamic (bulk) velocity, (2.5)
$\tilde{\mathbf{u}}$	reduced hydrodynamic (bulk) velocity, (3.11)
$\mathbf{v}$	velocity of molecules
$\mathbf{V}$	peculiar velocity of molecules, (2.10)
$\langle v \rangle$	mean thermal velocity of molecules, (2.42)
W	transmission probability, (2.94), Sec. 5.2.1.
x,y,z	spatial coordinates
$\tilde{x},\tilde{y},\tilde{z}$	dimensionless spatial coordinates, (3.3)
X_P, X_T	thermodynamic forces, Sec. 2.10.
$\alpha(\varphi), \alpha_{ij}$	accommodation coefficients, Sec. 3.
α	diffuse fraction in Maxwell's boundary condition, (2.23)
β_*	coefficient of the reduced velocity, (3.12)
γ	exponent of the thermomolecular pressure difference, (1.5)
δ	rarefaction parameter, (2.2)
ζ	ratio of the specific heats
κ	heat conductivity, (2.39), (2.41)
λ	mean free path, (2.3), (2.40)
Λ_{kn}	kinetic coefficients, Sec. 2.10.
μ	viscosity, (2.39), (2.41)
ν	collision frequency, (2.46)–(2.48)
ξ,η	curvilinear coordinates, (4.20), (4.26)
ξ_P	dimensionless gradient of the pressure, (3.10)
ξ_T	dimensionless gradient of the temperature, (3.10)
ρ	mass density of gas
ϱ	perturbation of the number density, (2.65)
σ	entropy production, (2.78)
σ_P	reduced viscous slip coefficient, (3.70)
σ_T	reduced thermal slip coefficient, (3.70)
Σ	tube cross section
τ	perturbation of the temperature, (2.65)
τ_w	distribution of the temperature along the capillary, (1.1)
Ω	region of the gas flow

Superscripts

ch	channel with an infinite width
ch, b	channel with a finite width b
or	orifice
sl	slit
th	tube

Subscripts

I	left container
II	right container
P	small pressure drop/gradient
T	small temperature drop/gradient
fm	free-molecular regime
*	given cross section of capillary
BGK	BGK model
S	S model

Abbreviations

BE	Boltzmann Equation, Sec. 2.2.
BGK	Bhatnagar Gross Krook, Sec. 2.5.1.
MC	Monte Carlo, Sec. 5.2.2.
RGD	Rarefied Gas Dynamics, Sec. 1.1.
TPD	Thermomolecular pressure difference, Sec. 1.2.

1. Introduction

1.1. Scope of the Review

Rarefied gas dynamics (RGD) is an active and fast developing scientific field. A biennial symposium attracts a large number of scientists and engineers working in this field. Recently, some monographs[11,27,30] describing latest achievements in the RGD were published. The starting point of the rarefied gas theory is the kinetic Boltzmann equation. Another very important aspect of the theory is the gas–surface interaction, which serves as a boundary condition for the kinetic equation. The monographs mentioned above describe the main properties of the kinetic equation, the properties of its boundary condition, and the principal methods of solution of the Boltzmann equation. So, they provide general information about the rarefied gas theory.

The present review is dedicated to one of the largest and most important branches of the RGD, namely the internal rarefied gas flows. The knowledge of this branch is applicable in many technologies such as: vacuum equipment, chemical apparatus, spaceship construction etc. Moreover, this branch plays a significant role in the development of the RGD as a whole. Because of the simplicity of numerical calculations, some types of internal rarefied gas flows serve as a test problem for new numerical methods. These flows are very sensitive to the nature of the gas–surface interaction. That is why they are used for indirect measurements of the gas–surface interaction parameters. To realize this task, an experimenter needs exact values of the mass flow rates through a capillary as a function of the gas rarefaction and of the gas–surface interaction parameters.

Today, much theoretical data on the internal gas flows are available in the literature. These data have not been widely applied by experimenters and engineers even though it is possible. There are three main reasons for this.

(1) The material on the rarefied gas flows is dispersed in many papers. Each describes only one aspect of the problem, while the flows depend on many parameters including the gas rarefaction, the geometrical size of the

capillary, the nature of the gas–surface interaction, and the nature of the intermolecular interaction.

(2) The theoretical results in this field are usually presented in terms of the microparameters such as the molecular mean free path and frequency of the intermolecular collisions. A special terminology was formed in the corresponding papers, which cannot be understood without the profound knowledge of the kinetic theory of gases. At the same time, it is not so trivial to relate these microparameters with the macroparameters measured in practice such as the pressure, the temperature, and the viscosity. Some papers contradict others regarding this question.

(3) The theoretical works are performed under suppositions idealizing the problem: the capillary has an infinite length, the gas is single, and the gaseous molecules are monatomic. In practice one deals with a capillary of finite length and with a gaseous mixture of polyatomic gases. Without special knowledge one does not know if the theoretical results obtained under ideal assumptions can be applied in some practical situations.

The present article provides numerical data and analytical formulas on the mass flow rate and on the heat flux through a capillary. It should be noted that the rarefied gas flows are complicated by the so-called cross effects, viz. the mass flow caused by temperature gradient and the heat flux caused by pressure gradient. These cross effects are described in this article.

The entire range of the main parameters determining the gas flow is considered. The capillary length varies from infinity when the end effects can be neglected to zero when the capillary degenerates into a thin slit or orifice. The pressure and temperature drops on the capillary ends are also assumed to be arbitrary. The drops vary from small values when the linear theory is valid to large values when the nonlinear equations must be applied. The principal parameter, which affects the gas flows, is the gas rarefaction. In the article, the entire range of this parameter is covered, from the regime when the intermolecular collisions can be discounted to the hydrodynamic regime.

Besides the flow rates and the heat fluxes, one more practically important phenomenon is described, namely, the effect of the thermomolecular pressure difference. This effect can serve for indirect pressure measurements and for measurements of the gas–surface interaction parameters.

The contents of this article are as follows: In the present section, the general statement of the problem is described. The main assumptions outlining the sphere of the applicability of the data presented in the review are given.

In Sec. 2 the main theoretical conceptions of the RGD are described. The relations between the microparameters (molecular mean free path, molecular mass, molecular diameter) with the macroparameters (pressure, temperature, number density, viscosity, thermal conductivity) are given. The engineers, who need to calculate the mass flow rates in some equipments, and the experimenters, who need to choose the best conditions for indirect measurements of the gas–surface interaction parameters or to confirm some theoretical conclusions, can easily relate the data presented here with practically measured quantities. Numerical methods applied to calculate the rarefied gas flows are described briefly in this section. For the reader who wants to study one or another method in depth, the corresponding references are given.

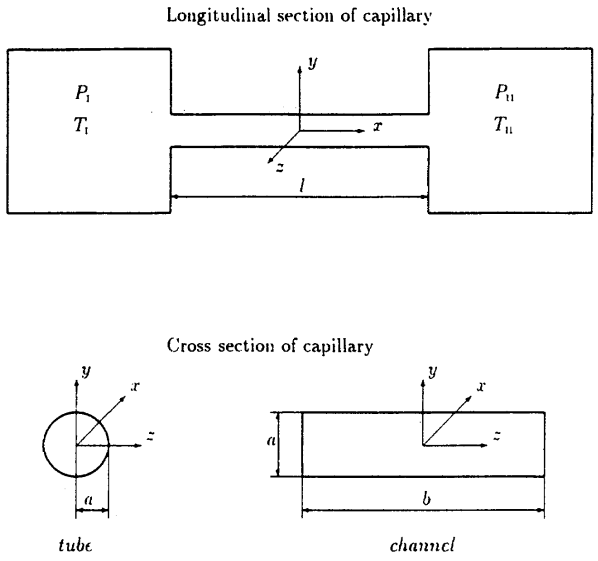

FIG. 1. Sketch of the gas flow through a capillary of arbitrary length.

In Sec. 3 the gas flow through long capillaries is considered. In this limit the end effects can be neglected. Moreover, the solution to the problem can be split into two stages. First, we calculate the flow rates through a given cross section of the capillary under the small gradients of the pressure and temperature. In the second stage we use an approach elaborated recently to calculate the flow rates as a function of the pressures and the temperatures on the capillary ends without any restrictions on their drops.

In Sec. 4 the other limit case is considered, viz. the capillary with a zero length. This means that the containers are separated by a thin partition having a slit or an orifice.

In Sec. 5 the intermediate values of the capillary length are regarded.

From the last two sections one concludes that information on these types of rarefied gas flows is very poor and there is a need for more research in this scientific field.

1.2. General Statement of the Problem

Consider two reservoirs containing the same gas and joined by a capillary of a length l as is shown in Fig. 1. Let P_I and T_I be the pressure and the temperature, respectively, of the gas in the left container; P_{II} and T_{II} are the pressure and the temperature, respectively, in the right container. There is a temperature distribution $T_w(x)$ on the capillary wall. This distribution can exist independently of the temperatures T_I and T_{II}. However we will not consider this specific situation and assume that

$$T_w(x)=T_I+(T_{II}-T_I)\tau_w(x), \tag{1.1}$$

where $\tau_w(x)$ is some given function satisfying the conditions

$$\tau_w(-l/2)=0, \quad \tau_w(l/2)=1.$$

Therefore, if $T_I=T_{II}$ then $T_w(x)=T_I=\text{const}$.

It is obvious that the pressure and temperature drops

$$\Delta P=(P_{II}-P_I), \quad \Delta T=(T_{II}-T_I) \tag{1.2}$$

cause the fluxes of the mass and heat through the capillary. The flow rate and the heat flux are defined as

$$\dot{M}=\frac{\Delta M}{\Delta t}, \quad \dot{E}=\frac{\Delta E}{\Delta t}, \tag{1.3}$$

respectively. Here, ΔM and ΔE are quantities of mass and heat, respectively, flowing through a cross section of the capillary per a time interval Δt.

In rarefied gases the flow rate and the heat flux depend on the drops of both pressure and temperature, i.e.,

$$\dot{M}=\dot{M}(\Delta P,\Delta T), \quad \dot{E}=\dot{E}(\Delta P,\Delta T). \tag{1.4}$$

This means that the mass flow can be caused not only by the pressure drop but also by the temperature drop, and the heat flux is caused not only by the temperature drop but also by the pressure drop.

This fact leads to an interesting phenomenon, the so-called thermomolecular pressure difference (TPD). If we assume that the system (the capillary+the reservoirs) is closed, the pressures P_I, P_{II} are equal each to other but the temperatures T_I, T_{II} are maintained different, then a gas begins to flow from the cold container to the hot one. This will cause a pressure difference between the reservoirs, and the mass flow in the opposite direction appears. When the whole mass flow rate through the capillary is zero the stationary state will be established. The established pressure ratio P_I/P_{II} in this state can be related to the maintained temperature ratio as

$$\frac{P_I}{P_{II}}=\left(\frac{T_I}{T_{II}}\right)^{\gamma}, \tag{1.5}$$

where γ is the exponent of the TPD, which can be related to the mass flow rate.

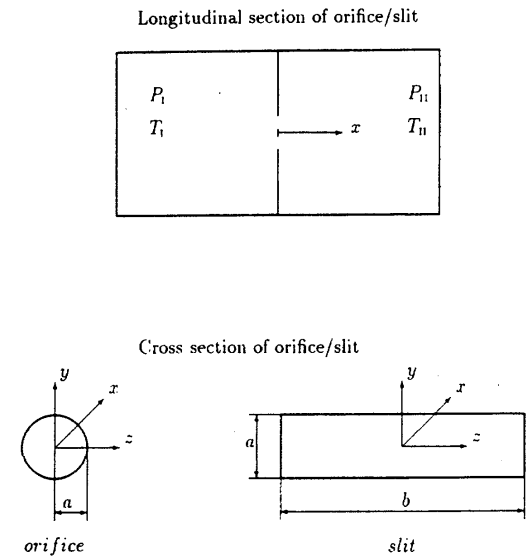

FIG. 2. Sketch of the gas flow through an orifice and slit.

1.3. Main Assumptions

We restrict ourselves by the following assumptions:

(i) The volume of the reservoirs are significantly larger than the volume of the capillary, so that the gas in the containers is in equilibrium far away from the capillary entrances. This assumption allows us to discount the form and size of the reservoirs.

(ii) The flow regime is stable, not turbulent. The criterion of the stability of the gas flow is the Reynolds number. The data on the critical Reynolds number can be found in many books on hydrodynamics, see e.g., Landau and Lifshitz,[73] Chapter III.

(iii) The molecular mean free path is significantly larger than the molecular diameter. This assumption allows us to consider only binary intermolecular collisions and to apply the Boltzmann equation. The molecular diameter is of the order 10^{-10} m, while the mean free path under normal conditions (the pressure is 1 atm and the temperature is 0 °C) is about 10^{-8} m. This assumption is violated if the pressure exceeds 10 atm.

(iv) The gas molecules are monatomic. This assumption allows us to neglect the internal degrees of freedom and to simplify the kinetic equation. In practice, usually one deals with polyatomic gases and hence, the natural question arises: are the results obtained for monatomic gases applicable to polyatomic ones? If the reply is negative, this article would be totally meaningless. The question on the applicability must be considered in every special case: some results are applicable, while others are not. At the end of every section, recommendations on the applicability of results to polyatomic gases are given.

(v) The gas is a single pure species. This assumption also allows us to simplify the kinetic equation. Since in practice gaseous mixtures are met more frequently than a single gas, the same question arises: are the results obtained for a single gas applicable to a gaseous mixture. This question will be discussed at the end of Sec. 2.13.

1.4. Types of Capillaries

We will consider two types of capillaries: the capillary with the round cross section will be called "tube," and the capillary with the rectangular cross section will be called "channel," (see Fig. 1). The word "capillary" will be used to indicate both "tube" and "channel." We denote the capillary length by l, the tube radius and the channel height by a. The channel width is denoted by b.

In the particular case $l=0$, i.e., the containers are divided only by an infinitesimally thin partition as is shown in Fig. 2, the capillary will be called the "orifice" instead of the "tube" and the "slit" instead of the "channel."

1.5. Mass Flow Rate and Heat Flux

1.5.1. Channel

The mass flow rate and the heat flux through a channel of finite width b are calculated as

$$\dot{M}^{\mathrm{ch},b}=\int_{-b/2}^{b/2}\int_{-a/2}^{a/2}\rho(\mathbf{r})u_x(\mathbf{r})\mathrm{d}y\mathrm{d}z, \tag{1.6}$$

$$\dot{E}^{\mathrm{ch},b}(x)=\int_{-b/2}^{b/2}\int_{-a/2}^{a/2}q_x(\mathbf{r})\mathrm{d}y\mathrm{d}z, \tag{1.7}$$

respectively. Here, $\mathbf{r}=(x,y,z)$ is the position vector, $\rho(\mathbf{r})$ is the local mass density of the gas, $u_x(\mathbf{r})$ is the x component of the hydrodynamic (bulk) velocity of the gas, and $q_x(\mathbf{r})$ is x component of the heat flow vector in the gas. The coordinates x,y,z are depicted in Fig. 1. Note that the mass flow rate does not depend on the x coordinate because of the mass impenetrability of the capillary walls. Since there are no heat impenetrable walls, the heat flux through a cross section of the capillary generally depends on the x coordinate.

In theoretical calculations, it is usually assumed that the width b is essentially larger than the height a and the flow field has the translational invariance in the z direction. In this case the flow rate and the heat flux are defined per unity of the width, i.e., as limits

$$\dot{M}^{\mathrm{ch}}=\lim_{b\to\infty}\left(\frac{1}{b}\dot{M}^{\mathrm{ch},b}\right)=\int_{-a/2}^{a/2}\rho(x,y)u_x(x,y)\mathrm{d}y, \tag{1.8}$$

$$\dot{E}^{\mathrm{ch}}(x)=\lim_{b\to\infty}\left(\frac{1}{b}\dot{E}^{\mathrm{ch},b}\right)=\int_{-a/2}^{a/2}q_x(x,y)\mathrm{d}y. \tag{1.9}$$

Further, we will use these definitions of the mass flow rate (1.8) and of the heat flux (1.9) through a channel.

1.5.2. Tube

The flow rate and the heat flux through a tube are calculated as

$$\dot{M}^{\mathrm{tb}}=2\pi\int_0^a\rho(x,r_-)u_x(x,r_-)r_-\mathrm{d}r_-, \tag{1.10}$$

$$\dot{E}^{\mathrm{tb}}(x)=2\pi\int_0^a q_x(x,r_-)r_-\mathrm{d}r_-, \tag{1.11}$$

where $r_-=\sqrt{y^2+z^2}$. The coordinates are depicted in Fig. 1.

1.6. Main Variables

In this article the mass flow rate $\dot{M}$ and the heat flux $\dot{E}$ are treated as functions of the following variables:

(i) The drops of the pressure ΔP and temperature ΔT. We also will use the ratios of the pressure $P_{\mathrm{I}}/P_{\mathrm{II}}$ and of the temperature $T_{\mathrm{I}}/T_{\mathrm{II}}$.

(ii) The rarefaction parameter of the gas, which is inversely proportional to the Knudsen number. Their definitions are given in Sec. 2.1.

(iii) The dimensionless capillary length $L=l/a$.

(iv) The parameters of the gas–surface interaction. All data presented here were obtained under the supposition of the diffuse-specular scattering of the gas molecules on the surface. This scattering law has a unique parameter, which is introduced in Sec. 2.3.

2. Basic Conceptions of Rarefied Gas Dynamics

2.1. Knudsen Number and Rarefaction Parameter

The principal parameter of the RGD is the Knudsen number, Kn, which characterizes the gas rarefaction. The Knudsen number is defined as the ratio

$$\mathrm{Kn}=\frac{\lambda}{a}, \tag{2.1}$$

where λ is the molecular mean free path, i.e., the average distance traveled by a molecule between collisions, and a is the characteristic scale of the gas flow. For the problem in question a is the radius of the tube or the height of the channel.

Regarding the value of the Knudsen number, we may distinguish three regimes of the gas flow. If the Knudsen number is very small ($\mathrm{Kn}\ll 1$), the mean free path is so small that the gas can be considered as a continuous medium and the hydrodynamic equations can be applied to the gas flow. That is why the regime is called *hydrodynamic*.

If the Knudsen number is very large ($\mathrm{Kn}\gg 1$), the mean free path is so large that the collisions of molecules with the capillary walls occur much more frequently than the collisions between molecules. Under this condition we may discount the intermolecular collisions and consider that every molecule moves independently of each other. This is the so-called *free-molecular* regime.

When the Knudsen number has some intermediate value we cannot consider the gas as a continuous medium. At the same time we cannot discount the intermolecular collisions. This regime is called *transition*.

This division of the regimes of flow is very important because the methods used for calculation of the gas flows essentially depend on the regime.

Usually another quantity characterizing the gas rarefaction is used instead of the Knudsen number, viz. the rarefaction parameter, defined as

$$\delta=\frac{\sqrt{\pi}}{2}\frac{a}{\lambda}=\frac{\sqrt{\pi}}{2}\frac{1}{\mathrm{Kn}}. \tag{2.2}$$

Large values of δ correspond to the hydrodynamic regime and small values of δ appropriate to the free molecular regime.

To calculate the Knudsen Kn number or the rarefaction parameter δ one needs to know the microparameter, such as the mean free path λ, which cannot be measured. If one tries to calculate λ directly, one finds that it depends on the molecular velocity and the molecular size. So, to obtain the mean free path one needs knowledge of other nonmeasurable quantities. Another manner to obtain the mean free path is to use its relations with the transport coefficients provided by the kinetic theory of gases. It has become customary to calculate λ via the viscosity coefficient μ as

$$\lambda=\frac{\sqrt{\pi}\mu}{2P}\left(\frac{2k_BT}{m}\right)^{1/2}, \tag{2.3}$$

where P is the pressure, T is the temperature, m is the molecular mass, and $k_B=1.380658\times10^{-23}$ J/K is the Boltzmann constant. This definition has the advantage that it contains the easily measurable quantities (P,T) and the quantities (μ,m) which can be found in Refs. 19 and 69 or in handbooks on Physics and Chemistry. Moreover the definition (2.3) allows us an easier comparison between results referring to different molecular models. In Sec. 2.4.2 the origin of the relation (2.3) will be described.

The mean free path λ can be also calculated via the thermal conductivity. This method gives slightly different values of λ. To avoid further confusion the mean free path at some given pressure P and at some given temperature T will be defined by the relation (2.3) only.

2.2. Boltzmann Equation

The state of a monatomic gas is described by the one-particle velocity distribution function $f(t,\mathbf{r},\mathbf{v})$, where t is the time, $\mathbf{r}$ is a vector of spatial coordinates, and $\mathbf{v}$ is a velocity of molecules. The distribution function is defined so as the quantity $f(t,\mathbf{r},\mathbf{v})\mathbf{dr}\mathbf{dv}$ is the number of particles in the phase volume $\mathbf{dr}\mathbf{dv}$ near the point $(\mathbf{r},\mathbf{v})$ at the time t.

All macrocharacteristics of the gas flow can be calculated via the distribution function:

number density

$$n(t,\mathbf{r})=\int f(t,\mathbf{r},\mathbf{v})\mathbf{dv}, \tag{2.4}$$

hydrodynamic (bulk) velocity

$$\mathbf{u}(t,\mathbf{r})=\frac{1}{n}\int \mathbf{v}\, f(t,\mathbf{r},\mathbf{v})\mathbf{dv}, \tag{2.5}$$

pressure

$$P(t,\mathbf{r})=\frac{m}{3}\int V^2 f(t,\mathbf{r},\mathbf{v})\mathbf{dv}, \tag{2.6}$$

stress tensor

$$P_{ij}(t,\mathbf{r})=m\int V_iV_j f(t,\mathbf{r},\mathbf{v})\mathbf{dv}, \tag{2.7}$$

temperature

$$T(t,\mathbf{r})=\frac{m}{3nk_B}\int V^2 f(t,\mathbf{r},\mathbf{v})\mathbf{dv}, \tag{2.8}$$

heat flow vector

$$\mathbf{q}(t,\mathbf{r})=\frac{m}{2}\int V^2\mathbf{V} f(t,\mathbf{r},\mathbf{v})\mathbf{dv}, \tag{2.9}$$

where $\mathbf{V}$ is the peculiar velocity

$$\mathbf{V}=\mathbf{v}-\mathbf{u}. \tag{2.10}$$

With help of (2.4), (2.6) and (2.8) the state equation is derived

$$P(\mathbf{r})=n(\mathbf{r})k_BT(\mathbf{r}). \tag{2.11}$$

Note that Eq. (2.11) is valid for any nonequilibrium state of the gas, while Pascal's law is valid only in equilibrium. In a nonequilibrium state the pressure defined by (2.6) is the average value over all directions. Further we will pass from the variables (n,T) to (P,T) and vice versa implying the relation (2.11).

The distribution function obeys the Boltzmann equation (BE),[25–27,30,39,57,71] which in the absence of external forces reads as

$$\frac{\partial f}{\partial t}+\mathbf{v}\cdot\frac{\partial f}{\partial\mathbf{r}}=Q(ff_*), \tag{2.12}$$

where $Q(ff_*)$ is the collision integral

$$Q(ff_*)=\int w(\mathbf{v},\mathbf{v}_*;\mathbf{v}',\mathbf{v}'_*)(f'f'_*-ff_*)\mathbf{dv}'\mathbf{dv}'_*\mathbf{dv}_*. \tag{2.13}$$

Here, the affixes to f correspond to those of their arguments $\mathbf{v}$: $f'=f(t,\mathbf{r},\mathbf{v}')$, $f_*=f(t,\mathbf{r},\mathbf{v}_*)$. The quantity $w(\mathbf{v},\mathbf{v}_*;\mathbf{v}',\mathbf{v}'_*)$ is the probability density that two molecules having the velocities $\mathbf{v}'$ and $\mathbf{v}'_*$ will have the velocities $\mathbf{v}$ and $\mathbf{v}_*$, respectively, after a binary collision between them.

The function w satisfies the two general relations:[76] the reciprocity property

$$w(\mathbf{v},\mathbf{v}_*;\mathbf{v}',\mathbf{v}'_*)=w(-\mathbf{v}',-\mathbf{v}'_*;-\mathbf{v},-\mathbf{v}_*), \tag{2.14}$$

and the unitary property

$$\int w(\mathbf{v},\mathbf{v}_*;\mathbf{v}',\mathbf{v}'_*)\mathbf{dv}\mathbf{dv}_*=\int w(\mathbf{v}',\mathbf{v}'_*;\mathbf{v},\mathbf{v}_*)\mathbf{dv}\mathbf{dv}_*. \tag{2.15}$$

Applying these relations the following inequality is easily proved, see Cercignani[26] (Chap.II Sec. 7), Ferziger and Kaper[57] (Sec. 4.2), Lifshitz and Pitaevskii[76] (Sec. 4)

$$\int Q(ff_*)\ln f\mathbf{dv}\leqslant 0. \tag{2.16}$$

Moreover, the collision integral obeys the rules

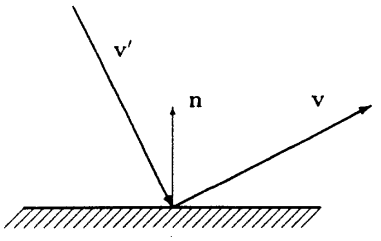

FIG. 3. The velocities of incident ($\mathbf{v}'$) and reflected ($\mathbf{v}$) molecules.

$$\int \psi(\mathbf{v})Q(ff_*)\mathrm{d}\mathbf{v}=0, \quad \psi(\mathbf{v})=1, m\mathbf{v}, \quad \frac{mv^2}{2}, \tag{2.17}$$

that follows from the conservation of the particles, momentum and energy in every collision.

2.3. Gas–Surface Interaction

On the boundary surface we need to relate the distribution function of incident particles f^- and the distribution function of molecules leaving the wall f^+. The relation can be written in a general form as, see Cercignani[26] (Chap. III), Cercignani *et al.*[30] (Chap. 8)

$$f^+(\mathbf{r},\mathbf{v})=\frac{H(v_n)}{|v_n|}\int H(-v_n')|v_n'|R(\mathbf{r},\mathbf{v}'\to\mathbf{v}) \times f^-(\mathbf{r},\mathbf{v}')\mathrm{d}\mathbf{v}', \tag{2.18}$$

where $H(x)$ is the Heaviside step function defined as

$$H(x)=\begin{cases}1 & \text{for } x>0,\\ 0 & \text{for } x<0,\end{cases} \tag{2.19}$$

$v_n=\mathbf{v}\cdot\mathbf{n}$ is a normal velocity component, n is the unit vector normal to the surface (see Fig. 3). $R(\mathbf{r},\mathbf{v}'\to\mathbf{v})$ is a scattering kernel satisfying the normalization condition

$$\int H(v_n)R(\mathbf{r},\mathbf{v}'\to\mathbf{v})\mathrm{d}\mathbf{v}=1. \tag{2.20}$$

Another obvious property of the kernel is that it cannot assume a negative value

$$R(\mathbf{r},\mathbf{v}'\to\mathbf{v})\geq 0.$$

If the surface is staying in local equilibrium at a temperature T_w, the kernel satisfies the reciprocity property, see Cercignani[26] (Chap III, Sec. 3)

$$H(-v_n')|v_n'|\exp\left(-\frac{mv'^2}{2k_BT_w}\right)R(\mathbf{r},\mathbf{v}'\to\mathbf{v}) = H(v_n)|v_n|\exp\left(-\frac{mv^2}{2k_BT_w}\right)R(\mathbf{r},-\mathbf{v}\to-\mathbf{v}'). \tag{2.21}$$

The most known model of the gas–surface interaction is the diffuse scattering having the following kernel

$$R(\mathbf{v}'\to\mathbf{v})=\frac{m^2v_n}{2\pi(k_BT_w)^2}\exp\left(-\frac{mv^2}{2k_BT_w}\right), \tag{2.22}$$

where T_w is the surface temperature. Physically this means that a particle coming to the surface "forgets" all information on its state before the interaction with the surface. Then, it leaves the surface with the Maxwellian distribution function. That is why the diffuse scattering is also called the perfect accommodation.

Calculations of rarefied gas flows based on the diffuse scattering sometimes give an understated flow rate instead of experimental results. To eliminate this discrepancy Maxwell[107] generalized the model (2.22) and considered that only α part of molecules is reflected diffusely but the reflection of the rest part $(1-\alpha)$ is specular. Maxwell's kernel reads as

$$R(\mathbf{v}'\to\mathbf{v})=(1-\alpha)\delta(\mathbf{v}'-\mathbf{v}+2\mathbf{n}v_n) + \alpha\frac{m^2v_n}{2\pi(k_BT_w)^2}\exp\left(-\frac{mv^2}{2k_BT_w}\right). \tag{2.23}$$

This model is widely used but it contradicts some experimental results on the TPD effect (see Sec. 5.2.5). That is why some other models were proposed. One of them is the Cercignani and Lampis[31] model, which reads as

$$R(\mathbf{v}'\to\mathbf{v})=\frac{m^2v_n}{2\pi\alpha_n\alpha_t(2-\alpha_t)(k_BT_w)^2} \times\exp\left\{-\frac{m[v_n^2+(1-\alpha_n)v_n'^2]}{2k_BT_w\alpha_n}-\frac{1}{\alpha_t(2-\alpha_t)} \times\frac{m[v_t-(1-\alpha_t)v_t']^2}{2k_BT_w}\right\}J_0\left(\frac{\sqrt{1-\alpha_n}mv_nv_n'}{\alpha_nk_BT_w}\right), \quad (0\leq\alpha_t\leq 2;\ 0\leq\alpha_n\leq 1), \tag{2.24}$$

where v_t is the tangential component of the molecular velocity, J_0 denotes the modified Bessel function of the first kind and zero order defined as

$$J_0(x)=(2\pi)^{-1}\int_0^{2\pi}\exp(x\cos\phi)\mathrm{d}\phi, \tag{2.25}$$

α_n has the physical sense of the accommodation coefficient for the part of the kinetic energy corresponding to the motion normal to the wall, and α_t is the accommodation coefficient of the tangential momentum.

The definition of the accommodation coefficients will be given in Sec. 2.9.

2.4. Analytical Solutions of the Boltzmann Equation

Generally speaking if one solves the BE (2.12) with the boundary conditions (2.18), one knows the distribution function $f(t,\mathbf{r},\mathbf{v})$. Then, one can calculate all moments (2.4)–(2.9) and finally one finds the flow rate M and the heat flux E. However the complexity of the BE does not allow us to perform this task in general. Recently, using powerful computers it became possible to solve numerically the BE only in

some simple cases. That is why a number of approximate methods of solution of the BE were elaborated. Here, we will consider the main ones.

2.4.1. Moment Method

The moments of the distribution function are defined as

$$M^{(N)}_{\alpha_1\dots\alpha_N}(t,\mathbf{r})=\int v_{\alpha_1}\dots v_{\alpha_N}f(t,\mathbf{r},\mathbf{v})d\mathbf{v},$$

$$\alpha_\beta=1,2,3,\quad \beta=1\dots N \quad (2.26)$$

$$\mathscr{M}^{(N)}_{\alpha_1\dots\alpha_N}(t,\mathbf{r})=\int V_{\alpha_1}\dots V_{\alpha_N}f(t,\mathbf{r},\mathbf{v})d\mathbf{v},$$

$$\alpha_\beta=1,2,3\quad \beta=1\dots N. \quad (2.27)$$

The M moments of the order N may be related with of $\mathscr{M}$ moments of the order N and lower, and vice versa.

The macrocharacteristics of the gas may be expressed in terms of these moments

$$n(t,\mathbf{r})=M^{(0)},\quad nu_i(t,\mathbf{r})=M^{(1)}_i,\quad P_{ij}(t,\mathbf{r})=m\mathscr{M}^{(2)}_{ij},$$

$$q_i=\frac{m}{2}(\mathscr{M}^{(3)}_{i11}+\mathscr{M}^{(3)}_{i22}+\mathscr{M}^{(3)}_{i33}). \quad (2.28)$$

The main idea of the method offered by Grad[60] is to represent the distribution function in the form of series

$$f(t,\mathbf{r},\mathbf{v})=f^{\mathrm{M}}_{\mathrm{loc}}\left(a^{(0)}H^{(0)}+a^{(1)}_{\alpha_1}H^{(1)}_{\alpha_1}+\dots+\frac{1}{N!}a^{(N)}_{\alpha_1\dots\alpha_N}H^{(N)}_{\alpha_1\dots\alpha_N}+\dots\right), \quad (2.29)$$

where $f^{\mathrm{M}}_{\mathrm{loc}}$ is the local Maxwellian defined as

$$f^{\mathrm{M}}_{\mathrm{loc}}(n,T,\mathbf{u})=n(t,\mathbf{r})\left\{\frac{m}{2\pi k_{\mathrm{B}}T(t,\mathbf{r})}\right\}^{3/2}\times\exp\left\{-\frac{m[\mathbf{v}-\mathbf{u}(t,\mathbf{r})]^2}{2k_{\mathrm{B}}T(t,\mathbf{r})}\right\}. \quad (2.30)$$

$H^{(N)}_{\alpha_1\dots\alpha_N}(V_1,V_2,V_3)$ are Hermite polynomials in the three independent variables determined by the relation

$$H^{(N)}_{\alpha_1\dots\alpha_N}(V_1,V_2,V_3)=(-1)^N\left(\frac{k_{\mathrm{B}}T}{m}\right)^{N/2}\exp\left\{\frac{mV^2}{2k_{\mathrm{B}}T}\right\}\times\frac{\partial^N}{\partial V_{\alpha_1}\dots\partial V_{\alpha_N}}\exp\left\{-\frac{mV^2}{2k_{\mathrm{B}}T}\right\}. \quad (2.31)$$

Using the orthogonality of the Hermite polynomials, we find

$$a^{(N)}_{\alpha_1\dots\alpha_N}(t,\mathbf{r})=\frac{1}{n}\int f(t,\mathbf{r},\mathbf{v})H^{(N)}_{\alpha_1\dots\alpha_N}d\mathbf{v}. \quad (2.32)$$

The coefficients $a^{(N)}$ may be expressed in terms of the moments

$$a^{(0)}=1,\quad a^{(1)}_i=0,\quad a^{(2)}_{ij}=\frac{m\mathscr{M}^{(2)}_{ij}}{P}-\delta_{ij},$$

$$a^{(3)}_{ijk}=\frac{m\mathscr{M}^{(3)}_{ijk}}{P}\sqrt{\frac{m}{k_{\mathrm{B}}T}}. \quad (2.33)$$

If we multiply both sides of the BE (2.12) by $H^{(N)}$ and integrate over the whole velocity space $\mathbf{v}$, we obtain

$$\int H^{(N)}\left(\frac{\partial f}{\partial t}+\mathbf{v}\cdot\frac{\partial f}{\partial\mathbf{r}}\right)d\mathbf{v}=\int H^{(N)}Q(ff_*)d\mathbf{v}. \quad (2.34)$$

Then, substituting (2.29) into the collision integral $Q(ff_*)$ in (2.34) we obtain the system of differential equations for an infinite set of the coefficients $a^{(N)}$. The left hand side of Eq. (2.34) is expressed as a linear combination of the derivatives of $a^{(N)}$ with respect to the time and the spatial coordinates. This part of the equation contains the moments of order up to $(N+1)$. The right hand side of Eq. (2.34) is expressed as a linear combination of double products of $a^{(N)}$. This part of the equation contains an infinite number of the coefficients $a^{(N)}$.

It is clear that to solve this system of equations we must retain only a finite number of the moments. If we retain N equations, the last one will contain the moment of the $N+1$ order. To close the system this moment must be related to the moments of the order lower than $N+1$. The relation is based on a physical rationale.

The boundary conditions can be derived by the same method. We multiply both sides of (2.18) by the functions $H^{(N)}_{\alpha_1\dots\alpha_N}$ and integrate with respect to $\mathbf{v}$, substituting the approximating functions (2.29) for $f(\mathbf{v})$ and $f(\mathbf{v}')$. As a results of these derivations we obtain a relation between the moments on the boundary.

One can see that this method assumes the distribution function to be continuous in the velocity variables, but it is approximately true only at the small Knudsen numbers. Thus, the method gives good results only near the hydrodynamic regime.

Details of the method are given in the literature.[10,26,27,71]

2.4.2. Chapman–Enskog Method

The distribution function can be expanded into the power series with respect to the small parameter such as the Knudsen number

$$f=f^{(0)}+\mathrm{Kn}\,f^{(1)}+\mathrm{Kn}^2f^{(2)}+\dots. \quad (2.35)$$

The Chapman–Enskog method assumes that the distribution function depends on the time and the coordinates only via the five moments being the parameters of the local Maxwellian: the number density $n(t,\mathbf{r})$, the three components of the bulk velocity $\mathbf{u}(t,\mathbf{r})$, and the temperature $T(t,\mathbf{r})$. Substituting (2.35) into the BE (2.12) and taking into account the assumption mentioned above, we find that $f^{(0)}$ is the local Maxwellian $f^{\mathrm{M}}_{\mathrm{loc}}$ defined by (2.30). The next approximation $f^{(n)}$ is expressed via the previous one $f^{(n-1)}$.

On the basis of the first approximation $f^{(1)}$ we obtain Newton's law

$$P_{ij}=P\delta_{ij}-2\mu S_{ij}, \tag{2.36}$$

and Fourier's law

$$\mathbf{q}=-\kappa\nabla T, \tag{2.37}$$

where S_{ij} is the rate of shear tensor

$$S_{ij}=\frac{1}{2}\left(\frac{\partial u_i}{\partial x_j}+\frac{\partial u_j}{\partial x_i}\right)-\frac{\delta_{ij}}{3}\nabla\cdot\mathbf{u}, \tag{2.38}$$

κ is the thermal conductivity. The explicit expressions of the transport coefficients μ and κ can be obtained if the intermolecular interaction law is given. For the hard sphere molecules the coefficients have the form

$$\mu=\frac{5}{16}\frac{\sqrt{\pi m k_B T}}{\pi d^2},\quad \kappa=\frac{75k_B}{64m}\frac{\sqrt{\pi m k_B T}}{\pi d^2}, \tag{2.39}$$

where d is the molecular diameter. Taking into account that the molecular mean free path λ is given by

$$\lambda=\frac{1}{\sqrt{2}n\pi d^2}, \tag{2.40}$$

see Bird[10] (Sec. 1.4), Ferziger and Kaper[57] (Sec. 2.4), expressions (2.39) turn into

$$\mu=\frac{5\pi}{32}\langle v\rangle mn\lambda\simeq\frac{1}{2}\langle v\rangle mn\lambda,$$

$$\kappa-\frac{75\pi k_B}{128}\langle v\rangle n\lambda\sim\frac{15k_B}{8}\langle v\rangle n\lambda, \tag{2.41}$$

where $\langle v\rangle$ is the mean thermal velocity

$$\langle v\rangle=\left(\frac{8k_BT}{\pi m}\right)^{1/2}. \tag{2.42}$$

Namely the expression (2.41) for μ has been used in (2.3) to relate the mean free path with the macroparameters. From (2.41) it is easily obtained the relation between the viscosity μ and the thermal conductivity κ

$$\kappa=\frac{15k_B}{4m}\mu. \tag{2.43}$$

With the help of Newton's law (2.36) the equation of the momentum balance gives us the Navier–Stokes equation

$$\rho\frac{du_i}{dt}=-\frac{dP}{dx_i}+2\mu\sum_{j=1}^{3}\frac{\partial S_{ij}}{\partial x_j}. \tag{2.44}$$

The Chapman–Enskog method is based on the expansion (2.35) with respect to the small Knudsen numbers. So, like the moment method, the Chapman–Enskog method also is applicable only for the small Knudsen numbers. Usually, it is used to obtain the explicit expressions of the transport coefficients in the hydrodynamic equations.

Details of the method are given in the literature.[10,26,27,39,57,71]

2.5. Model Kinetic Equations

The Grad and Chapman–Enskog methods are applied near the hydrodynamic regime. To describe gas flows at an arbitrary rarefaction, it is necessary to develop another approach to the solution of the BE. The main idea of the method suitable at any Knudsen number is to simplify the collision integral retaining its fundamental properties such as (2.16) and (2.17). Then, one may apply some exact method of solution to these approximate equations. The simplified equations are called the model kinetic equations.

2.5.1. BGK Equation

An early model equation was proposed by Bhatnagar, Gross and Krook[9] (BGK) and independently by Welander.[165] They presented the collision integral as

$$Q_{BGK}(ff_*)=\nu[f^M_{loc}(n,T,\mathbf{u})-f(t,\mathbf{r},\mathbf{v})], \tag{2.45}$$

where f^M_{loc} is the local Maxwellian (2.30). The local values of the number density $n(t,\mathbf{r})$, bulk velocity $\mathbf{u}(t,\mathbf{r})$ and temperature $T(t,\mathbf{r})$ are calculated via the distribution function $f(t,\mathbf{r},\mathbf{v})$ in accordance with the definitions (2.4), (2.5) and (2.8), respectively. The quantity ν is the collision frequency, which is assumed to be independent of the molecular velocity. One can verify that the model collision integral obeys both fundamental properties (2.16) and (2.17).

The collision frequency ν can be chosen by various methods. One of them is to choose ν so that by solving the model equation by the Chapman–Enskog method the expression of the viscosity μ would be the same as given in the full collision integral. Regarding this we obtain

$$\nu(t,\mathbf{r})=\frac{P(t,\mathbf{r})}{\mu(T)}. \tag{2.46}$$

Note that ν is a local quantity, because the pressure is a function of t and $\mathbf{r}$ and the viscosity μ also depends on t and $\mathbf{r}$ via the temperature T.

Another way to choose ν is as follows:

$$\nu(t,\mathbf{r})=\frac{5k_B}{2m}\frac{P(t,\mathbf{r})}{\kappa(t,\mathbf{r})}=\frac{2}{3}\frac{P(t,\mathbf{r})}{\mu(T)}, \tag{2.47}$$

where relation (2.43) has been used. Solving the BGK equation with this ν, one obtains the correct expression of the heat conductivity κ.

A third way to choose ν is to put the frequency as the ratio of the mean thermal velocity (2.42) to the mean free path, i.e.,

$$\nu=\frac{\langle v\rangle}{\lambda}=\frac{4}{\pi}\frac{P(t,\mathbf{r})}{\mu(T)}, \tag{2.48}$$

where Eqs. (2.3) and (2.42) have been used. This follows from the fact that the mean time between two successive collisions is equal to $1/\nu$ and on the other hand it is equal to $\lambda/\langle v\rangle$. It would seem that this choice of frequency is physically justified. But mathematically it gives the correct expression neither for the viscosity μ nor for the thermal conductivity κ.

A shortcoming of this model equation is that the correct expressions for the viscosity and heat conductivity cannot be proved simultaneously. As a result, the Prandtl number that the BGK model gives is unity instead of the correct value of 2/3. To avoid this shortcoming some modifications were offered.

One modification of this model was introduced by Krook.[72] He assumed that the frequency ν depends on the molecular velocity $\mathbf{v}$, because a computation of the collision frequency for physical models (rigid spheres, finite range potentials) shows that ν varies with the molecular velocity. All basic properties are retained, but to satisfy (2.17) the moments appearing in the local Maxwellian of the modified model are not the local density, velocity and temperature of the gas, but some other local parameters.

2.5.2. S-Model

The S model proposed by Shakhov[130] is also a modification of the BGK model giving the correct Prandtl number. The collision integral of this model is written down as

$$Q_S(ff_*)=\frac{P}{\mu}\left\{f^M_{\rm loc}\left[1+\frac{2m}{15\,n(k_BT)^2}\,\mathbf{q}\cdot\mathbf{V}\left(\frac{mV^2}{2k_BT}-\frac{5}{2}\right)\right]-f(t,\mathbf{r},\mathbf{v})\right\}. \tag{2.49}$$

This model has another shortcoming: the inequality (2.16) can be proved only for the linearized S model. In the nonlinear form one can neither prove nor disprove the inequality. But the conservation laws (2.17) are valid for the S model in any form.

2.5.3. Ellipsoidal Model

Another model[37,65] with the correct Prandtl number has the collision integral in the following form

$$Q_{El}(ff_*)=\nu\left\{\frac{n}{\pi^{3/2}}(\det A)^{1/2}\times\exp\left[-\sum_{i,j=1}^{3}A_{ij}(v_i-u_i)(v_j-u_j)\right]-f\right\}, \tag{2.50}$$

where

$$A=\|A_{ij}\|=\left\|\frac{2k_BT}{m\ \mathrm{Pr}}\delta_{ij}-\frac{2(1-\mathrm{Pr})P_{ij}}{nm\ \mathrm{Pr}}\right\|^{-1},$$

where Pr is the Prandtl number. If we let Pr = 1, we recover the BGK model. It is also impossible to prove the inequality (2.16) for this model.

2.5.4. Applicability of the Model Equations

Conclusions on the applicability of the model equations can be made from a comparison of numerical data based on them with those obtained from the exact BE. In Sec. 3 this comparison is carefully performed on the basis of the simplest internal gas flow, viz. the flow between two parallel plates. From this comparison the following anticipated recommendations can be given: (i) any isothermal gas flow can be successfully calculated with the help of the BGK model; (ii) the S model is an ideal equation to describe the linear nonisothermal gas flows; (iii) the ellipsoidal model is not recommended for practical calculations.

2.6. Linearized Boltzmann Equation

2.6.1. Linearization Near the Absolute Maxwellian

If the state of the gas is weakly nonequilibrium, we may linearize the BE by the standard manner. The distribution function can be presented as

$$f(t,r,v)=f_0^M[1+h(t,\mathbf{r},\mathbf{v})],\quad |h|\ll 1, \tag{2.51}$$

where f_0^M is the absolute Maxwellian with the equilibrium number density n_0 and the equilibrium temperature T_0

$$f_0^M=n_0\left(\frac{m}{2\pi k_BT_0}\right)^{3/2}\exp\left(-\frac{mv^2}{2k_BT_0}\right). \tag{2.52}$$

Substituting (2.51) into (2.12) the linearized BE is easily derived

$$\frac{\partial h}{\partial t}+\hat{D}h-\hat{L}h=0. \tag{2.53}$$

The operators $\hat{D}$ and $\hat{L}$ are defined as

$$\hat{D}h=\mathbf{v}\cdot\frac{\partial h}{\partial\mathbf{r}}, \tag{2.54}$$

$$\hat{L}h=\int f_0^M(\mathbf{v}_*)w(\mathbf{v},\mathbf{v}_*;\mathbf{v}',\mathbf{v}'_*)\times(h'+h'_*-h-h_*)d\mathbf{v}_*d\mathbf{v}'_*d\mathbf{v}'. \tag{2.55}$$

Let us introduce the operator of the time reversal

$$\hat{T}\varphi(\mathbf{r},\mathbf{v})=\varphi(\mathbf{r},-\mathbf{v}) \tag{2.56}$$

and two scalar products

$$(\varphi,\psi)=\int f_0^M\varphi(\mathbf{r},\mathbf{v})\psi(\mathbf{r},\mathbf{v})d\mathbf{v},\quad((\varphi,\psi))=\int_\Omega(\varphi,\psi)d\mathbf{r}, \tag{2.57}$$

where Ω is the region of the gas flow. Using (2.14) and (2.15) the following relations can be proved

$$(\hat{T}\hat{L}\varphi,\psi)=(\hat{T}\hat{L}\psi,\varphi), \tag{2.58}$$

$$((\hat{T}\hat{L}\varphi,\psi))=((\hat{T}\hat{L}\psi,\varphi)). \tag{2.59}$$

The moments of the distribution function can be expressed via the perturbation function h and the scalar product (2.57) as

$$n=n_0+(1,h),\quad T=T_0+\frac{m}{3k_Bn_0}(v^2,h)-\frac{T_0}{n_0}(1,h), \tag{2.60}$$

$$\mathbf{u}=\frac{1}{n_0}(\mathbf{v},h), \quad \mathbf{q}=\frac{m}{2}(v^2\mathbf{v},h)-\frac{5}{2}k_BT_0(\mathbf{v},h). \tag{2.61}$$

2.6.2. Linearization Near the Local Maxwellian

In some cases it is more convenient to linearize near the local Maxwellian, i.e., to represent the distribution function as

$$f(t,\mathbf{r},\mathbf{v})=f^M_{loc}(n,T,0)[1+h(t,\mathbf{r},\mathbf{v})], \tag{2.62}$$

where f^M_{loc} is defined by (2.30). Here, the moments $n(t,\mathbf{r})$ and $T(t,\mathbf{r})$ may depend on the coordinates. If we substitute (2.62) into the BE (2.12) we obtain

$$\frac{\partial h}{\partial t}+\hat{D}h-\hat{L}h=-\mathbf{v}\cdot\left[\frac{1}{n}\frac{\partial n}{\partial \mathbf{r}}+\left(\frac{mv^2}{2k_BT}-\frac{3}{2}\right)\frac{1}{T}\frac{\partial T}{\partial \mathbf{r}}\right]. \tag{2.63}$$

One can see that in the case $n(t,\mathbf{r})=n_0$ and $T(t,\mathbf{r})=T_0$ the last equation takes the form (2.53).

2.7. Linearized Model Equations

In the case of the weak nonequilibrium the local Maxwellian (2.30) can be related to the absolute Maxwellian (2.52) as

$$f^M_{loc}(n,T,\mathbf{u})=f^M_0\left[1+\varrho+\frac{m}{k_BT_0}\mathbf{v}\cdot\mathbf{u}+\tau\left(\frac{mv^2}{2k_BT_0}-\frac{3}{2}\right)\right], \tag{2.64}$$

where

$$\varrho=\frac{n-n_0}{n_0}, \quad \tau=\frac{T-T_0}{T_0}. \tag{2.65}$$

Equation (2.64) is valid if

$$|\varrho|\ll 1, \left|\sqrt{\frac{m}{k_BT_0}}\mathbf{u}\right|\ll 1, \quad |\tau|\ll 1.$$

Substituting (2.51) and (2.64) into (2.45) we obtain

$$Q_{BGK}(ff_*)=\nu f^M_0\left[\varrho+\frac{m}{k_BT_0}\mathbf{v}\cdot\mathbf{u}+\tau\left(\frac{mv^2}{2k_BT_0}-\frac{3}{2}\right)-h\right]. \tag{2.66}$$

Then, the linearized collision operator takes the form

$$\hat{L}_{BGK}h=\nu_0\left[\varrho+\frac{m}{k_BT_0}\mathbf{v}\cdot\mathbf{u}+\tau\left(\frac{mv^2}{2k_BT_0}-\frac{3}{2}\right)-h\right]. \tag{2.67}$$

Note that here the frequency ν has its value in the equilibrium state, because the consideration of its variation gives us the terms of the second order of the smallness, which are negligible.

The analogous procedure with the S model (2.49) gives us the following collision operator

$$\hat{L}_Sh=\frac{P_0}{\mu_0}\left[\varrho+\frac{m}{k_BT_0}\mathbf{v}\cdot\mathbf{u}+\tau\left(\frac{mv^2}{2k_BT_0}-\frac{3}{2}\right)+\frac{2m}{15n_0(k_BT_0)^2}\mathbf{q}\cdot\mathbf{v}\left(\frac{mv^2}{2k_BT_0}-\frac{5}{2}\right)-h\right], \tag{2.68}$$

where $P_0=n_0k_BT_0$ and $\mu_0=\mu(T_0)$.

2.8. Linearized Boundary Conditions

The linearized boundary conditions are easily obtained substituting (2.51) into (2.18) combining with (2.20) and (2.21)

$$h^+=\hat{A}h^-+h^+_w-\hat{A}h^-_w, \quad h_w=\frac{T_w-T_0}{T_0}\left(\frac{mv^2}{2k_BT_0}-\frac{5}{2}\right). \tag{2.69}$$

The upper indexes "+" and "−" in (2.69) mean the perturbation function of the reflected and incident molecules, respectively. The scattering operator $\hat{A}$ is defined as

$$\hat{A}h^-=\frac{H(v_n)}{|v_n|\exp[-mv^2/(2k_BT_0)]}\int H(-v_n')|v_n'|\times\exp\left(-\frac{mv'^2}{2k_BT_0}\right)h(\mathbf{v}')R(\mathbf{v}'\to\mathbf{v})d\mathbf{v}'. \tag{2.70}$$

Let us introduce one more scalar product

$$(\varphi,\psi)_B=\int H(v_n)v_nf^M_0\,\varphi(\mathbf{r},\mathbf{v})\psi(\mathbf{r},\mathbf{v})d\mathbf{v}, \quad \mathbf{r}\in\partial\Omega, \tag{2.71}$$

where $\partial\Omega$ is the surface bounding the gas flow.

Using the normalization (2.20) and the reciprocity of the scattering kernel (2.21) one obtains the following relation[26]

$$(\hat{T}\varphi^-,\hat{A}\psi^-)_B=(\hat{T}\psi^-,\hat{A}\varphi^-)_B. \tag{2.72}$$

2.9. Accommodation Coefficients

In some cases it is not necessary to know the scattering kernel, it is enough to know only its integral characteristics such as the accommodation coefficients $\alpha(\varphi)$. For a surface having a temperature T_0 the accommodation coefficient is defined as

$$\alpha(\varphi)=\frac{\int H(-v_n)\varphi(\mathbf{v})|v_n|f d\mathbf{v}-\int H(v_n)\varphi(\mathbf{v})|v_n|f d\mathbf{v}}{\int H(-v_n)\varphi(\mathbf{v})|v_n|f d\mathbf{v}-\int H(v_n)\varphi(\mathbf{v})|v_n|f^M_0 d\mathbf{v}}, \tag{2.73}$$

where f^M_0 is defined by (2.52), and $\varphi(\mathbf{v})$ is some function of the molecular velocity. One can see that the accommodation coefficient $\alpha(\varphi)$ defined by (2.73) depends on the distribution function of the impinging molecules. Restricting this distribution function we obtain a more meaningful definition. If we represent f as

$$f=f^M_0(1+\hat{T}\psi), \tag{2.74}$$

then Eq. (2.73) can be written as

$$\alpha(\varphi,\psi)=1-\frac{(\varphi^+,\hat{T}\psi^-)_B}{(\hat{T}\varphi^-,\psi^+)_B}=1-\frac{(\hat{A}\varphi^-,\hat{T}\psi^-)_B}{(\hat{T}\varphi^-,\psi^+)_B}$$

$$=1-\frac{(\hat{A}\psi^-,\hat{T}\varphi^-)_B}{(\hat{T}\varphi^-,\psi^+)_B}, \tag{2.75}$$

where Eq. (2.72) has been used.

It is easily verified that in Maxwell's kernel (2.23) α is the accommodation coefficient of any quantity φ for any perturbation function ψ.

In the Cercignani–Lampis kernel (2.24) α_t is the accommodation coefficient of tangential momentum, i.e., $\alpha_t=\alpha(mv_t,\psi)$ for any ψ. The coefficient α_n is the accommodation coefficient for the part of the kinetic energy corresponding to the motion normal to the wall, i.e., $\alpha_n=\alpha(mv_n^2,\psi)$ for any ψ. If one tries to compute other accommodation coefficients using the Cercignani–Lampis model, one concludes that they depend on the distribution function ψ.

Let us take a set of of physically meaningful quantities φ_i and let $\varphi=\varphi_i$, $\psi=\varphi_j$. We obtain a matrix of the accommodation coefficients

$$\alpha_{ij}=1-\frac{(\hat{A}\varphi_i^-,\hat{T}\varphi_j^-)_B}{(\hat{T}\varphi_i^-,\varphi_j)_B}. \tag{2.76}$$

With the help of (2.72) one can prove that the matrix α_{ij} is symmetric. The set $\varphi_1=v_n$, $\varphi_2=v_{t1}$, $\varphi_3=v_{t2}$ and $\varphi_4=v^2$ leads us to the four accommodation coefficients:[109] α_{11}, $\alpha_{22}=\alpha_{33}$, α_{44}, and $\alpha_{14}=\alpha_{41}$, which are generally used.

The accommodation coefficient of the tangential momentum α_{22} is most important in the problem of the internal rarefied gas flow. The accommodation coefficients are usually measured indirectly, e.g., via the mass flow rate through a capillary. Data on the coefficients can be found in the literature.[3,7,122,125,126,154] From these data one can see that for light gases, such as helium and neon, the accommodation coefficients may differ significantly from unity, while for heavy gases, e.g., krypton, xenon, the coefficients are close to unity. The gas–surface interaction for a contaminated surface is closer to the diffuse scattering than the interaction with a surface specially treated. A chemical cleaning of the surface increases the deviation of the accommodation coefficients from the unity. So, if one deals with a sufficiently heavy gas and with an ordinarily contaminated surface, one may assume the perfect accommodation of gas on the surface.

2.10. Onsager's Reciprocity Relations

If we restrict ourselves by the linear region of physical laws, all irreversible phenomena can be described in the quite general form

$$J_k=\sum_n \Lambda_{kn}X_n, \tag{2.77}$$

where X_k are independent thermodynamic forces, J_k are conjugated thermodynamic fluxes and Λ_{kn} are kinetic coefficients. If the set of the fluxes is chosen so as the entropy production in the system is expressed as the sum

$$\sigma=\sum_n J_nX_n, \tag{2.78}$$

the Onsager theorem[118] establishes the following relations between the kinetic coefficients

$$\Lambda_{kn}=\Lambda_{nk}. \tag{2.79}$$

Casimir[21] generalized these relations regarding forces with a different time parity. However, all thermodynamic forces considered here have the same time parity, which is why we retain the reciprocity relations just in the form (2.79).

Onsager[118] proved the relations (2.79) for insulated systems. De Groot and Mazur[51] derived them for systems in local equilibrium. However, we are going to consider open systems admitting a heat exchange with the surroundings and not being in local equilibrium, which is destroyed at a large rarefaction of the gas. For our purpose the best approach is based on the BE, which was elaborated by Loyalka,[87] by Bosch *et al.*,[159] by Bishaev and Rykov,[13–16] by Freedlender[58] and by Sharipov.[132–139,143] The explicit expressions for the thermodynamic fluxes and the kinetic coefficients in the case of rarefied gas flow through a capillary are given below.

Since the Onsager reciprocity relations are valid for a weak nonequilibrium state, we assume the relative drops of the pressure and temperature to be small

$$\left|\frac{P_{II}-P_I}{P_I}\right|\ll 1, \quad \left|\frac{T_{II}-T_I}{T_I}\right|\ll 1. \tag{2.80}$$

Further it is reasonable to assume these drops to be thermodynamic forces

$$X_P=\frac{P_{II}-P_I}{P_I}, \quad X_T=\frac{T_{II}-T_I}{T_I}. \tag{2.81}$$

Moreover, we consider the stationary gas flow.

In Refs. 136–138 it was shown that to satisfy (2.78) the thermodynamic fluxes must have the following form

$$J_P=-n_I\int_{\Sigma_-} u_x d\Sigma, \tag{2.82}$$

$$J_T=-\frac{1}{k_BT_I}\left(\int_{\Sigma^{II}} q_x d\Sigma-\int_{\Sigma_w^c} q_n\tau_w d\Sigma\right), \tag{2.83}$$

where Σ_- is any cross section of the capillary, Σ^{II} is the cross section bounding the right container and the capillary, Σ_w^c is the lateral surface of the capillary, $q_n=(\mathbf{q}\cdot\mathbf{n})$ is the normal of the heat flow vector, where the unit vector $\mathbf{n}$ is directed into the capillary, and τ_w is the temperature distribution (1.1).

Because of the smallness of the pressure and temperature drops the solution of the linearized BE (2.53) or (2.63) can be decomposed as

$$h(\mathbf{r},\mathbf{v})=h_{\mathrm{P}}(\mathbf{r},\mathbf{v})X_{\mathrm{P}}+h_{\mathrm{T}}(\mathbf{r},\mathbf{v})X_{\mathrm{T}}. \tag{2.84}$$

Substituting (2.84) into (2.61) one can see that the moments of the distribution function are decomposed to

$$\mathbf{u}=\mathbf{u}_{\mathrm{P}}X_{\mathrm{P}}+\mathbf{u}_{\mathrm{T}}X_{\mathrm{T}},\quad \mathbf{q}=\mathbf{q}_{\mathrm{P}}X_{\mathrm{P}}+\mathbf{q}_{\mathrm{T}}X_{\mathrm{T}}. \tag{2.85}$$

Substituting (2.85) into (2.82) and (2.83) and comparing with (2.77) we obtain the explicit expressions of the kinetic coefficients

$$\Lambda_{\mathrm{PP}}=-n_{\mathrm{I}}\int_{\Sigma_{\perp}} u_{x\mathrm{P}}\mathrm{d}\Sigma, \tag{2.86}$$

$$\Lambda_{\mathrm{PT}}=-n_{\mathrm{I}}\int_{\Sigma_{\perp}} u_{x\mathrm{T}}\mathrm{d}\Sigma, \tag{2.87}$$

$$\Lambda_{\mathrm{TP}}=-\frac{1}{k_{\mathrm{B}}T_{\mathrm{I}}}\left(\int_{\Sigma^{\mathrm{II}}} q_{x\mathrm{P}}\mathrm{d}\Sigma-\int_{\Sigma_w^c} q_{n\mathrm{P}}\tau_w\mathrm{d}\Sigma\right), \tag{2.88}$$

$$\Lambda_{\mathrm{TT}}=-\frac{1}{k_{\mathrm{B}}T_{\mathrm{I}}}\left(\int_{\Sigma^{\mathrm{II}}} q_{x\mathrm{T}}\mathrm{d}\Sigma-\int_{\Sigma_w^c} q_{n\mathrm{T}}\tau_w\mathrm{d}\Sigma\right). \tag{2.89}$$

The physical sense of the coefficients is as follows: Λ_{PP} describes the Poiseuille flow, i.e., the mass flow rate caused by the pressure drop, Λ_{PT} describes the thermal creep, i.e., the mass flow rate caused by the temperature drop, Λ_{TP} corresponds to the mechanocaloric heat flux, i.e., the heat flux caused by the pressure drop, and Λ_{TT} is the ordinary heat flux caused by the temperature drop.

Starting from equalities (2.59) and (2.72) Sharipov[136–138] proved the Onsager relation (2.79), i.e., $\Lambda_{\mathrm{PT}}=\Lambda_{\mathrm{TP}}$, which is valid for any gas rarefaction, for any gas–surface interaction law, and for any temperature distribution τ_w along the capillary.

De Groot and Mazur[51] derived the analogous expressions assuming that the walls are heat impenetrable. This means that $q_n=0$ at $\mathbf{r}\in\Sigma_w^c$. If we assume the same, the kinetic coefficients (2.88) and (2.89) are reduced to

$$\Lambda_{\mathrm{TP}}=-\frac{1}{k_{\mathrm{B}}T_{\mathrm{I}}}\int_{\Sigma_-} q_{x\mathrm{P}}\mathrm{d}\Sigma,\quad \Lambda_{\mathrm{TT}}=-\frac{1}{k_{\mathrm{B}}T_{\mathrm{I}}}\int_{\Sigma_-} q_{x\mathrm{T}}\mathrm{d}\Sigma, \tag{2.90}$$

coinciding with the expressions by de Groot and Mazur.[51]

In the case of infinite capillary the kinetic coefficients Λ_{TP} and Λ_{TT} also take the form (2.90), because a local equilibrium is established in a capillary element and the normal heat flow vector q_n disappears.

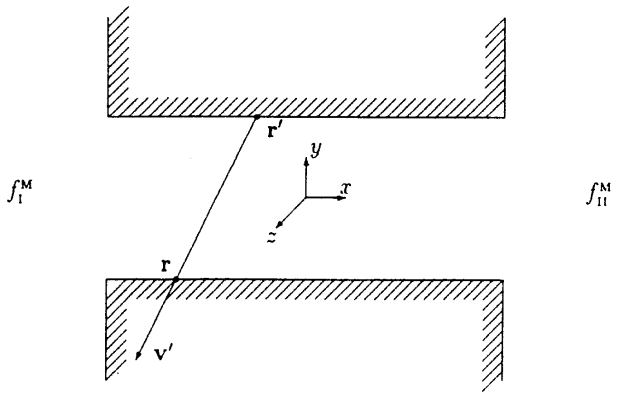

FIG. 4. Illustration to the derivation of Clausing's equation.

2.11. Methods of Computation in the Free-Molecular Regime

2.11.1. Clausing's Equation

If the Knudsen number is very large so that every molecule moves without any collisions with others, the collision integral is equal to zero. To obtain the distribution function in this regime we need only to integrate the left hand side of the BE (2.12) taking into account the boundary condition (2.18). As a result we obtain the integral equation, which has the form (2.18) where $f^-(\mathbf{r},\mathbf{v}')$ is replaced by the Maxwellian

$$f_{\mathrm{I}}^{\mathrm{M}}=\frac{P_{\mathrm{I}}}{k_{\mathrm{B}}T_{\mathrm{I}}}\left(\frac{m}{2\pi k_{\mathrm{B}}T_{\mathrm{I}}}\right)^{3/2}\exp\left(-\frac{mv^2}{2k_{\mathrm{B}}T_{\mathrm{I}}}\right), \tag{2.91}$$

or

$$f_{\mathrm{II}}^{\mathrm{M}}=\frac{P_{\mathrm{II}}}{k_{\mathrm{B}}T_{\mathrm{II}}}\left(\frac{m}{2\pi k_{\mathrm{B}}T_{\mathrm{II}}}\right)^{3/2}\exp\left(-\frac{mv^2}{2k_{\mathrm{B}}T_{\mathrm{II}}}\right), \tag{2.92}$$

if a molecule with the velocity $\mathbf{v}'$ comes to point $\mathbf{r}$ from the left or right container, respectively. $f^-(\mathbf{r},\mathbf{v}')$ is replaced by $f^+(\mathbf{r}',\mathbf{v}')$ if the molecules comes from point $\mathbf{r}'$ being on the capillary surface (see Fig. 4). Resolving the derived integral equation we obtain the distribution function and hence the flow rate and the heat flux.

In the case of the diffuse-specular scattering (2.23) the integral equation is simplified and takes the following form

$$n_{\mathrm{w}}(x)=\int_{-l/2}^{l/2}\mathscr{K}(x,x')n_{\mathrm{w}}(x')\mathrm{d}x'+\mathscr{N}(x), \tag{2.93}$$

where $n_{\mathrm{w}}(x)$ is number of molecules impinging with the capillary wall per time unit and per area unit in the point with the longitudinal coordinate x. The functions $\mathscr{K}(x,x')$ and $\mathscr{N}(x)$ are determined by the capillary form and its dimensionless length L. Resolving this integral equation we can find the flow rate and the heat flux.

The derivation of Clausing's equation (2.93) can be found in Cercignani[26] (Chap.V, Sec.8.) and Kogan[71] (Sec. 6.3). Methods of solution of integral equations are described in Sec. 2.12.4.

2.11.2. Test Particle Monte Carlo Method

The test particle Monte Carlo method[10,11] implies a simulation of the motion of a large number of particles. Since there is no interaction between the molecules we may simulate the motion of every particle separately. First, we generate a particle on the entrance cross section of the capillary with the Maxwellian distribution of the velocity and the uniform distribution over the cross section. Then, we find the trajectory of the particle and calculate the point of the collision of this particle with the capillary wall. It may happen that the particle will pass the capillary without any collision with the wall. In this case we generate a new particle on the capillary entrance. If the particle falls on the wall, we simulate its scattering according to the gas–surface interaction law and obtain the post-interaction velocity of the particle. Then, we find a new point of the interaction with the wall. The procedure is repeated until the particle goes out the capillary. Then, we generate a new particle on the entrance cross section.

The particle can go out through the same capillary entrance where it has been generated (i.e., the particle has not passed through the capillary) and through the opposite entrance (i.e., the particle has passed through the capillary). Testing a lot of the particles we may calculate the transmission probability as

$$W=\frac{N_p}{N}, \tag{2.94}$$

where N_p is the number molecules passed through the capillary and N is the number of the generated particles. The transmission probability is easily related to the mass flow rate, see Sec. 5.2.1.

Bird[10] has reported a program to calculate the transmission probability W through a tube for the diffuse scattering (2.22) on the wall.

2.12. Methods of Computation in the Transition Regime

2.12.1. Discrete Velocity Method

We choose a set of values of the velocity $\mathbf{v}_i$ and interpolate the distribution function in terms of its values corresponding to the velocities $\mathbf{v}_i$. The collision integral is expressed via the values $f_i(t,\mathbf{r})=f(t,\mathbf{r},\mathbf{v}_i)$. Thus, the integro-differential BE is replaced by a system of differential equations for the functions $f_i(t,\mathbf{r})$. The differential equations can be solved numerically by a finite difference method. Then, the distribution function moments are calculated using some quadrature. The method can be optimized[147] if we take into account a solution in the hydrodynamic regime. This method gives good results in the entire range of the Knudsen number.

Details of the method are given by Kogan[1] (Sec. 3.13) and elsewhere.[130,140,147]

2.12.2. Variational Method

To use the variational method we need a variational principle, which can be formulated in the following form. Let us consider a linear equation written in the quite general form

$$\hat{\mathscr{L}}h=\mathscr{S}, \tag{2.95}$$

where $\hat{\mathscr{L}}$ is a some linear operator and $\mathscr{S}$ is a source function. If the linear operator $\hat{\mathscr{L}}$ is self-adjoint with respect to a certain scalar product (,), i.e., for any functions φ and ψ we have

$$(\hat{\mathscr{L}}\varphi,\psi)=(\hat{\mathscr{L}}\psi,\varphi), \tag{2.96}$$

then the functional

$$J(\tilde{h})=(\tilde{h},\hat{\mathscr{L}}\tilde{h})-2(\mathscr{S},\tilde{h}) \tag{2.97}$$

is easily shown to satisfy

$$\delta J=0 \tag{2.98}$$

if and only if $\tilde{h}=h+\delta h$, where h is the solution of Eq. (2.95) and δh is infinitesimal.

We may represent the function $\tilde{h}$ in some analytical form containing some undetermined constants c_i. Usually, the analytical form (so-called trial functions) is chosen from some physical reasonings or from the solutions in the hydrodynamic regime. Then, the trial function is inserted into the functional $J(\tilde{h})$ and J becomes a function of the constant c_i; setting equal to zero the partial derivatives of this function with respect to c_i, we obtain a system which determines the best values of the c_i according to the variational principle.

The advantage of this method is that it requires essentially less computational effort than a direct numerical method, e.g., the discrete velocity method, but it gives only an approximate solution. The precision depends on the choice of the trial function. The great shortcoming of the method is that one cannot estimate the error of the variational solution. That is why the variation solution should be compared with a direct numerical solution for few Knudsen numbers.

Details of the method are given by Cercignani.[26]

2.12.3. Integro-Moment Method

Let the gas flow be a steady weak nonequilibrium that is possible under the small pressure and temperature drops. If the collision integral is replaced by the BGK model or by the S model we can reduce the kinetic equation to the system of integral equations having the following form

$$M_i(\mathbf{r})=\sum_{j=1}^{N}\int_{\Omega}\mathscr{K}_{ij}(\mathbf{r},\mathbf{r}')M_j(\mathbf{r}')d\mathbf{r}'+\mathscr{I}_i(\mathbf{r}),\quad 1\leqslant i\leqslant N, \tag{2.99}$$

where $M_i(\mathbf{r})$ is the moments of the distribution function, Ω is the region of the gas flow, $\mathscr{K}_{ij}(\mathbf{r},\mathbf{r}')$ and $\mathscr{I}_i(\mathbf{r})$ are some functions to be defined in every specific problem. In Sec. 3.3 the expressions of these functions are given for the gas flow through an infinite capillary.

The system (2.99) includes those moments that the model collision integral contains. If we apply the BGK equation, the set of the moments is: $n(\mathbf{r})$, $\mathbf{u}(\mathbf{r})$ and $T(\mathbf{r})$. In one-dimensional flows the density and temperature fields are known and the system (2.99) is reduced to the one equation containing only longitudinal component of the bulk velocity. If one applies the S model, the set of the moments is added by the heat flow vector $\mathbf{q}(\mathbf{r})$.

A derivation of the integral equations (2.99) can be found in the literature.[4,34,45,71,155]

2.12.4. Solution of Integral Equations

The method of solution to the integral equations (2.93) and (2.99) will be demonstrated below for the one-dimensional equation written as

$$M(y)=\int_a^b \mathscr{K}(y,y')M(y')\mathrm{d}y'+\mathscr{J}(y), \quad (2.100)$$

where $\mathscr{K}(y,y')$ and $\mathscr{J}(y)$ are some given functions.

Variational method: The equation (2.100) is a particular case of Eq. (2.95) with the operator

$$\hat{\mathscr{L}}M=M(y)-\int_a^b \mathscr{K}(y,y')M(y')\mathrm{d}y'. \quad (2.101)$$

If we apply a model collision operator satisfying the condition (2.59) and the boundary condition satisfying (2.72), the operator $\hat{\mathscr{L}}$ is always self-adjoint with respect to the scalar product

$$(\varphi,\psi)=\int_a^b \varphi(y)\psi(y)\mathrm{d}y. \quad (2.102)$$

The variational method assumes the moment $M(y)$ to be presented as

$$M(y)=\sum_{i=1}^{K} c_i\varphi_i(y), \quad (2.103)$$

where $\varphi_i(y)$ is a set of basic functions to be chosen from some physical reasonings, and c_i are constants to be calculated. Applying the variational principle described in Sec. 2.12.2. the system of algebraic equations is obtained for these constants:

$$\sum_{i=1}^{K} (\hat{\mathscr{L}}\varphi_i,\varphi_j)c_i=(\mathscr{J},\varphi_j), \quad 1\leqslant j\leqslant K. \quad (2.104)$$

Thus, if one numerically calculates the matrix $(\hat{\mathscr{L}}\varphi_i,\varphi_j)$ and the vector $(\mathscr{J},\varphi_j)$ one knows the constants c_i and hence the moments $M(y)$.

The Bubnov–Galerkin variational method described by Mikhlin[110] and widely applied to the capillary gas flows, gives the same equation system for the coefficients c_i.

Direct numerical method: The integral equation (2.100) can be solved directly. The interval $[a,b]$ is divided on segments $[y_k,y_{k+1}]$, where $1\leqslant k\leqslant K$, $y_1=a$ and $y_{K+1}=b$. Then, the integral equation is replaced by the following system of the algebraic equations

$$M(y_{n+1/2})=\sum_{k=1}^{K} M(y_{k+1/2})\int_{y_k}^{y_{k+1}} \mathscr{K}(y_{n+1/2},y')\mathrm{d}y' + \mathscr{J}(y_{n+1/2}), \quad (2.105)$$

where $1\leqslant n\leqslant K$, $y_{k+1/2}$ is some point between y_k and y_{k+1}. Solving this system we find the moment M in the points $y_{k+1/2}$.

If the order of the algebraic system is large the iterative method of its solution is applied. Mathematically this means a numerical construction of the Neumann-Liouville series.

2.12.5. Method of Elementary Solutions

The main idea of the method of elementary solutions is to separate the variables, to construct a complete set of separated variable solutions ("elementary solutions"), then to represent the general solution of the kinetic equation as a superposition of the elementary solutions, and finally to use the boundary conditions to determine the coefficients of the superposition. For simple one-dimensional gas flows this method allows us to reduce the model kinetic equation to an integral equation for the perturbation function. Then one has to apply some numerical procedure to solve this integral equation.

Details of the method are given by Cercignani[26] (Chap.VI).

2.12.6. Direct Simulation Monte Carlo Method

The region of the gas flow is divided into a network of cells. The dimensions of the cells must be such that the change in flow properties across each cell is small. The time is advanced in discrete steps of magnitude Δt, such that Δt is small compared with the mean time between two successive collisions.

The molecular motion and intermolecular collision are uncoupled over the small time interval Δt by the repetition of the following procedure:

(i) The molecules are moved through the distance determined by their velocities and Δt. If the trajectory passes the boundary a simulation of the gas–surface interaction is performed according to a given law. New molecules are generated at boundaries across which there is an inward flux.

(ii) A representative number of collisions appropriate to Δt and the number of molecules in the cell is computed. The pre-collision velocities of the molecules involved in the collision are replaced by the post-collision values in accordance with a given law of the intermolecular interaction.

After a sufficient number of the repetitions we may calculate any moment of the distribution function. Details of the method are given by Bird.[10,11]

2.13. Gaseous Mixtures

To describe a gaseous mixture having N components we need to consider N distribution functions $f_i(t,\mathbf{r},\mathbf{v})$, $1\leqslant i\leqslant N$, and the system of the Boltzmann equations

$$\frac{\partial f_i}{\partial t}+\mathbf{v}\cdot\frac{\partial f_i}{\partial \mathbf{r}}=\sum_{j=1}^{N} Q_{ij}(f_i f_j), \quad 1\leqslant i\leqslant N, \quad (2.106)$$

where Q_{ij} is the integral describing the collisions between species i and j. The methods of solution to this equation system are based on the same ideas as those to solve the single equation (2.12). The problem is that the computational efforts drastically increase if we pass from a single gas to a gaseous mixture. Moreover, in a mixture new phenomena appear, such as the mass and heat fluxes caused by a concentration gradient, the diffusion caused by gradients of the pressure, temperature and concentration. These phenomena complicate treatment of the gaseous mixture. That is why there are very few papers[36,44,156,175] on the gaseous mixture flows. Therefore, it is very attractive to use the single gas results for a gaseous mixture.

It is obvious that the phenomena mentioned in the previous paragraph cannot be described in the frame of the single gas. Concerning the other phenomena, viz, the mass and heat flux caused by the pressure and temperature gradients, it is possible to offer two approaches to describe a gaseous mixture based on the data obtained for a single gas.

(i) The first approach is that we substitute a gaseous mixture by a single gas having the mean molecular mass. This means if n_i is the number density and m_i is the molecular mass of species i, we consider that the "single" gas has the number density $n=\Sigma_i n_i$ and the molecular mass $m=\Sigma_i n_i m_i/n$. This approach can be justified only in the hydrodynamic regime.

(ii) The second approach is that we consider the flow of every component independently of each other. Applying the single gas theory to every component of the mixture we calculate the mass and heat flux as a sum of the fluxes in these components. This approach is justified only in the free-molecular regime. In the transition regime both approaches give approximate results which can be used for an estimate.

3. Gas Flow Through Long Capillaries

3.1. Remarks

In this section we consider long capillaries so that $L=l/a\gg 1$. What does it mean physically? The pressure and the temperature relax significantly quicker over a cross section than in the capillary as a whole. Thus, we may assume that the pressure and the temperature do not depend upon the diametric coordinates, i.e.,

$$P=P(x), \quad P(-l/2)=P_{\mathrm{I}}, \quad P(l/2)=P_{\mathrm{II}}, \quad (3.1)$$

$$T=T(x), \quad T(-l/2)=T_{\mathrm{I}}, \quad T(l/2)=T_{\mathrm{II}}. \quad (3.2)$$

The coordinates (x,y,z) are given in Fig. 1. Near the capillary ends this assumption may be violated, but for the long capillaries the influence of the end effect can be neglected.

Since the thermal conductivity of the capillary walls is significantly larger than the thermal conductivity of gases, the temperature distribution $T(x)$ is determined by the thermal properties of the capillary and must be given without a solution to the kinetic equation. The pressure distribution $P(x)$ is not known *a priori*, but must be found as a solution of the kinetic equation.

For further derivations we will use the following dimensionless coordinates

$$\tilde{x}=x/a, \quad \tilde{y}=y/a, \quad \tilde{z}=z/a. \quad (3.3)$$

Let us consider a cross section $\tilde{x}=\tilde{x}_*$ of the capillary being far away from the capillary ends. The pressure and the temperature near this cross section ($|\tilde{x}-\tilde{x}_*|\sim 1$) can be presented as

$$P(\tilde{x})=P(\tilde{x}_*)+\left.\frac{dP}{d\tilde{x}}\right|_{\tilde{x}=\tilde{x}_*}(\tilde{x}-\tilde{x}_*)+\frac{1}{2}\left.\frac{d^2P}{d\tilde{x}^2}\right|_{\tilde{x}=\tilde{x}_*}(\tilde{x}'-\tilde{x}_*)^2, \quad (3.4)$$

$$T(\tilde{x})=T(\tilde{x}_*)+\left.\frac{dT}{d\tilde{x}}\right|_{\tilde{x}=\tilde{x}_*}(\tilde{x}-\tilde{x}_*)+\frac{1}{2}\left.\frac{d^2T}{d\tilde{x}^2}\right|_{\tilde{x}=\tilde{x}_*}(\tilde{x}'-\tilde{x}_*)^2, \quad (3.5)$$

where $|\tilde{x}'-\tilde{x}_*|<|\tilde{x}-\tilde{x}_*|$. The estimation of the derivations shows that

$$\frac{1}{P}\frac{dP}{d\tilde{x}}\sim\frac{P_{\mathrm{II}}-P_{\mathrm{I}}}{P_{\mathrm{av}}L}=O\left(\frac{1}{L}\right), \quad \frac{1}{T}\frac{dT}{d\tilde{x}}\sim\frac{T_{\mathrm{II}}-T_{\mathrm{I}}}{T_{\mathrm{av}}L}=O\left(\frac{1}{L}\right), \quad (3.6)$$

$$\frac{1}{P}\frac{d^2P}{d\tilde{x}^2}\sim\frac{P_{\mathrm{II}}-P_{\mathrm{I}}}{P_{\mathrm{av}}L^2}=O\left(\frac{1}{L^2}\right), \quad \frac{1}{T}\frac{d^2T}{d\tilde{x}^2}\sim\frac{T_{\mathrm{II}}-T_{\mathrm{I}}}{T_{\mathrm{av}}L^2}=O\left(\frac{1}{L^2}\right), \quad (3.7)$$

where

$$P_{\mathrm{av}}=\frac{P_{\mathrm{I}}+P_{\mathrm{II}}}{2}, \quad T_{\mathrm{av}}=\frac{T_{\mathrm{I}}+T_{\mathrm{II}}}{2}. \quad (3.8)$$

Since $L\gg 1$, the first derivatives are small. The second derivatives have the second order of the smallness and can be omitted in (3.4) and (3.5). Finally we have

$$P(\tilde{x})=P_*[1+\xi_{\mathrm{P}}(\tilde{x}-\tilde{x}_*)],$$
$$T(\tilde{x})=T_*[1+\xi_{\mathrm{T}}(\tilde{x}-\tilde{x}_*)], \quad (3.9)$$

where $P_*=P(\tilde{x}_*)$, $T_*=T(\tilde{x}_*)$, and

$$\xi_{\mathrm{P}}=\frac{1}{P_*}\left.\frac{dP}{d\tilde{x}}\right|_{\tilde{x}=\tilde{x}_*}, \quad \xi_{\mathrm{T}}=\frac{1}{T_*}\left.\frac{dT}{dx}\right|_{\tilde{x}=\tilde{x}_*}. \quad (3.10)$$

Thus, we may conclude that: (i) near a given section $\tilde{x}_*$ on a distance of the order of the capillary diameter a, the pres-

sure P, and the temperature T linearly depend on $\tilde{x}$; (ii) the gradients of the pressure ξ_P and of the temperature ξ_T are small, i.e., $|\xi_P| \ll 1$ and $|\xi_T| \ll 1$.

Equations (3.9) have been obtained without any assumption on the pressure and temperature drops. Even with large drops, the representation (3.9) remains valid. Such representation of the pressure and temperature distributions allows us to split the solution of the problem into two stages. In the first stage we will find the flow rate through the section $\tilde{x}=\tilde{x}_*$ as a function of P_* and T_* assuming the gradients ξ_P and ξ_T to be small and constant. In the second stage considering a variation of ξ_P and ξ_T along the capillary on a distance of the order of the capillary length we will calculate the mass flow rate and the heat flux through the capillary as a function of the pressures P_I, P_{II} and the temperatures T_I, T_{II} on the capillary ends.

3.2. Input Equations

Let us introduce the dimensionless molecular velocity, bulk velocities and heat flow vector as

$$\mathbf{c}=\beta_* \mathbf{v}, \quad \tilde{\mathbf{u}}=\beta_* \mathbf{u}, \quad \tilde{\mathbf{q}}=\frac{\beta_*}{P_*}\mathbf{q}, \tag{3.11}$$

respectively. Here

$$\beta_*=\left(\frac{m}{2k_B T_*}\right)^{1/2}. \tag{3.12}$$

Since in the first stage we assume the pressure and the temperature gradients to be small and constant, we may linearize the kinetic equation with respect to the gradients ξ_P and ξ_T. Let us perform the linearization near the local Maxwellian $f^M_{loc}(n,T,0)$ defined by (2.30), where $n(\tilde{x})=P(\tilde{x})/k_B T(\tilde{x})$. The pressure $P(\tilde{x})$ and the temperature $T(\tilde{x})$ are determined by (3.9). So, introducing the perturbation function h as (2.62), where h does not depend on the x coordinate, we reduce Eq. (2.63) as follows:

$$\hat{\tilde{D}}h-\hat{\tilde{L}}h=-c_x\,\xi_P-c_x\left(c^2-\tfrac{5}{2}\right)\xi_T, \tag{3.13}$$

$$\hat{\tilde{D}}=a\beta_*\,\hat{D}, \quad \hat{\tilde{L}}=a\beta_*\hat{L}, \tag{3.14}$$

where $\hat{D}$ is defined by (2.54) and $\hat{L}$ is defined by (2.55). The derivative with respect to the time has been omitted, because we consider a steady flow. Since h does not depend on the x coordinate, the reduced differential operator $\hat{\tilde{D}}$ has the form

$$\hat{\tilde{D}}h=c_y\frac{\partial h}{\partial \tilde{y}}, \quad \hat{\tilde{D}}h=c_y\frac{\partial h}{\partial \tilde{y}}+c_z\frac{\partial h}{\partial \tilde{z}} \tag{3.15}$$

for the channel and tube, respectively.

If one applies the BGK model (2.45), the reduced collision operator $\hat{\tilde{L}}$ takes the form

$$\hat{\tilde{L}}_{BGK}h=\tilde{\nu}_{BGK}(2c_x\tilde{u}_x-h), \quad \tilde{\nu}_{BGK}=a\beta_*\nu, \tag{3.16}$$

where $\tilde{\nu}_{BGK}$ is the dimensionless collision frequency for this model. If one applies the S model (2.68), the reduced collision operator $\hat{\tilde{L}}$ has the following form:

$$\hat{\tilde{L}}_S h=\tilde{\nu}_S\left[2c_x\,\tilde{u}_x+\frac{4}{15}\,\tilde{q}_x c_x\left(c^2-\frac{5}{2}\right)-h\right],$$

$$\tilde{\nu}_S=a\beta_*\frac{P_*}{\mu(T_*)}, \tag{3.17}$$

where $\tilde{\nu}_S$ is the dimensionless collision frequency for the S model. Here we have regarded that the bulk velocity and the heat flow vector have the longitudinal component only expressed via the perturbation function as

$$\tilde{u}_x=\frac{1}{\pi^{3/2}}\int \exp(-c^2)c_x h\,dc, \tag{3.18}$$

$$\tilde{q}_x=\frac{1}{\pi^{3/2}}\int \exp(-c^2)c_x\left(c^2-\frac{5}{2}\right)h\,dc. \tag{3.19}$$

As has been indicated in Sec. 2.5.1. the BGK model admits several ways to choose the collision frequency ν. Therefore, the expression of the dimensionless collision frequency $\tilde{\nu}_{BGK}$ depends on the choice of ν. The most preferable choice is Eq. (2.46), because it provides the correct description of the mass flow rate caused by the pressure gradient in the hydrodynamic regime. So, using (2.46) with (2.11), (2.41), (2.42) and (3.12) we have

$$\tilde{\nu}_{BGK}=\frac{\sqrt{\pi}}{2}\frac{a}{\lambda_*}=\delta, \tag{3.20}$$

where λ_* is the mean free path at the pressure P_* and the temperature T_*. Here, the definition of δ (2.2) has been used.

So, the choice of the collision frequency (2.46) leads to the equality between $\tilde{\nu}_{BGK}$ and the rarefaction parameter δ. The other expressions of ν, i.e., (2.47) and (2.48), lead to other relations between $\tilde{\nu}_{BGK}$ and δ, which we will use only in specific cases. So, presenting the results based on the BGK model we will imply the relation (3.20) if the other relations are not mentioned.

For the S model there is the unique relation between the dimensionless frequency $\tilde{\nu}_S$ and the rarefaction parameter δ. One can easily verify that they are equal to each other

$$\tilde{\nu}_S=\delta. \tag{3.21}$$

Since Equation (3.13) is linear, its solution h can be decomposed as

$$h=h_P\xi_P+h_T\xi_T. \tag{3.22}$$

From (3.18) and (3.19) one can see that the bulk velocity $\tilde{u}_x$ and heat flow vector $\tilde{q}_x$ are decomposed to

$$\tilde{u}_x=\tilde{u}_{xP}\xi_P+\tilde{u}_{xT}\xi_T, \quad \tilde{q}_x=\tilde{q}_{xP}\xi_P+\tilde{q}_{xT}\xi_T. \tag{3.23}$$

Substituting (3.22) into (3.13) and considering that the gradients ξ_P and ξ_T are independent, we obtain two independent equations

$$\hat{D}h_P-\hat{L}h_P=-c_x, \quad \hat{D}h_T-\hat{L}h_T=-c_x(c^2-\tfrac{5}{2}). \tag{3.24}$$

The first of them describes the gas flow caused only by the pressure gradient and the second one describes the flow caused only by the temperature gradient.

Let us introduce the reduced flow rate and the reduced heat flux as:

for channel

$$G_*^{ch}=\frac{\dot{M}^{ch}}{aP_*\beta_*}=2\int_{-1/2}^{1/2}\tilde{u}_x d\tilde{y},$$

$$Q_*^{ch}=\frac{2\beta_*\dot{E}^{ch}}{aP_*}=2\int_{-1/2}^{1/2}\tilde{q}_x d\tilde{y}, \tag{3.25}$$

for tube

$$G_*^{tb}=\frac{\dot{M}^{tb}}{\pi a^2P_*\beta_*}=4\int_0^1\tilde{u}_x\tilde{r}_\perp d\tilde{r}_\perp,$$

$$Q_*^{tb}=\frac{2\beta_*\dot{E}^{tb}}{\pi a^2P_*}=4\int_0^1\tilde{q}_x\tilde{r}_\perp d\tilde{r}_\perp, \tag{3.26}$$

where $\tilde{r}_\perp=\sqrt{\tilde{y}^2+\tilde{z}^2}$. If we introduce the following notations:

for channel

$$G_{*P}^{ch}=-2\int_{-1/2}^{1/2}\tilde{u}_{xP}d\tilde{y}, \quad G_{*T}^{ch}=2\int_{-1/2}^{1/2}\tilde{u}_{xT}d\tilde{y}, \tag{3.27}$$

$$Q_{*P}^{ch}=2\int_{-1/2}^{1/2}\tilde{q}_{xP}d\tilde{y}, \quad Q_{*T}^{ch}=-2\int_{-1/2}^{1/2}\tilde{q}_{xT}d\tilde{y}, \tag{3.28}$$

for tube

$$G_{*P}^{tb}=-4\int_0^1\tilde{u}_{xP}\tilde{r}_\perp d\tilde{r}_\perp, \quad G_{*T}^{tb}=4\int_0^1\tilde{u}_{xT}\tilde{r}_\perp d\tilde{r}_\perp, \tag{3.29}$$

$$Q_{*P}^{tb}=4\int_0^1\tilde{q}_{xP}\tilde{r}_\perp d\tilde{r}_\perp, \quad Q_{*T}^{tb}=-4\int_0^1\tilde{q}_{xT}\tilde{r}_\perp d\tilde{r}_\perp, \tag{3.30}$$

with the help of (3.23), (3.25) and (3.26) we obtain[a]

$$G_*=-G_{*P}\xi_P+G_{*T}\xi_T, \quad Q_*=Q_{*P}\xi_P-Q_{*T}\xi_T. \tag{3.31}$$

Thus, G_{*P}, G_{*T}, Q_{*P}, Q_{*T} are the dimensionless coefficients of proportionality between the flow rate/the heat flux in the capillary section $\tilde{x}=\tilde{x}_*$ and the *local* gradients of the pressure ξ_P and temperature ξ_T. They are introduced so as to be always positive.

The introduced coefficients are related with the thermodynamic fluxes (2.82) and (2.83) as:

for channel

$$J_P=-\frac{an_*}{2\beta_*}G_*^{ch}, \quad J_T=-\frac{an_*}{2\beta_*}Q_*^{ch}, \tag{3.32}$$

for tube

$$J_P=-\frac{\pi a^2n_*}{2\beta_*}G_*^{tb}, \quad J_T=-\frac{\pi a^2n_*}{\beta_*}Q_*^{tb}. \tag{3.33}$$

In the expressions of J_T the second term must be omitted because in a long capillary there is no gas–surface heat exchange. The kinetic coefficients take the form

$$\Lambda_{PP}=AG_{*P}, \quad \Lambda_{PT}=-AG_{*T}, \quad \Lambda_{TP}=-AQ_{*P},$$
$$\Lambda_{TT}=AQ_{*T}, \tag{3.34}$$

where

$$A^{ch}=\frac{an_*}{2\beta_*}, \quad A^{tb}=\frac{\pi a^2n_*}{2\beta_*}, \tag{3.35}$$

for channel and tube, respectively. Based on these relations, we may use the same terminology that was introduced for the kinetic coefficients Λ_{nk} in Sec. 2.10, i.e., G_{*P} is the Poiseuille flow, G_{*T} is the thermal creep, Q_{*P} is the mechanocaloric heat flux, and Q_{*T} is the ordinary heat flux.

From Onsager 's relation (2.79) and the relations (3.34) we have

$$G_{*T}=Q_{*P}. \tag{3.36}$$

This relation is very useful. Since G_{*T} and Q_{*P} are calculated from the two independent equations (3.24), the relation (3.36) serves as an additional criterion of the numerical precision. On the other hand, if one is going to calculate only the flow rate, i.e., only the coefficients G_{*P} and G_{*T}, one does not need to solve the second equation (3.24); computing Q_{*P} from the first equation (3.24) one immediately gets G_{*T} from (3.36).

Below, the flow rates G_{*P}, G_{*T} and the heat fluxes Q_{*P}, Q_{*T} will be presented here as a function of the rarefaction parameter δ. Note that δ without a subscript is referred to the *local* pressure P_* and the *local* temperature T_*. With the help of (2.2) and (2.3) the rarefaction parameter δ is related to P_* and T_* as

$$\delta=\frac{\sqrt{\pi}}{2}\frac{a}{\lambda_*}=\frac{aP_*}{\mu(T_*)}\left(\frac{m}{2k_BT_*}\right)^{1/2}. \tag{3.37}$$

Here, it should be noted that to relate the parameter δ with the pressure P_* and temperature T_* we have to indicate the type of gas, because the relation (3.37) contains two specific characteristics of gas: the molecular mass m and the viscosity μ. But representing the dimensionless flow rates G_{*P}, G_{*T}, Q_{*P}, Q_{*T} as a function of the rarefaction parameter δ,

[a]If the superscripts ch and tb are omitted the corresponding expression is valid for both channel and tube.

it is not necessary to specify the gas. These coefficients have been introduced so as their relations with the parameter δ do not contain any specific characteristic of gas.

3.3. Application of the Integro-Moment Method

In general form the integro-moments method is described in Sec. 2.12.3. Since this method is most applicable to the one-dimensional rarefied gas flows, below the integral equations for this case will be written down.

3.3.1. Channel Flow

From the BGK model we have two independent equations for the channel flow

$$\tilde{u}_{xm}(\tilde{y})=\int_{-1/2}^{1/2}\mathscr{K}_{11}(\tilde{y},\tilde{y}')\tilde{u}_{xm}(\tilde{y}')\mathrm{d}\tilde{y}'+\mathscr{S}_{1m}(\tilde{y}),\qquad m=\mathrm{P,T}. \tag{3.38}$$

The heat flow vector is calculated via the bulk velocity

$$\tilde{q}_{xm}(\tilde{y})=\int_{-1/2}^{1/2}\mathscr{K}_{21}(\tilde{y},\tilde{y}')\tilde{u}_{xm}(\tilde{y}')\mathrm{d}\tilde{y}'+\mathscr{S}_{2m}(\tilde{y}),\qquad m=\mathrm{P,T}. \tag{3.39}$$

From the S model we have two independent systems of simultaneous equations:

$$\begin{pmatrix}\tilde{u}_{xm}(\tilde{y})\\ \tilde{q}_{xm}(\tilde{y})\end{pmatrix}=\int_{-1/2}^{1/2}\begin{pmatrix}\mathscr{K}_{11}(\tilde{y},\tilde{y}') & \mathscr{K}_{12}(\tilde{y},\tilde{y}')\\ \mathscr{K}_{21}(\tilde{y},\tilde{y}') & \mathscr{K}_{22}(\tilde{y},\tilde{y}')\end{pmatrix}\times\begin{pmatrix}\tilde{u}_{xm}(\tilde{y}')\\ \tilde{q}_{xm}(\tilde{y}')\end{pmatrix}\mathrm{d}\tilde{y}'+\begin{pmatrix}\mathscr{S}_{1m}(\tilde{y})\\ \mathscr{S}_{2m}(\tilde{y})\end{pmatrix},\quad m=\mathrm{P,T}. \tag{3.40}$$

The derivation of such types of equations can be found in the literature.[22,28,47,155,166]

In the case of the diffuse (2.22) scattering the kernels $\mathscr{K}_{ij}$ and the free terms $\mathscr{S}_{im}$ have the following form:

$$\mathscr{K}_{11}=\frac{\delta}{\sqrt{\pi}}I_{-1},\quad \mathscr{K}_{21}=\frac{\delta}{\sqrt{\pi}}\left(I_1-\frac{1}{2}I_{-1}\right),$$
$$\mathscr{K}_{12}=\frac{2}{15}\mathscr{K}_{21},\quad \mathscr{K}_{22}=\frac{2\delta}{15\sqrt{\pi}}\left(I_3-I_1+\frac{9}{4}I_{-1}\right), \tag{3.41}$$
$$\mathscr{S}_{1\mathrm{P}}=-\frac{1}{2\delta}\int_{-1/2}^{1/2}\mathscr{K}_{11}\mathrm{d}\tilde{y}',\quad \mathscr{S}_{2\mathrm{P}}=-\frac{1}{2\delta}\int_{-1/2}^{1/2}\mathscr{K}_{21}\mathrm{d}\tilde{y}',$$
$$\mathscr{S}_{1\mathrm{T}}=\mathscr{S}_{2\mathrm{P}},\quad \mathscr{S}_{2\mathrm{T}}=-\frac{15}{4\delta}\int_{-1/2}^{1/2}\mathscr{K}_{22}\mathrm{d}\tilde{y}'.$$

Here, I_n are the special transcendental functions defined as

$$I_n=I_n(t)=\int_0^\infty c^n\exp\left(-c^2-\frac{t}{c}\right)\mathrm{d}c. \tag{3.42}$$

In (3.41) the argument t is $(\delta|\tilde{y}-\tilde{y}'|)$.

For the diffuse-specular scattering (2.23) the expressions of $\mathscr{K}_{ij}$ and $\mathscr{S}_{im}$ can be found in the literature.[47,91,166]

3.3.2. Tube Flow

From the BGK model we have two analogous integral equations for the tube flow

$$\tilde{u}_{xm}(\tilde{\mathbf{r}}_\perp)=\int_{\Sigma_\perp}\mathscr{K}_{11}(\tilde{\mathbf{r}}_\perp,\tilde{\mathbf{r}}_\perp')\tilde{u}_{xm}(\tilde{\mathbf{r}}_\perp')\mathrm{d}\tilde{\mathbf{r}}_\perp'+\mathscr{S}_{1m}(\tilde{\mathbf{r}}_\perp),\qquad m=\mathrm{P,T}, \tag{3.43}$$

where $\tilde{\mathbf{r}}_\perp=(\tilde{y},\tilde{z})$ is the two-dimensional reduced position vector and $\Sigma_\perp$ is the tube cross section. The heat flow vector is calculated as

$$\tilde{q}_{xm}(\tilde{\mathbf{r}}_\perp)=\int_{\Sigma_\perp}\mathscr{K}_{21}(\tilde{\mathbf{r}}_\perp,\tilde{\mathbf{r}}_\perp')\tilde{u}_{xm}(\tilde{\mathbf{r}}_\perp')\mathrm{d}\tilde{\mathbf{r}}_\perp'+\mathscr{S}_{2m}(\tilde{\mathbf{r}}_\perp),\qquad m=\mathrm{P,T}. \tag{3.44}$$

From the S model we have two independent systems of simultaneous equations

$$\begin{pmatrix}\tilde{u}_{xm}(\tilde{\mathbf{r}}_\perp)\\ \tilde{q}_{xm}(\tilde{\mathbf{r}}_\perp)\end{pmatrix}=\int_{\Sigma_\perp}\begin{pmatrix}\mathscr{K}_{11}(\tilde{\mathbf{r}}_\perp,\tilde{\mathbf{r}}_\perp') & \mathscr{K}_{12}(\tilde{\mathbf{r}}_\perp,\tilde{\mathbf{r}}_\perp')\\ \mathscr{K}_{21}(\tilde{\mathbf{r}}_\perp,\tilde{\mathbf{r}}_\perp') & \mathscr{K}_{22}(\tilde{\mathbf{r}}_\perp,\tilde{\mathbf{r}}_\perp')\end{pmatrix}\times\begin{pmatrix}\tilde{u}_{xm}(\tilde{\mathbf{r}}_\perp')\\ \tilde{q}_{xm}(\tilde{\mathbf{r}}_\perp')\end{pmatrix}\mathrm{d}\tilde{\mathbf{r}}_\perp'+\begin{pmatrix}\mathscr{S}_{1m}(\tilde{\mathbf{r}}_\perp)\\ \mathscr{S}_{2m}(\tilde{\mathbf{r}}_\perp)\end{pmatrix},\quad m=\mathrm{P,T}. \tag{3.45}$$

The derivation of such types of equations can be found in the literature.[35,45,154,151]

In the case of the diffuse scattering (2.22) the kernels $\mathscr{K}_{ij}$ and the free terms $\mathscr{S}_{im}$ take the following form:

$$\mathscr{K}_{11}=\frac{\delta}{\pi|\tilde{\mathbf{r}}_\perp-\tilde{\mathbf{r}}_\perp'|}I_0,\quad \mathscr{K}_{21}=\frac{\delta}{\pi|\tilde{\mathbf{r}}_\perp-\tilde{\mathbf{r}}_\perp'|}(I_2-I_0),$$
$$\mathscr{K}_{12}=\frac{2}{15}\mathscr{K}_{21},\quad \mathscr{K}_{22}=\frac{2\delta}{15\pi|\tilde{\mathbf{r}}_\perp-\tilde{\mathbf{r}}_\perp'|}\left(I_4-2I_2+\frac{5}{2}I_0\right), \tag{3.46}$$
$$\mathscr{S}_{1\mathrm{P}}=-\frac{1}{2\delta}\int_{\Sigma_\perp}\mathscr{K}_{11}\mathrm{d}\tilde{\mathbf{r}}_\perp',\quad \mathscr{S}_{2\mathrm{P}}=-\frac{1}{2\delta}\int_{\Sigma_\perp}\mathscr{K}_{21}\mathrm{d}\tilde{\mathbf{r}}_\perp',$$
$$\mathscr{S}_{1\mathrm{T}}=\mathscr{S}_{2\mathrm{P}},\quad \mathscr{S}_{2\mathrm{T}}=-\frac{15}{4\delta}\int_{\Sigma_\perp}\mathscr{K}_{22}\mathrm{d}\tilde{\mathbf{r}}_\perp'.$$

Here, the argument t of the special functions I_n is $(\delta|\mathbf{r}_\perp-\mathbf{r}_\perp'|)$.

The expressions of $\mathscr{K}_{ij}$ and $\mathscr{S}_{im}$ for the diffuse-specular scattering (2.23) can be found in the literature.[45,125,154]

3.3.3. Special Functions I_n

Here, some useful properties of the special functions I_n defined by (3.42) will be given [see Abramovitz[1] (p.1001)]. The functions of the different order n are related as

$$\frac{dI_n(t)}{dt} = -I_{n-1}(t), \tag{3.47}$$

$$2I_n(t) = (n-1)I_{n-2}(t) + tI_{n-3}(t). \tag{3.48}$$

The power series representation has the form

$$2I_1(t) = \sum_{k=0}^{\infty} (a_k \ln t + b_k)t^k, \tag{3.49}$$

$$a_k = \frac{-2a_{k-2}}{k(k-1)(k-2)},$$

$$b_k = \frac{-2b_{k-2} - (3k^2 - 6k + 2)a_k}{k(k-1)(k-2)}, \quad k > 2,$$

$$a_0 = a_1 = 0, \quad a_2 = -b_0, \quad b_0 = 1, \quad b_1 = -\sqrt{\pi},$$

$$b_2 = 0.6341754927.$$

The asymptotic representation of $I_n(t)$ at $t \to \infty$ is as follows:

$$I_n(t) \sim \sqrt{\frac{\pi}{3}}\, 3^{-n/2} v^{n/2} \exp(-v) \sum_{k=0}^{\infty} \frac{a_k}{v^k}, \quad v = 3\left(\frac{t}{2}\right)^{2/3}, \tag{3.50}$$

$$a_0 = 1, \quad a_1 = \frac{1}{12}(3n^2 + 3n - 1),$$

$$12(k+2)a_{k+2} = -(12k^2 + 36k - 3n^2 - 3n + 25)a_{k+1} + \frac{1}{2}(n-2k)(2k+3-n)(2k+3+2n)a_k.$$

3.3.4. Trial Functions for the Variational Solution

The above given integral equations can be solved by the direct numerical method or by the variational method described in Sec. 2.12.4. To apply the variational method the following trial functions are usually used:

$$\tilde{u}_{xm} = c_{1m} + c_{2m}\tilde{y}^2, \quad \tilde{u}_{xm} = c_{1m} + c_{2m}\tilde{r}_\perp^2, \quad m = \mathrm{P,T} \tag{3.51}$$

for channel and tube, respectively. The trial function for the heat flow vector is a constant

$$\tilde{q}_{xm} = c_{3m}, \quad m = \mathrm{P,T}. \tag{3.52}$$

Then, according to the method described in Sec. 2.12.4, one obtains from (3.40) or (3.45) (S model) the following algebraic equation systems for the constant c_{1m}, c_{2m} and c_{3m}:

$$\sum_{j=1}^{3} \mathscr{A}_{ij} c_{jm} = \mathscr{B}_{im}, \quad m = \mathrm{P,T}, \tag{3.53}$$

where $\mathscr{A}_{ij}$ is a symmetric matrix. The elements of this matrix and the free terms $\mathscr{B}_{im}$ have the form

for channel

$$\mathscr{A}_{11} = 1 - \int_{-1/2}^{1/2} \mathscr{K}_{11}\, d\tilde{y}'\, d\tilde{y},$$

$$\mathscr{A}_{12} = \frac{1}{12} - \int_{-1/2}^{1/2} \mathscr{K}_{11}\tilde{y}'^2\, d\tilde{y}'\, d\tilde{y},$$

$$\mathscr{A}_{13} = -\int_{-1/2}^{1/2} \mathscr{K}_{12}\, d\tilde{y}'\, d\tilde{y},$$

$$\mathscr{A}_{22} = \frac{1}{80} - \int_{-1/2}^{1/2} \mathscr{K}_{11}\tilde{y}'^2\tilde{y}^2\, d\tilde{y}'\, d\tilde{y},$$

$$\mathscr{A}_{23} = -\int_{-1/2}^{1/2} \mathscr{K}_{12}\tilde{y}^2\, d\tilde{y}'\, d\tilde{y},$$

$$\mathscr{A}_{33} = 1 - \int_{-1/2}^{1/2} \mathscr{K}_{22}\, d\tilde{y}'\, d\tilde{y},$$

$$\mathscr{B}_{1m} = \int_{-1/2}^{1/2} \mathscr{S}_{1m}\, d\tilde{y}, \quad \mathscr{B}_{2m} = \int_{-1/2}^{1/2} \mathscr{S}_{1m}\tilde{y}^2\, d\tilde{y},$$

$$\mathscr{B}_{3m} = \int_{-1/2}^{1/2} \mathscr{S}_{2m}\, d\tilde{y},$$

for tube

$$\mathscr{A}_{11} = 1 - \frac{1}{\pi}\int_{\Sigma_\perp} \mathscr{K}_{11}\, d\tilde{\mathbf{r}}_\perp'\, d\tilde{\mathbf{r}}_\perp,$$

$$\mathscr{A}_{12} = \frac{1}{2} - \frac{1}{\pi}\int_{\Sigma_\perp} \mathscr{K}_{11}\tilde{r}_\perp'^2\, d\tilde{\mathbf{r}}_\perp'\, d\tilde{\mathbf{r}}_\perp,$$

$$\mathscr{A}_{13} = -\frac{1}{\pi}\int_{\Sigma_\perp} \mathscr{K}_{12}\, d\tilde{\mathbf{r}}_\perp'\, d\tilde{\mathbf{r}}_\perp,$$

$$\mathscr{A}_{22} = \frac{1}{3} - \frac{1}{\pi}\int_{\Sigma_\perp} \mathscr{K}_{11}\tilde{r}_\perp'^2\tilde{r}_\perp^2\, d\tilde{\mathbf{r}}_\perp'\, d\tilde{\mathbf{r}}_\perp,$$

$$\mathscr{A}_{23} = -\frac{1}{\pi}\int_{\Sigma_\perp} \mathscr{K}_{12}\tilde{r}_\perp^2\, d\tilde{\mathbf{r}}_\perp'\, d\tilde{\mathbf{r}}_\perp,$$

$$\mathscr{A}_{33} = 1 - \frac{1}{\pi}\int_{\Sigma_\perp} \mathscr{K}_{22}\, d\tilde{\mathbf{r}}_\perp'\, d\tilde{\mathbf{r}}_\perp,$$

$$\mathscr{B}_{1m} = \frac{1}{\pi}\int_{\Sigma_\perp} \mathscr{S}_1\, d\tilde{\mathbf{r}}_\perp, \quad \mathscr{B}_{2m} = \frac{1}{\pi}\int_{\Sigma_\perp} \mathscr{S}_1\tilde{r}_\perp^2\, d\tilde{\mathbf{r}}_\perp,$$

$$\mathscr{B}_{3m} = \frac{1}{\pi}\int_{\Sigma_\perp} \mathscr{S}_2\, d\tilde{\mathbf{r}}_\perp.$$

The coefficients $\mathscr{A}_{ij}$ and $\mathscr{B}_{im}$ can be calculated numerically for any value of the rarefaction parameter δ. Then, resolving the systems (3.53) one knows the bulk velocity (3.51) and the heat flow vector (3.52) and consequently all coefficients defined by (3.27)–(3.30).

3.4. Transition Regime

3.4.1. Plane Poiseuille Flow

Diffuse scattering: Among all types of flows considered in this article the plane Poiseuille flow $G_{*\mathrm{P}}^{\mathrm{ch}}$ under the supposition of the diffuse scattering (2.22) is the most deeply inves-

TABLE 1. Reduced flow rate G^{ch}_{*P} vs δ: diffuse scattering, different methods

	G^{ch}_{*P}							
δ	a	b	c	d	e	f	g	h
0.01	3.0499	3.0489	2.2114	...	...	...	3.0519	...
0.1	2.0328	2.0314	1.9829	1.8818	2.0861	2.0327	2.0397	1.9318
0.2	1.8083	1.8079	1.8167	1.6994	1.8465	...	...	1.7407
0.5	1.6017	1.6017	1.6050	1.5491	1.6166	1.6018	1.6147	1.5607
1.0	1.5379	1.5389	1.5381	1.5116	1.5343	1.5386	1.5541	1.5086
2.0	1.5912	1.5942	1.5950	1.5491	1.5709	1.5948	...	1.5681
4.0	1.8450	1.8440	1.8459	1.7958	1.8075	1.8459	...	...
5.0	1.9895	1.9883	1.9908	1.9634	1.9485	1.9907	2.0080	1.9637
7.0	2.2904	2.2914	2.2945	2.2782	2.2482	2.2949	...	...
10.0	2.7558	2.7638	2.7681	2.7536	2.7790	2.7686	2.7863	2.7350

[a]Cercignani and Daneri (Ref. 28), Eq. (3.38) (BGK), direct numerical method.
[b]Cercignani and Pagani (Ref. 34), Eq. (3.38) (BGK), variational method.
[c]Huang *et al.* (Ref. 66), Eq. (3.13) with (3.16) (BGK), discrete velocity method.
[d]Loyalka and Lang (Ref. 99), BE for Maxwell's molecules, variational method.
[e]Loyalka and Lang (Ref. 99), Model eq. with variable collision frequency, variational method.
[f]Loyalka *et al.* (Ref. 102), Eq. (3.13) with (3.16) (BGK), method of elementary solutions.
[g]Chernyak *et al.* (Ref. 42), Eq. (3.40) (S model), direct numerical method.
[h]Hickey and Loyalka (Ref. 63), Eq. (3.13) with (2.54) (BE), discrete velocity method.

tigated theoretically. The list of papers describing this kind of rarefied gas flow is very long. Some estimations of the flow rate G^{ch}_{*P} can be found in the literature.[22,158,166,178] These works provide only a qualitative behavior of the coefficient G^{ch}_{*P}. Some results obtained on the basis of the BE by the moment method are presented in the literature.[67,78,119,120,153] An analysis of the plane Poiseuille flow based on the method of elementary solutions is given in the literature.[24,38]

Numerical results obtained from the BGK model by various methods can be found in the literature.[17,20,28,34,47,66,68,79,87,91,99,102,147,148] Numerical results based on the S model are presented by Chernyak *et al.*[42] Results based on numerical calculation of the BE are available in the literature.[63,97,116]

Thus, due to the simplicity of this type of flow the coefficient G^{ch}_{*P} was obtained using various kinetic equations and applying almost all methods elaborated in the RGD. Below, an analysis of the above mentioned numerical results is given.

Cercignani and Daneri[28] solved the integral equation (3.38) (BGK) by the direct numerical method. Their results are presented in the second column of Table 1. Then, Cercignani and Pagani[34] (third column) solved the same integral equation by the variational method, which gives a good agreement with the exact numerical solution.[28] Huang *et al.*[66] solved Eq. (3.13) with (3.16) (BGK) by the discrete velocity method. The results are presented in the fourth column of Table 1. One can see that there is good agreement with the previous results in the transition and hydrodynamic regimes. The disagreement at small δ is explained by the numerical grid used by Huang *et al.*[66] which was not sufficiently dense.

Loyalka and Lang[99] solved the BE for Maxwellian molecules (fifth column) and the model equation with the variable collision frequency ν appropriate to the rigid spheres (sixth column) by the variational method. It can be seen that the BE for Maxwellian molecules gives rather understated

TABLE 2. Reduced flow rate G^{ch}_{*P} vs δ by Ohwada *et al.* (Ref. 116): diffuse scattering, BE

δ	G^{ch}_{*P}	δ	G^{ch}_{*P}
0.0393	2.2958	0.785	1.5148
0.0524	2.1816	0.982	1.5066
0.0785	2.0318	1.31	1.5124
0.0982	1.9556	1.96	1.5602
0.131	1.8642	2.62	1.6304
0.196	1.7498	3.93	1.7998
0.262	1.6796	5.24	1.9876
0.393	1.5982	7.85	2.386
0.524	1.5542		

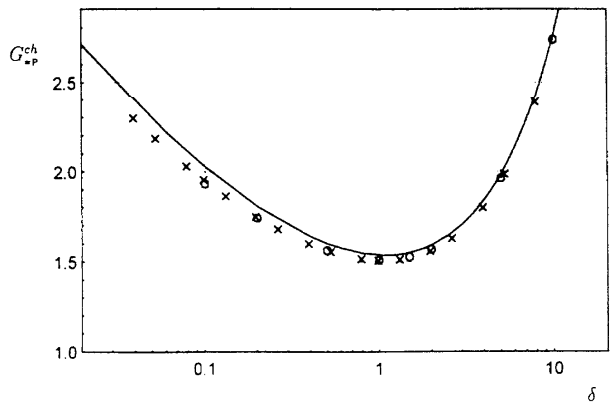

FIG. 5. Reduced flow rate G^{ch}_{*P} vs δ at diffuse scattering: solid line—BGK by Cercignani and Pagani (Ref. 34), crosses—BE by Ohwada *et al.* (Ref. 116), circles—BE by Hickey and Loyalka (Ref. 63).

TABLE 3. Reduced flow rate G^{ch}_{*P} vs δ, complete data by Cercignani & Pagani (Ref. 34): diffuse scattering, BGK

δ	G^{ch}_{*P}	δ	G^{ch}_{*P}
0.01	3.0489	1.5	1.5530
0.02	2.7107	1.6	1.5598
0.03	2.5234	1.7	1.5674
0.04	2.3964	1.8	1.5757
0.05	2.3016	1.9	1.5847
0.06	2.2217	2.0	1.5942
0.07	2.1655	2.5	1.6480
0.08	2.1140	3.0	1.7092
0.09	2.0698	3.5	1.7751
0.1	2.0314	4.0	1.8440
0.2	1.8079	4.5	1.9153
0.3	1.7092	5.0	1.9883
0.4	1.6408	5.5	2.0627
0.5	1.6017	6.0	2.1381
0.6	1.5761	6.5	2.2144
0.7	1.5591	7.0	2.2914
0.8	1.5482	7.5	2.3690
0.9	1.5416	8.0	2.4472
1.0	1.5389	8.5	2.5258
1.1	1.5379	9.0	2.6048
1.2	1.5394	9.5	2.6041
1.3	1.5427	10.0	2.7638
1.4	1.5473	10.5	2.8438

results, while the variable collision frequency model gives fairly good results.

Loyalka *et al.*[102] solved the BGK model by the method of elementary solutions, which gives good agreement with the integro-moment method in the whole range of the rarefaction parameter δ. The results are given in the seventh column of Table 1.

Chernyak *et al.*[42] solved the integral equation (3.40) (S model) by both variational and direct numerical methods. They also obtained a perfect agreement between the two methods. In the eighth column of Table 1 their results based on the direct numerical method are presented. One can see that there is a fine agreement between the solutions based on the BGK equation and that based on the S model.

Hickey and Loyalka[63] (ninth column) solved numerically the BE for rigid spheres. One can see that the disagreement between the model equations (BGK and S model) and the exact BE is within 2%.

Ohwada *et al.*[116] also solved the BE. But they introduced the rarefaction parameter as $\delta = 2a/(\sqrt{\pi}\lambda_*)$. This definition of δ follows from the BGK model with the frequency (2.48). Therefore, the values of δ given by Ohwada *et al.*[116] must be recalculated. Their results are presented separately in Table 2 with the parameter δ recalculated in our notations. A comparison of these results with those obtained by Hickey and Loyalka[63] is performed in Fig. 5. One can see that the two numerical solutions of the BE obtained independently are in a good agreement between themselves. The numerical data by Cercignani and Pagani[34] based on the BGK model are also shown in Fig. 5.

The numerical results based on the BGK model, i.e., Refs. 17, 20, 47, 79, 87, 91, 97, 147, 148, are in a good agreement with the data described above. The results of the paper[68] are erroneous as is pointed out by Loyalka.[89]

Thus, from this analysis we may conclude that the most simple way to calculate the coefficient G^{ch}_{*P} is to apply the variational method based on the trial functions (3.51) to the BGK equation. This method gives reliable results with modest calculation efforts. The complete data on the coefficient G^{ch}_{*P} obtained by Cercignani and Pagani[34] using this method are presented in Table 3.

Diffuse-specular scattering: The first results for the diffuse-specular scattering (2.23) were obtained by Chernyak *et al.*[47] based on Eq. (3.38) (BGK) solved by the variational method. Then, Loyalka[91] solved the same equation by the direct numerical method. In the paper by Loyalka *et al.*[102] the numerical solution of the BGK equation by the method of elementary solutions is given. To perform a comparison between these results all of them are presented in Table 4. One can see that the variational results by Chernyak *et al.*[47] differ from the exact results by Loyalka.[91,102] At the same time, the results of the works[91,102] obtained by the two quite different methods are in good agreement between them. So, we conclude that the results by Loyalka[91] are reliable. His complete data are given in Table 5.

Loyalka and Hickey[97] solved the BE by the discrete velocity method. Their results are given in Table 5. Unfortunately, it is impossible to compare the solution based on the BGK model[91] with the BE solution,[97] because they were obtained for different values of the gas–surface interaction parameter α.

TABLE 4. Reduced flow rate G^{ch}_{*P} vs δ and α: different methods

	G^{ch}_{*P}					
	$\alpha = 0.88$			$\alpha = 0.80$		
δ	a	b	c	a	b	c
0.05	2.6456	2.7383	2.7383	2.9206	3.0897	3.0897
0.1	2.3261	2.4060	2.4060	2.5605	2.7077	2.7077
1.0	1.7348	1.7921	1.7920	1.8914	2.0019	2.0018
10.0	2.9529	3.0241	3.0177	3.0836	3.2305	3.2241

[a]Chernyak *et al.* (Ref. 47), Eq. (3.38) (BGK), variational method.
[b]Loyalka (Ref. 91), Eq. (3.38) (BGK), direct numerical method.
[c]Loyalka *et al.* (Ref. 102), Eq. (3.13) with (3.16) (BGK), method of elementary solutions.

TABLE 5. Reduced flow rate G^{ch}_{*P} vs δ and α, complete data

	G^{ch}_{*P}						
	Loyalka (Ref. 91)[a]					Loyalka and Hickey (Ref. 97)[b]	
δ	$\alpha=0.96$	$\alpha=0.92$	$\alpha=0.88$	$\alpha=0.84$	$\alpha=0.80$	$\alpha=0.75$	$\alpha=0.50$
0.001	4.5646	4.8773	5.2149	5.5808	5.9788	...	...
0.01	3.2417	3.2417	3.6697	3.9095	4.1695	...	...
0.02	2.8770	3.0548	3.2463	3.4530	3.6771	...	...
0.03	2.6755	3.0381	3.0131	3.2021	3.4070	...	...
0.04	2.5390	2.6915	2.8556	3.0328	3.2249	...	...
0.05	2.4373	2.5823	2.7383	2.9069	3.0897	...	...
0.07	2.2916	2.4259	2.5706	2.7270	2.8967	...	...
0.09	2.1893	2.3163	2.4532	2.6011	2.7618	...	...
0.1	2.1482	2.2723	2.4060	2.5507	2.7077	2.7860	4.3628
0.25	...	...	...	...	...	2.4065	3.7697
0.3	1.7945	1.8937	2.0011	2.1176	2.2448	...	...
0.5	1.6863	1.7776	1.8766	1.9844	2.1023	2.2128	3.4748
0.7	1.6398	1.7272	1.8220	1.9254	2.0388	...	...
0.75	...	...	...	...	...	2.1449	3.3694
0.8	1.6202	1.7052	1.7976	1.8986	2.0092	...	...
0.9	...	...	...	...	...	2.1269	3.3392
1.0	1.6163	1.7005	1.7921	1.8921	2.0019	2.1204	3.3270
1.1	...	...	...	...	...	2.1171	3.3192
1.2	...	...	...	...	...	2.1164	3.3149
1.25	1.6174	1.7001	1.7902	1.8887	1.9969	...	...
1.3	...	...	...	...	...	2.1178	3.3136
1.4	...	...	...	...	...	2.1209	3.3144
1.5	1.6289	1.7107	1.7999	1.8974	2.0046	2.1254	3.3171
2.0	1.6694	1.7503	1.8386	1.9352	2.0414	2.1625	3.3491
2.5	1.7233	1.8039	1.8918	1.9881	2.0939	...	...
3.0	1.7847	1.8653	1.9531	2.0493	2.1551	2.2748	3.4618
3.5	1.8510	1.9316	2.0196	2.1158	2.2217	...	...
4.0	1.9205	2.0013	2.0894	2.1858	2.2918	...	...
5.0	2.0661	2.1472	2.2356	2.3324	2.4388	2.5555	3.7496
6.0	2.2173	2.2988	2.3876	2.4848	2.5916	...	...
7.0	2.3722	2.4541	2.5433	2.6408	2.7480	2.8625	4.0633
9.0	2.6807	2.7722	2.8620	2.9601	3.0679	...	...
10.0	2.8512	2.9340	3.0241	3.1225	3.2305	3.3407	4.5490

[a]Equation (3.38), (BGK), direct numerical method.
[b]Equation (3.13) with (2.54) (BE), discrete velocity method.

3.4.2. Cylindrical Poiseuille Flow

Diffuse scattering: Some analytical results on the coefficient G^{tb}_{*P} for the diffuse scattering (2.22) can be found in Refs. 56, 151, 157, 176, which are restricted by the small range of the rarefaction parameter. These results will not be considered here. Let us analyze the results obtained for the entire range of δ.

TABLE 6. Reduced flow rate G^{tb}_{*P} vs δ: diffuse scattering, different methods

	G^{tb}_{*P}				
δ	a	b	c	d	e
0.01	1.4768	1.4801	1.4763	1.4800	1.4681
0.1	1.4043	1.4039	1.4039	1.4101	1.3984
1.0	1.4594	1.4576	1.4582	1.4758	1.4499
10.0	3.5821	3.5573	3.5633	3.5749	3.5608

[a]Cercignani and Sernagiotto (Ref. 35), Eq. (3.43) (BGK), direct numerical method.
[b]Cercignani and Pagani (Ref. 33), Eq. (3.43) (BGK), variational method.
[c]Lo and Loyalka (Ref. 79), Eq. (3.43) (BGK), optimized numerical method.
[d]Sharipov (Ref. 141), Eq. (3.13) with (3.17) (S model), discrete velocity method.
[e]Loyalka and Hamoodi (Ref. 95), (3.13) with (2.54) (BE), discrete velocity method.

To calculate G^{tb}_{*P} Cercignani and Sernagiotto[35] solved the integral equation (3.43) (BGK) by direct numerical methods. Their results are presented in the second column of Table 6. Then, Cercignani and Pagani[33] (third column) resolved the same integral equation by the variational method, which gives good agreement with the exact solution. Lo and Loyalka[79] (fourth column) also solved this integral equation by the optimized numerical method with great precision. These results can be considered as a most exact numerical solution of the BGK model. Sharipov[141] (fifth column) solved the S model, i.e., Eq. (3.13) with (3.17), by the discrete velocity method. Loyalka and Hamoodi[95] (sixth column) numerically solved the BE for a rigid sphere gas.

From Table 6 one can see that there is good agreement between the results based on the BGK model and those obtained from the S model. The disagreement between the

TABLE 7. Reduced flow rate G^{tb}_{*P} vs δ, complete data: diffuse scattering

	G^{tb}_{*P}				G^{tb}_{*P}		
δ	a	b	c	δ	a	b	c
0.0	1.5045	1.5045	...	1.5	...	...	1.5512
0.0001	1.5026	...	...	1.6	1.5753	1.5956	...
0.001	...	...	1.4845	1.8	1.6171	1.6373	...
0.002	1.4962	...	...	2.0	1.6608	1.6799	1.6573
0.004	1.4902	...	...	3.0	1.8850	1.9014	1.8795
0.006	1.4852	...	...	4.0	2.1188	2.1315	...
0.008	1.4808	...	...	5.0	2.3578	2.3666	2.3472
0.01	1.4768	1.4800	1.4704	6.0	2.5999	2.6049	...
0.02	1.4608	1.4636	...	7.0	2.8440	2.8455	2.8282
0.04	1.4391	1.4418	...	8.0	3.0894	3.0878	...
0.08	1.4131	1.4168	...	9.0	3.3355	3.3314	...
0.1	1.4043	1.4101	1.4039	10.0	3.5821	3.5749	3.5623
0.2	1.3820	1.3911	1.3812	20.0	6.0411	6.0492	...
0.3	1.3767	1.3876	1.3756	30.0	8.5333	8.5392	...
0.4	1.3796	1.3920	1.3782	40.0	11.0295	11.036	...
0.5	...	...	1.3857	50.0	13.5269	13.459	...
0.6	1.3982	1.4130	1.3963	60.0	16.0254	...	...
0.8	1.4261	1.4425	1.4238	70.0	18.5244	...	...
1.0	1.4594	1.4758	1.4567	80.0	21.0234	...	...
1.2	1.4959	1.5158	...	90.0	23.5219	...	...
1.4	1.5348	1.5550	...	100.0	26.0214	...	...

[a]Cercignani and Sernagiotto (Ref. 35) and Lo and Loyalka (Ref. 79), BGK.
[b]Sharipov (Ref. 141), S model.
[c]Loyalka and Hamoodi (Ref. 95), BE.

model equation solutions and that obtained from the BE is within 2%, which can be considered reasonable.

The numerical data on the coefficient G^{tb}_{*P} can be also found in Refs. 46, 81, 84, 91, 104, 123, 125, 160. All these results are in good agreement with the exact solution by Lo and Loyalka.[79]

The complete data on the coefficient G^{tb}_{*P} based on the BGK equation, S model and BE are presented in Table 7.

Diffuse-specular scattering: Numerical data on the coefficient G^{tb}_{*P} based on the BGK model with the diffuse-specular scattering (2.23) are available in Refs. 81, 91, 123 [direct numerical solution of Eq. (3.43)] and in Refs. 124, 125 [variational solution of Eq. (3.43)]. The numerical solution obtained from the S model by the discrete velocity method is given by Sharipov.[141] A comparison between these results is performed in Table 8. The results by Porodnov *et al.*[125] are not presented because they are very close to the results of the paper.[124]

From Table 8 one can see that: (i) the results by Loyalka[91] are erroneous, since they do not coincide with all the rest of the data, even with the data obtained later by himself with collaborators;[81] (ii) there is good agreement between the different methods of solution and between the different model equations. At $\delta = 10$ the disagreement between the variational and exact methods is about 2%. But for large δ the variational method gives a sufficiently high precision. Moreover, the solution of the S model[141] obtained with great precision gave good agreement with the variational solution. Thus, we may conclude that the variational solution of the BGK model by Porodnov *et al.*[124,125] and the discrete veloc-

TABLE 8. Reduced flow rate G^{tb}_{*P} vs δ and α: different methods

	G^{tb}_{*P}								
	$\alpha = 0.8$					$\alpha = 0.6$			
δ	a	b	c	d	e	b	c	d	e
0.01	2.1662	2.187	2.187	2.1827	2.1853	3.374	3.374	3.3381	3.3374
0.1	1.9211	1.993	1.992	1.9988	2.0043	2.944	2.950	2.9542	2.9597
1.0	1.6531	1.930	1.937	1.9363	1.9514	2.706	2.689	2.7215	2.7277
10.0	3.5823	4.025	4.092	4.1021	4.0343	4.785	4.878	4.9487	4.7703

[a]Loyalka (Ref. 91), Eq. (3.43) (BGK), direct numerical method.
[b]Porodnov and Tukhvetov (Ref. 124), Eq. (3.43) (BGK), variational method.
[c]Porodnov and Tukhvetov (Ref. 123), Eq. (3.43) (BGK), direct numerical method.
[d]Lo *et al.* (Ref. 81), Eq. (3.43) (BGK), direct numerical method.
[e]Sharipov (Ref. 141), Eq. (3.13) with (3.17) (S model), discrete velocity method.

TABLE 9. Reduced flow rate G^{tb}_{*P} vs δ and α by Porodnov *et al.* (Refs. 124 and 125): BGK

	G^{tb}_{*P}					
δ	$\alpha=0.98$	$\alpha=0.94$	$\alpha=0.90$	$\alpha=0.84$	$\alpha=0.80$	$\alpha=0.6$
0.01	1.534	1.657	1.791	2.026	2.187	3.374
0.02	1.516	1.635	1.764	1.983	2.144	3.255
0.04	1.492	1.605	1.728	1.933	2.085	3.137
0.06	1.475	1.585	1.703	1.899	2.045	3.044
0.08	1.462	1.569	1.685	1.873	2.014	...
0.1	1.452	1.556	1.668	1.853	1.992	2.944
0.2	1.426	1.523	1.627	1.806	1.931	...
0.4	1.420	1.510	1.615	1.768	1.888	2.720
0.6	1.437	1.523	1.621	1.772	1.888	2.691
0.8	1.464	1.547	1.638	1.791	1.904	...
1.0	1.496	1.578	1.668	1.818	1.930	2.706
2.0	1.693	1.773	1.861	2.007	2.116	2.879
3.0	1.914	1.994	2.081	2.227	2.336	3.096
4.0	2.145	2.225	2.312	2.458	2.567	3.327
5.0	2.381	2.461	2.548	2.694	2.803	3.565
6.0	2.620	2.700	2.787	2.934	3.003	...
7.0	2.862	2.942	3.029	3.167	3.285	...
8.0	3.105	3.185	3.272	3.420	3.529	4.293
9.0	3.349	3.430	3.517	3.664	3.778	...
10.0	3.595	3.675	3.761	3.910	4.019	4.785

ity solution of the S model by Sharipov[141] are most reliable.

In Table 9 the complete data on the coefficient G^{tb}_{*P} based on the variational solution of the BGK model[124,125] are presented. The complete data on this coefficient based on the S-model[141] are given in Table 10.

3.4.3. Plane Thermal Creep Flow

Diffuse scattering: To calculate the thermal creep G^{ch}_{*T} Loyalka[87] solved the integral equation (3.43) (BGK), which implies the diffuse scattering (2.22), by the variational method. Then, he solved the same equation by the direct numerical method.[89] In the work[102] the data obtained from the BGK model by the method of elementary solutions are presented. In Table 11 a comparison between these three solutions is performed. One can see that there is good agreement between them.

TABLE 10. Reduced flow rate G^{tb}_{*P} vs δ and α by Sharipov (Ref. 141): S model

	G^{tb}_{*P}			G^{tb}_{*P}	
δ	$\alpha=0.8$	$\alpha=0.6$	δ	$\alpha=0.8$	$\alpha=0.6$
0.0005	2.2484	3.4875	0.9	1.9373	2.7183
0.001	2.2437	3.4751	1.0	1.9514	2.7277
0.005	2.2131	3.4001	1.2	1.9859	2.7559
0.01	2.1853	3.3374	1.4	2.0214	2.7861
0.02	2.1442	3.2488	1.6	2.0593	2.8201
0.03	2.1141	3.1853	1.8	2.0991	2.8568
0.04	2.0901	3.1355	2.0	2.1402	2.8956
0.05	2.0703	3.0945	3.0	2.3585	3.1074
0.06	2.0534	3.0599	4.0	2.5881	3.3342
0.07	2.0388	3.0299	5.0	2.8233	3.5677
0.08	2.0259	3.0037	6.0	3.0620	3.8050
0.09	2.0145	2.9805	7.0	3.3030	4.0446
0.1	2.0043	2.9597	8.0	3.5455	4.2858
0.2	1.9444	2.8346	9.0	3.7893	4.5281
0.3	1.9169	2.7710	10.0	4.0343	4.7703
0.4	1.9056	2.7367	20.0	6.5086	7.2387
0.5	1.9033	2.7184	30.0	8.9965	9.7105
0.6	1.9069	2.7101	40.0	11.491	12.185
0.7	1.9144	2.7085	50.0	13.972	14.656
0.8	1.9248	2.7117			

Chernyak *et al.*[42] solved the integral equation (3.40) (S model) by the direct numerical method (fifth column) and by the variational one (sixth column). These results also coincide perfectly each with other.

The seventh column contains the results by Loyalka and Hickey[97] based on the BE solved by the discrete velocity method. The results by Ohwada *et al.*[116] based on the BE are presented separately in Table 12, where δ is recalculated according to our definition.

A comparison between the results obtained from the different equations is performed also in Fig. 6. From this figure we may conclude that: (i) the numerical solutions of the BE equation obtained by Loyalka and Hickey[97] (circles) and by Ohwada *et al.*[116] (crosses) for the different values of δ are in a good agreement; (ii) the solution of the S model (square) is closer to the BE solution than the BGK solution (solid line).

From Table 11 and Fig. 6 one can see that unlike the coefficient G^{ch}_{*P}, for the thermal creep G^{ch}_{*T} there is no agreement between the results obtained from the different model equations. The S model gives the disagreement (about 8%) with the BE solution, which can be regarded as reasonable. The disagreement of the BGK model solution with the BE solution reaches 30%. This large disagreement is a consequence of the fact that the BGK model does not give the correct value of the Prandtl number. The dimensionless collision frequency $\tilde{\nu}_{BGK}$ related with the rarefaction parameter δ by (3.20) provides the correct values of the Poiseuille flow

TABLE 11. Reduced flow rate G^{ch}_{*T} vs δ: diffuse scattering, different methods

	G^{ch}_{*T}					
δ	a	b	c	d	e	f
0.001	1.8394	1.8289	...	...	...	...
0.01	1.2334	1.2348	...	1.2470	1.2469	...
0.1	0.6948	0.6944	0.6949	0.7328	0.7283	0.7966
1.0	0.2950	0.2948	0.2948	0.3656	0.3653	0.3890
10.0	0.0663	0.06553	0.0660	0.09834	0.09707	0.0898

[a]Loyalka (Ref. 89), Eq. (3.43) (BGK), direct numerical method.
[b]Loyalka (Ref. 89), Eq. (3.43) (BGK), variational method.
[c]Loyalka *et al.* (Ref. 102), Eq. (3.13) with (3.16) (BGK), method of elementary solutions.
[d]Chernyak *et al.* (Ref. 42), (3.40) (S model), direct numerical method.
[e]Chernyak *et al.* (Ref. 42), (3.40) (S model), variational method.
[f]Loyalka and Hickey (Ref. 97), (3.13) with (2.54) (BE) direct numerical method.

G_{*P}. But it cannot provide the correct value of the thermal creep.

The numerical data based on the BGK model can be corrected using the expression of the frequency ν in the form (2.47). Then, the relation between the dimensionless collision frequency $\tilde{\nu}_{BGK}$ defined by (3.16) with the rarefaction parameter δ will be as follows

$$\tilde{\nu}_{BGK} = \tfrac{2}{3}\delta \tag{3.54}$$

instead of (3.20). So, to use the collision frequency ν in the form (2.47) we have to recalculate the rarefaction parameter δ.

The dashed line in Fig. 6 corresponds to the dependence of G^{ch}_{*T} on the recalculated δ. One can see that the BGK model with the collision frequency $\tilde{\nu}_{BGK}$ related with δ by (3.54) gives good agreement with the BE solution for the coefficient G^{ch}_{*T}. But one must bear in mind that the BGK model with (3.54) gives an incorrect value of the coefficient G_{*P} in the transition and hydrodynamic regimes.

The numerical data on the coefficient G_{*T} are available also in the literature.[17,80,91,103] All these results are in good agreement with the data given above. The results of the work[68] are erroneous as is pointed out by Loyalka.[89] Unfortunately, the data based on the S model, which would be very useful here, are presented very poorly by Chernyak *et al.*[42]

The complete data based on the BGK model[89] are given in Table 13. The coefficient G^{ch}_{*T} is presented as a function of the dimensionless collision frequency $\tilde{\nu}_{BGK}$. The rarefaction parameter recalculated by (3.54) is also given. The complete data based on the BE[97] are given in Table 14.

Diffuse-specular scattering: The numerical data on the plane thermal creep G^{ch}_{*T} for the diffuse-specular scattering (2.23) are available in the literature.[80,91,97,102,103] The results obtained by Loyalka *et al.*[97] on the basis of the BE are presented in Table 14. The results obtained by Loyalka[91] based on the BGK model with the dimensionless collision frequency defined by (3.54), are given in Table 15. The data of the papers[80,102,103] coincide with those obtained by Loyalka.[91]

3.4.4. Cylindrical Thermal Creep Flow

Diffuse scattering: Numerical data on the cylindrical thermal creep G^{tb}_{*T} based on the BGK model assuming diffuse scattering (2.22) were obtained by Loyalka,[84] who solved the integral equation (3.43) by the direct numerical method. His results are presented in the second column of Table 16. Chernyak *et al.*[46] (third column) solved the same equation by the variational method. Valougeorgis and Thomas[160] (fourth

TABLE 12. Reduced flow rate G^{ch}_{*T} vs δ by Ohwada *et al.* (Ref. 116): diffuse scattering, BE

δ	G^{ch}_{*T}	δ	G^{ch}_{*T}
0.0393	0.9968	0.785	0.4240
0.0524	0.9338	0.982	0.3916
0.0785	0.8484	1.31	0.3460
0.0982	0.8030	1.96	0.2838
0.131	0.7460	2.62	0.2418
0.196	0.6690	3.93	0.1870
0.262	0.6164	5.24	0.1522
0.393	0.5448	7.85	0.1106
0.524	0.4954		

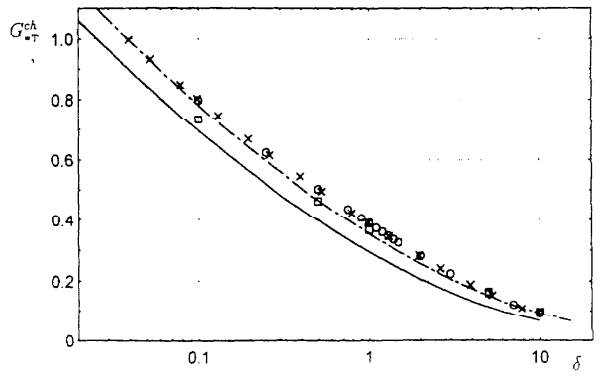

FIG. 6. Reduced flow rate G^{ch}_{*T} vs δ at diffuse scattering: solid line—BGK by Loyalka (Ref. 89), dashed line—BGK with recalculated δ, squares—S model by Chernyak *et al.* (Ref. 42), circles—BE by Loyalka and Hickey (Ref. 97), crosses—BE by Ohwada *et al.* (Ref. 116).

TABLE 13. Reduced flow rate G_{*T}^{ch} vs δ by Loyalka (Ref. 89): diffuse scattering, BGK

$\tilde{\nu}_{BGK}$	δ	G_{*T}^{ch}	$\tilde{\nu}_{BGK}$	δ	G_{*T}^{ch}
0.001	0.00067	1.8394	1.5	1.0	0.2413
0.005	0.00333	1.4134	2.0	1.333	0.2064
0.01	0.00667	1.2334	2.5	1.667	0.1811
0.02	0.0133	1.0606	3.0	2.0	0.1620
0.04	0.0267	0.8958	3.5	2.33	0.1464
0.05	0.0333	0.8450	4.0	2.67	0.1340
0.06	0.04	0.8043	5.0	3.33	0.1145
0.08	0.0533	0.7418	6.0	4.0	0.1000
0.1	0.0667	0.6948	7.0	4.67	0.0888
0.2	0.133	0.5578	8.0	5.33	0.0798
0.4	0.267	0.4351	9.0	6.0	0.0725
0.5	0.333	0.3986	10.0	6.67	0.0663
0.6	0.4	0.3699	20.0	13.3	0.0361
0.8	0.533	0.3268	30.0	20.0	0.0249
1.0	0.667	0.2950	40.0	26.7	0.0191

column) solved the BGK equation by the method of elementary solutions. One can see that there is good agreement between all these results. Note that the data of the papers[46,84,160] are presented in Table 16 implying the relation (3.20).

Sharipov[141] solved Eq. (3.13) with (3.17) (S model) by the discrete velocity method. His results are presented in the fifth column of Table 16. There is no agreement between the BGK model solution and that based on the S model. This disagreement was discussed in Sec. 3.4.3, where it was pointed out that the S model supplies more reliable results. Therefore, the complete data based on the BGK model are not presented here. The complete data based on the S model[141] are presented in Table 17.

The results based on the BGK model and being in good agreement with the data by Loyalka[84] can be found also in the literature.[81,91,104,125,123]

TABLE 14. Reduced flow rate G_{*T}^{ch} vs δ and α by Loyalka and Hickey (Ref. 97): BE

	G_{*T}^{ch}		
δ	$\alpha=1$	$\alpha=0.75$	$\alpha=0.5$
0.1	0.7966	1.0864	1.5632
0.25	0.6243	0.8118	1.0999
0.5	0.5036	0.6225	0.7903
0.75	0.4359	0.5193	0.6304
0.9	0.4060	0.4752	0.5646
1.0	0.3890	0.4505	0.5285
1.1	0.3737	0.4285	0.4970
1.2	0.3598	0.4089	0.4694
1.3	0.3472	0.3012	0.4448
1.4	0.3355	0.3752	0.4228
1.5	0.3248	0.3606	0.4030
2.0	0.2810	0.3027	0.3274
3.0	0.2226	0.2307	0.2393
5.0	0.1574	0.1570	0.1566
7.0	0.1212	0.1190	0.1165
10.0	0.0898	0.0871	0.0842

Diffuse-specular scattering: The results of the cylindrical thermal creep flow for the diffuse-specular scattering (2.23) based on the integral equation (3.43) (BGK) are available in the literature[81,91,123] (direct numerical solution) and in the work[125] (variational method). The data based on the S model were obtained by Sharipov.[141] Since the S model gives more reliable results, the results based on the BGK model are not presented here. We only note that: (i) There is a good agreement between the results of the Refs. 81, 125, 123; (ii) the results of the work in Ref. 91 are erroneous.

The complete data by Sharipov[141] on the cylindrical thermal creep G_{*T}^{tb} obtained from the S model for the different gas–surface interaction parameters α are given in Table 17.

3.4.5. Mechanocaloric Heat Flux

Due to the Onsager relation (3.36) the reduced mechanocaloric heat flux Q_{*P} is equal to the thermal creep G_{*T}. So, there is no point in considering the coefficient Q_{*P} here. We only note that there is a difference in the profiles $\tilde{u}_{xT}$ and $\tilde{q}_{xP}$. Information on the profiles can be found in the literature.[42,80,81,97,103,104,123]

3.4.6. Plane Heat Flux

Diffuse scattering: Results on the heat flux through a channel Q_{*T}^{ch} for the diffuse scattering (2.22) are available in the following papers: Loyalka[87] solved the integral equation (3.38) (BGK) by the variational method; Chernyak *et al.*[42] solved the integral equation (3.40) (S model) by both direct numerical and variational method; Lo and Loyalka[80] solved Eq. (3.38) (BGK) by the direct numerical method; and Loyalka and Hickey[97] solved the BE by the discrete velocity method. A comparison between these results is performed in Table 18. One can see that there is a disagreement between variational (second column) and direct numerical (third column) solutions of the BGK model. Most probably in the paper[87] the coefficient Q_{*T}^{ch} was calculated incorrectly. The exact (forth column) and variational (fifth column) solutions of the S model are in good agreement.

A comparison of the different solutions is also performed in Fig. 7. One can see that the solution of the S model (squares) is closer to the BE solution (crosses) than the BGK model solution (solid line). As well as for the thermal creep G_{*T}, this disagreement is a consequence of the BGK model having the incorrect Prandtl number. The BGK model gives more reasonable values of Q_{*T}^{ch}, if the collision frequency $\tilde{\nu}_{BGK}$ is related with the rarefaction parameter δ by (3.54). The recalculated data are presented by the dashed line in Fig. 7.

Since the BGK equation gives unreliable results on the coefficient Q_{*T}^{ch} and the results based on the S model[42] are presented very poorly, we restrict ourselves by the presentation of the complete data based on the BE[97] only. The data are given in Table 19.

Diffuse-specular scattering: The thermal flux for the diffuse-specular scattering (2.23) is calculated by Lo and

TABLE 15. Reduced flow rate G^{ch}_{*T} vs δ and α by Loyalka (Ref. 91): BGK

		G^{ch}_{*T}				
$\tilde{\nu}_{BGK}$	δ	$\alpha=0.96$	$\alpha=0.92$	$\alpha=0.88$	$\alpha=0.84$	$\alpha=0.80$
0.001	0.0007	1.9752	2.1058	2.2465	2.3987	2.5638
0.01	0.0067	1.3074	1.3839	1.4659	1.5539	1.6488
0.02	0.0133	1.1196	1.1813	1.2473	1.3180	1.3940
0.03	0.02	1.0141	1.0677	1.1249	1.1861	1.2517
0.04	0.0267	0.9416	0.9897	1.0409	1.0956	1.1543
0.05	0.0333	0.8867	0.9307	0.9775	1.0275	1.0809
0.07	0.0467	0.8066	0.8447	0.8851	0.9281	0.9740
0.09	0.06	0.7489	0.7828	0.8196	0.8567	0.8973
0.1	0.0667	0.7253	0.7574	0.7914	0.8275	0.8660
0.3	0.2	0.5000	0.5165	0.5338	0.5520	0.5712
0.5	0.3333	0.4089	0.4197	0.4310	0.4428	0.4552
0.7	0.4667	0.3538	0.3615	0.3695	0.3778	0.3864
0.9	0.6	0.3152	0.3209	0.3268	0.3329	0.3392
1.0	0.6667	0.2997	0.3046	0.3098	0.3150	0.3205
1.25	0.8333	0.2681	0.2717	0.2753	0.2790	0.2829
1.5	1.0	0.2437	0.2462	0.2488	0.2515	0.2543
2.0	1.3333	0.2075	0.2088	0.2102	0.2115	0.2129
2.5	1.6667	0.1816	0.1822	0.1828	0.1834	0.1841
3.0	2.0	0.1619	0.1621	0.1622	0.1624	0.1625
3.5	2.3333	0.1463	0.1461	0.1460	0.1459	0.1457
4.0	2.6667	0.1335	0.1332	0.1329	0.1325	0.1322
5.0	3.3333	0.1138	0.1133	0.1127	0.1122	0.1117
6.0	4.0	0.0992	0.0986	0.0980	0.0974	0.0967
7.0	4.6667	0.0879	0.0873	0.0867	0.0860	0.0854
9.0	6.0	0.0716	0.0710	0.0704	0.0698	0.0691
10.0	6.6667	0.0655	0.0649	0.0643	0.0637	0.0631

Loyalka[80] on the basis of the BGK equation and by Loyalka and Hickey[97] on the basis of the BE. The results of the last paper, which are more reliable, are presented in Table 19.

3.4.7. Cylindrical Heat Flux

The cylinder thermal flux was calculated only by Lo *et al.*[81] on the basis of the integral equation (3.43) (BGK) by the direct numerical method. The results are presented in Table 20, where the relation (3.54) has been used.

TABLE 16. Reduced flow rate G^{tb}_{*T} vs δ: diffuse scattering, different methods

	G^{tb}_{*T}			
δ	a	b	c	d
0.0001	0.7515	0.7515	0.7515	...
0.001	0.7467	0.7467	0.7466	0.7486
0.01	0.7179	0.7178	0.7177	0.7243
0.1	0.5976	0.5975	0.5968	0.6210
1.0	0.3220	0.3214	0.3217	0.3959
10.0	0.0687	0.0683	0.0686	0.1014

[a]Loyalka (Ref. 84), Eq. (3.43) (BGK), direct numerical solution.
[b]Chernyak *et al.* (Ref. 46), Eq. (3.43) (BGK), variational method.
[c]Valougeorgis and Thomas (Ref. 160), Eq. (3.13) with (3.16) (BGK), method of elementary solutions.
[d]Sharipov (Ref. 141), Eq. (3.13) with (3.17) (S model), discrete velocity method.

3.5. Free-Molecular Regime

In the free-molecular regime ($\delta=0$) the flow rate and the heat flux can be calculated analytically. At $\delta=0$ all kernels in the integral equations (3.38)–(3.40) and (3.43)–(3.45) are equal to zero and the moments $\tilde{u}_x$, $\tilde{q}_x$ are equal to the free terms. But for the channel flow the free terms contain the function $I_0(\delta|\tilde{y}-\tilde{y}'|)$. From the representation (3.49) one can see that at $\delta\to 0$ this function and hence the free terms tend to infinity. As a result the bulk velocity and the heat flow vector in the channel also tend to infinity in the free-molecular regime. This unphysical behavior is explained by the degenerate geometry: the channel is infinite in two directions. If we restrict the channel at least in one direction (length or width) the bulk velocity and the heat flow vector immediately will be finite quantities.

So, the expressions of the moments and the flow rates through the channel given below describe only their asymptotic behavior at $\delta\to 0$. From (3.38), (3.39), (3.43) and (3.44) with the free terms for the diffuse-specular scattering (2.23) we have

$$\tilde{u}^{ch}_{xP}=\frac{\ln\delta}{2\sqrt{\pi}}\,\frac{(2-\alpha)}{\alpha},\qquad \tilde{u}^{tb}_{xP}(r_\perp)=-\frac{E(r_\perp^2)}{\sqrt{\pi}}\,\frac{(2-\alpha)}{\alpha}, \tag{3.55}$$

$$\tilde{u}_{xT}=-\tfrac{1}{2}\,\tilde{u}_{xP},\qquad \tilde{q}_{xP}=\tilde{u}_{xT},\qquad \tilde{q}_{xT}=\tfrac{9}{4}\tilde{u}_{xP}, \tag{3.5}$$

TABLE 17. Reduced flow rate G^{tb}_{*T} vs δ and α by Sharipov (Ref. 141): S model

	G^{tb}_{*T}				G^{tb}_{*T}		
δ	$\alpha=1.0$	$\alpha=0.8$	$\alpha=0.6$	δ	$\alpha=1.0$	$\alpha=0.8$	$\alpha=0.6$
0.0005	0.7502	1.1215	1.7365	0.9	0.4092	0.4567	0.5140
0.001	0.7486	1.1166	1.7237	1.0	0.3959	0.4372	0.4865
0.005	0.7366	1.0838	1.6452	1.2	0.3721	0.4035	0.4402
0.01	0.7243	1.0530	1.5775	1.4	0.3514	0.3754	0.4029
0.02	0.7042	1.0070	1.4807	1.6	0.3330	0.3513	0.3718
0.03	0.6884	0.9719	1.4093	1.8	0.3165	0.3303	0.3456
0.04	0.6752	0.9432	1.3512	2.0	0.3016	0.3118	0.3230
0.05	0.6637	0.9186	1.3036	3.0	0.2439	0.2443	0.2445
0.06	0.6536	0.8970	1.2617	4.0	0.2042	0.2009	0.1971
0.07	0.6444	0.8778	1.2247	5.0	0.1752	0.1704	0.1651
0.08	0.6359	0.8603	1.1916	6.0	0.1531	0.1479	0.1420
0.09	0.6281	0.8444	1.1616	7.0	0.1359	0.1305	0.1245
0.1	0.6210	0.8297	1.1341	8.0	0.1220	0.1167	0.1108
0.2	0.5675	0.7244	0.9435	9.0	0.1106	0.1055	0.09979
0.3	0.5303	0.6558	0.8255	10.0	0.1014	0.09620	0.09079
0.4	0.5015	0.6050	0.7415	20.0	0.05426	0.05104	0.04746
0.5	0.4779	0.5648	0.6769	30.0	0.03685	0.03452	0.03187
0.6	0.4576	0.5315	0.6250	40.0	0.02785	0.02600	0.02388
0.7	0.4397	0.5031	0.5820	50.0	0.02212	0.02080	0.01874
0.8	0.4237	0.4784	0.5455				

where $E(x)$ is the complete elliptic integral of the second kind defined as

$$E(x)=\int_0^{\pi/2}(1-x\sin^2\phi)^{1/2}\mathrm{d}\phi. \tag{3.57}$$

The flow rates and the heat fluxes (3.27)–(3.30) take the form

$$G^{ch}_{*P}=-\frac{\ln\delta\,(2-\alpha)}{\sqrt{\pi}\,\alpha},\quad G^{tb}_{*P}=\frac{8}{3\sqrt{\pi}}\frac{(2-\alpha)}{\alpha}, \tag{3.58}$$

$$G_{*T}=\tfrac{1}{2}G_{*P},\quad Q_{*P}=G_{*T},\quad Q_{*T}=\tfrac{9}{4}G_{*P}. \tag{3.59}$$

The same result can be obtained via the integral equation systems (3.40) and (3.45).

TABLE 18. Reduced heat flux Q^{ch}_{*T} vs δ: diffuse scattering, different methods

	Q^{ch}_{*T}				
δ	a	b	c	d	e
0.01	5.4225	6.6742	6.7343	6.7343	···
0.1	3.3008	3.8460	4.0553	4.0500	3.8669
1.0	1.3180	1.4182	1.7543	1.7535	1.7846
10.0	0.1742	0.2334	0.3407	0.3402	0.3467

[a]Loyalka (Ref. 87), Eq. (3.38) (BGK), direct numerical method.
[b]Lo and Loyalka (Ref. 80), Eq. (3.38) (BGK), variational method.
[c]Chernyak *et al.* (Ref. 42), Eq. (3.43) (S model), direct numerical method.
[d]Chernyak *et al.* (Ref. 42), Eq. (3.43) (S model), variational method.
[e]Loyalka and Hickey (Ref. 97), Eq. (3.13) with (2.54) BE, discrete velocity method.

3.6. Near Free-Molecular Regime

One of the methods to obtain the analytical expressions of the flow rate and heat flux for the small values of the rarefaction parameter δ is as follows. We use the expansion (3.49) retaining a finite number of the terms. With the help of this expansion we can obtain analytical expressions of the coefficients $\mathcal{A}_{ij}$ and $\mathcal{B}_{im}$ of the algebraic system (3.53). Then, this algebraic system can be resolved analytically. Having the analytical expressions of the coefficients c_{1m}, c_{2m}, c_{3m} one easily obtains the bulk velocity (3.51) and the heat flow vector (3.52). Then, the flow rates and the heat fluxes are calculated by (3.27)–(3.30).

For the tube flow this task was done by Chernyak *et al.*[43] Under the supposition of the diffuse scattering (2.22) they obtained the flow rates and the heat fluxes up to the terms of order δ^2:

$$G^{tb}_{*P}=1.5045+\delta\ln\delta-0.3842\delta-0.8024\delta^2, \tag{3.60}$$

$$G^{tb}_{*T}=Q^{tb}_{*P}=0.7523+\delta\ln\delta+0.1158\delta-1.2036\delta^2, \tag{3.61}$$

$$Q^{tb}_{*T}=3.3851+2.5\delta\ln\delta-0.4604\delta-2.6078\delta^2. \tag{3.62}$$

Since these expressions have a small number of the terms, they give good precision in the very small range of δ. But applying the method described here, one can obtain the asymptotic formulas of the flow rates and the heat fluxes up to any order of δ.

Note, the algebraic system (3.53) and hence the expressions (3.60)–(3.62) are based on the S model.

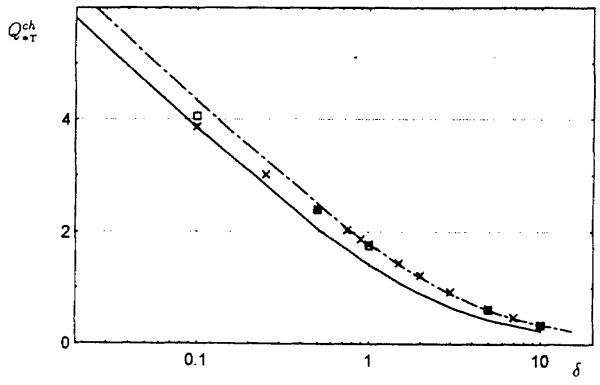

FIG. 7. Reduced heat flux Q^{ch}_{*T} vs δ at diffuse scattering: solid line—BGK by Lo and Loyalka (Ref. 80), dashed line—BGK with recalculated δ, squares—S model by Chernyak *et al.* (Ref. 42), crosses—BE by Loyalka and Hickey (Ref. 97).

TABLE 19. Reduced heat flux Q^{ch}_{*T} vs δ and α by Loyalka and Hickey (Ref. 97): BE

	Q^{ch}_{*T}		
δ	$\alpha=1.0$	$\alpha=0.75$	$\alpha=0.5$
0.1	3.8669	5.3371	7.7430
0.25	3.0187	3.9702	5.4179
0.5	2.3918	2.9969	3.8420
0.75	2.0333	2.4635	3.0290
0.9	1.8750	2.2355	2.6959
1.0	1.7846	2.1077	2.5136
1.1	1.7036	1.9948	2.3552
1.2	1.6305	1.8942	2.2161
1.3	1.5639	1.8038	2.0930
1.4	1.5030	1.7220	1.9832
1.5	1.4470	1.6476	1.8845
2.0	1.2217	1.3568	1.5103
3.0	0.9331	1.0044	1.0821
5.0	0.6319	0.6602	0.6903
7.0	0.4761	0.4909	0.5064
10.0	0.3167	0.3540	0.3616

TABLE 20. Reduced heat flux Q^{tb}_{*T} vs δ and α by Lo *et al.* (Ref. 81): BGK

		Q^{tb}_{*T}		
$\tilde{\nu}_{BGK}$	δ	$\alpha=1.0$	$\alpha=0.8$	$\alpha=0.6$
0.01	0.0067	3.2700	4.7987	7.2535
0.02	0.0133	3.1883	4.6135	6.8518
0.04	0.0267	3.0569	4.3294	6.2629
0.06	0.04	2.9485	4.1056	5.8195
0.1	0.0667	2.7703	3.7555	5.1579
0.4	0.2667	2.0146	2.4648	3.0152
0.6	0.4	1.7290	2.0428	2.4059
1.0	0.6667	1.3560	1.5356	1.7285
2.0	1.333	0.8849	0.9554	1.0227
3.0	2.0	0.6563	0.6939	0.7271
4.0	2.667	0.5210	0.5445	0.5640
5.0	3.333	0.4318	0.4478	0.4605
8.0	5.333	0.2867	0.2918	0.2969
10.0	6.667	0.2335	0.2367	0.2400

3.7. Hydrodynamic Regime

In the hydrodynamic regime ($\delta\to\infty$) the mass flow rate can be found from the Navier–Stokes equation (2.44). Its solution with the stickiness boundary condition (i.e., the bulk velocity is equal to zero on the wall) for an infinite capillary is well known, see e.g., Refs. 12, 73, 149. The dimensional velocity profile has the form

$$u_x^{ch}(y)=-\frac{1}{2\mu}\frac{dP}{dx}\left[\left(\frac{a}{2}\right)^2-y^2\right],$$

$$u_x^{tb}(r_\perp)=-\frac{1}{4\mu}\frac{dP}{dx}(a^2-r_\perp^2) \tag{3.63}$$

for the channel and tube, respectively. Here $r_\perp=\sqrt{y^2+z^2}$. From (3.63) with the help of (2.41), (3.11) and (3.23) we obtain the expression for the dimensionless velocities:

$$\tilde{u}_{xP}^{ch}(\tilde{y})=-\frac{\delta}{2}\left(\frac{1}{4}-\tilde{y}^2\right),\quad \tilde{u}_{xP}^{tb}(\tilde{r}_\perp)=-\frac{\delta}{4}(1-\tilde{r}_\perp^2),$$

$$\tilde{u}_{xT}=0. \tag{3.64}$$

For the reduced flow rates (3.27) and (3.29) we have

$$G^{ch}_{*P}=\frac{\delta}{6},\quad G^{tb}_{*P}=\frac{\delta}{4},\quad G_{*T}=0. \tag{3.65}$$

The heat flux can be easily found from Fourier's law (2.37), which for the capillary flow takes the form

$$q_x=-\kappa\frac{dT}{dx}. \tag{3.66}$$

With the help of (2.41), (3.11) and (3.23) we have

$$\tilde{q}_{xP}=0,\quad \tilde{q}_{xT}=-\frac{15}{8\delta}, \tag{3.67}$$

for both channel and tube. For the reduced heat fluxes (3.28) and (3.30) we obtain

$$Q_{*P}=0,\quad Q_{*T}=\frac{3.75}{\delta}. \tag{3.68}$$

3.8. Slip Regime of the Gas Flow

3.8.1. Definition of the Slip Coefficients

In the previous section we have obtained the flow rates assuming the stickiness boundary condition. However, the bulk velocity is not equal to zero on the wall because there is a slip of the gas. The tangential velocity u_t of the gas near the wall is proportional to its normal gradient and to the longitudinal temperature gradient, i.e.,

$$u_t=A_P\frac{\partial u_t}{\partial x_n}+A_T\frac{\partial T}{\partial x_t}, \tag{3.69}$$

where x_t is the coordinate tangential to the surface, x_n is the normal coordinate, and A_P and A_T are coefficients to be ob-

tained with the help of the kinetic equation. Here, it is more convenient to introduce the dimensionless slip coefficients as follows:

$$\sigma_P=\frac{\sqrt{\pi}}{2\lambda}A_P, \quad \sigma_T=\frac{1}{\lambda}\left(\frac{\pi m T}{2k_B}\right)^{1/2}A_T. \tag{3.70}$$

Taking into account the slip boundary condition (3.69) we have the following velocity profiles:

$$u_x^{ch}=-\frac{1}{2\mu}\frac{dP}{dx}\left[\left(\frac{a}{2}\right)^2-y^2+aA_P\right]+A_T\frac{dT}{dx}, \tag{3.71}$$

$$u_x^{tb}=-\frac{1}{4\mu}\frac{dP}{dx}(a^2-r_\perp^2+aA_P)+A_T\frac{dT}{dx}. \tag{3.72}$$

From (3.71) and (3.72) with the help of (3.11), (3.23) and (3.70) we obtain

$$\tilde{u}_{xP}^{ch}=-\frac{\delta}{2}\left(\frac{1}{4}-\tilde{y}^2\right)-\frac{\sigma_P}{2}, \quad \tilde{u}_{xT}^{ch}=\frac{\sigma_T}{2\delta}, \tag{3.73}$$

$$\tilde{u}_{xP}^{tb}=-\frac{\delta}{4}(1-\tilde{r}_\perp^2)-\frac{\sigma_P}{2}, \quad \tilde{u}_{xT}^{tb}=\frac{\sigma_T}{2\delta}. \tag{3.74}$$

Then, the reduced flow rates take the form

$$G_{*P}^{ch}=\frac{\delta}{6}+\sigma_P, \quad G_{*T}^{ch}=\frac{\sigma_T}{\delta}, \tag{3.75}$$

$$G_{*P}^{tb}=\frac{\delta}{4}+\sigma_P, \quad G_{*T}^{tb}=\frac{\sigma_T}{\delta}. \tag{3.76}$$

3.8.2. Viscous Slip Coefficient

To obtain the viscous slip coefficient σ_P one has to consider a stationary rarefied gas flow in the semi-infinite space $x_n \geq 0$ over an infinite plate having a constant temperature T and fixed at $x_n=0$. The behavior of the gas is described by the linearized kinetic equation. At the surface ($x_n=0$) the perturbation function h satisfies the boundary condition (2.18). At infinity ($x_n \to \infty$) it is assumed that the perturbation function coincides with the Chapman–Enskog solution with the tangential bulk velocity having a small normal gradient.

The detailed technique of solution of this problem and numerical data on the coefficient σ_P can be found in the literature.[6,23,29,34,70,86,88,90,96,98,100,115,155,167,170,177] Here, we consider the main rigorous results.

Diffuse scattering: Albertoni *et al.*[6] applying the method of elementary solutions to the BGK model and assuming the diffuse scattering (2.22), obtained

$$\sigma_P=1.016. \tag{3.77}$$

This can be considered as the most exact results based on the BGK model.

Loyalka and Ferziger[100] and Cercignani *et al.*[29] calculated the coefficient σ_P using other kinetic models. They found that the slip coefficient varies in the range

$$0.9624 \leq \sigma_P \leq 1.0185, \tag{3.78}$$

TABLE 21. Viscous slip coefficient σ_P vs α

	σ_P		
α	a	b	c
0.1	17.1031	17.0058	17.2332
0.2	8.2249	8.1524	8.2721
0.3	5.2551	5.1928	5.2770
0.4	3.7626	3.7069	3.7734
0.5	2.8612	2.8107	2.8664
0.6	2.2554	2.2093	2.2576
0.7	1.8187	1.7766	1.8194
0.8	1.4877	1.4494	1.4877
0.9	1.2272	1.1925	1.2270
1.0	1.0162	0.9849	1.0160

[a]Loyalka *et al.* (Ref. 101), BGK.
[b]Wakabayashi *et al.* (Ref. 163), BE.
[c]Equation (3.80).

i.e., it is only slightly model dependent.

The direct numerical solution of the BE for rigid spheres obtained by Loyalka and Hickey[96] and by Ohwada *et al.*[115] give the following values[b]

$$\sigma_P=0.9845 \quad \text{and} \quad \sigma_P=0.9849, \tag{3.79}$$

respectively. One can see that agreement between these results is perfect. So, the value $\sigma_P=0.985$ can be considered as the most reliable one for perfect accommodation.

Diffuse-specular scattering: Applying the variational method to the BE of Maxwellian molecules and assuming the diffuse scattering (2.23) Loyalka[83] obtained the following expression for the slip coefficient:

$$\sigma_P(\alpha)=\frac{2-\alpha}{\alpha}[\sigma_P(1)-0.1211(1-\alpha)]. \tag{3.80}$$

The same results were obtained by him in the paper[86] using an approximate method. The same expression (3.80) was also obtained by Suetin and Chernyak[155] from the S model equation. Zhdanov and Zaznoba[176] obtained this expression from the BE by the moment method.

Exact numerical calculations of the slip coefficient σ_P based on the BGK equation over the whole range of α were carried out by Loyalka *et al.*[101] Wakabayashi *et al.*[163] performed a numerical calculation of the BE by the discrete velocity method. In Table 21 these results and $\sigma_P(\alpha)$ calculated by (3.80) with $\sigma_P(1)=1.016$ are presented. It can be seen that there is good agreement between Eq. (3.80) and the numerical data based on the BGK model.[101] The values of σ_P obtained from the BE[163] differ very slightly from the BGK solution. Thus, Eq. (3.80) can be successfully used in practical calculations.

[b]The value given by Ohwada *et al.* (Ref. 115) must be multiplied by $\pi/4$.

3.8.3. Thermal Slip Coefficient

To obtain the thermal slip coefficient σ_T one has to consider a stationary rarefied gas flow in the semi-infinite space $x_n \geq 0$ over an infinite plate fixed at $x_n = 0$ and having a linear temperature distribution

$$T_w(x_t) = T_0(1 + \xi_{wT} x_t), \tag{3.81}$$

where ξ_{wT} is a given constant. This temperature distribution is established in the gas over the whole space occupied by him.

At the surface ($x_n = 0$) the perturbation function h satisfies the boundary condition (2.18). At infinity ($x_n \to \infty$) the function h tends to the Chapman–Enskog solution, corresponding to the heat transfer in the gas by a constant temperature gradient.

Two points should be noted here.

(i) First, sometimes in the literature the temperature jump coefficient is called "the temperature slip coefficient" (see, e.g., Refs. 70, 83). This could cause confusion, because one may think that "the temperature slip coefficient" is the same as the thermal slip coefficient. Here, we will not consider the temperature jump coefficient. We only point out that to obtain it one has to consider a temperature gradient, which is *normal* to the surface.

(ii) Second, since the BGK model has the Prandtl number equal to unity rather than 2/3, to compute σ_T we must be careful in the choice of the collision frequency ν in (2.45). The appropriate choice is that which leads to the correct heat conduction coefficient, i.e., the expression (2.47). Thus, all results based on the BGK model presented below will imply this choice of the frequency ν; even an original work uses the expression (2.46).

The detailed calculation of σ_T and numerical data can be found in the literature.[54,85,88,92–94,101,115,117,150,155,169,172,173] Let us analyze the main rigorous results.

Diffuse scattering: An accurate numerical calculations based on the BGK model with the diffuse scattering (2.22) were performed by Sone,[150] Williams,[169] Loyalka[94,101] and Onishi.[117] All of them obtained the same result, namely

$$\sigma_T = \tfrac{3}{2} 0.766 = 1.149. \tag{3.82}$$

The variational method applied to both the BGK model[85,88,92] and the S model[155] gave the following value:

$$\sigma_T = 9/8 = 1.125. \tag{3.83}$$

The same value has been obtained in the work[85] from the BE for Maxwellian molecules. But the model equation with a collision frequency appropriate to rigid sphere molecules[85] gives the value

$$\sigma_T = 0.9876. \tag{3.84}$$

The direct numerical solution of the BE for rigid spheres obtained by Loyalka[93] and by Ohwada *et al.*[115] gave the following values in our notations

TABLE 22. Thermal slip coefficient σ_T vs α

	σ_T				
α	a	b	c	d	e
0.0	0.7500	0.7500	0.7755	0.7500	0.7500
0.1	0.7925	0.7925	···	0.7899	0.7875
0.2	0.8344	0.8344	0.8286	0.8299	0.8250
0.3	0.8758	0.8757	···	0.8698	0.8625
0.4	0.9165	0.9164	0.8789	0.9097	0.9000
0.5	0.9567	0.9565	···	0.9497	0.9375
0.6	0.9963	0.9961	0.9266	0.9896	0.9750
0.7	1.0354	1.0352	···	1.0295	1.0125
0.8	1.0739	1.0737	0.9720	1.0694	1.0500
0.9	1.1119	1.1118	···	1.1094	1.0875
1.0	1.1495	1.1493	1.0152	1.1493	1.1250

[a]Loyalka *et al.* (Ref. 101), Integral equation based on BGK, direct numerical solution.
[b]Onishi (Ref. 117), Integral equation based on BGK, variational method.
[c]Wakabayashi *et al.* (Ref. 163), BE, discrete velocity method.
[d]Equation (3.86).
[e]Equation (3.87).

$$\sigma_T = \frac{3}{2} 0.6725 = 1.009, \quad \text{and} \quad \sigma_T = \frac{\pi}{2} 0.646 = 1.015, \tag{3.85}$$

respectively. One can see that there is a fine agreement between these two results. So, the value $\sigma_T = 1.01$ can be considered as the most reliable one for the diffuse scattering.

Diffuse-specular scattering: Based on the BGK equation with the diffuse-specular scattering (2.23) Loyalka and Cipolla[94] applying the method of elementary solutions obtained the expression

$$\sigma_T = 0.75 + 0.3993\alpha. \tag{3.86}$$

The variational method applied to the BGK and S models[88,94,155] gives the following expression:

$$\sigma_T = 0.75 + 0.375\alpha. \tag{3.87}$$

The same expression was obtained by Zhdanov and Zaznoba[176] from the BE by the moment method.

Loyalka *et al.*[101] solved the BGK model by the integro-moment method. The integral equation was solved by the exact numerical method. Onishi[117] also obtained the integral equation based on the BGK model. Then, the equation was solved by the variational method. Wakabayashi *et al.*[163] solved the BE by the discrete velocity method.

In Table 22 numerical results of the works[101,117,163] are presented and compared with the expressions (3.86) and (3.87). It can be seen that the expression (3.86) describes finely the numerical results based on the BGK model.[101,117] The disagreement between the BE solution and that based on the BGK model varies from 3% for $\alpha = 0$ to 12% for $\alpha = 1$.

3.9. Near Hydrodynamic Regime

In the two previous sections we obtained the expansions of the flow rates and heat fluxes for the large rarefaction param-

eter δ. The approach based on the Navier–Stokes equation with the slip boundary condition allows us to obtain the terms of the order $O(\delta)$ and $O(1)$ for $G_{*\mathrm{P}}$ and the terms of the order $O(1/\delta)$ for $G_{*\mathrm{T}}$. But using the approach described in Sec. 3.6 we may find more terms in the expansion. The unique difference from the approach for the small δ is that: the expansion (3.50) of the special functions I_n is used. With the help of this expansion we obtain the analytical expressions of the coefficients $\mathcal{A}_{ij}$ and $\mathcal{B}_{im}$ of the system (3.53). Then, we do the same as in Sec. 3.6 up to the analytical expressions for the flow rates and for the heat fluxes.

The method of elementary solutions based on the BGK model also allows us to obtain the analytical expressions of the flow rates and the heat fluxes. The following asymptotic formula ($\delta\to\infty$) of the plane Poiseuille flow $G^{\mathrm{ch}}_{*\mathrm{P}}$ for the diffuse scattering (2.22) was obtained by Williams[168]

$$G^{\mathrm{ch}}_{*\mathrm{P}}=\frac{\delta}{6}+1.0162+\frac{1.0653}{\delta}-\frac{2.1354}{\delta^2}. \tag{3.88}$$

Loyalka and Hickey[98] using the BE obtained the coefficients $G^{\mathrm{ch}}_{*\mathrm{P}}$, $G^{\mathrm{ch}}_{*\mathrm{T}}$, $Q^{\mathrm{ch}}_{*\mathrm{P}}$ and $Q^{\mathrm{ch}}_{*\mathrm{T}}$ for the diffuse scattering:

$$G^{\mathrm{ch}}_{*\mathrm{P}}=\frac{\delta}{6}+0.9790+\frac{0.7089}{\delta}-\frac{1.0872}{\delta^2}, \tag{3.89}$$

$$G^{\mathrm{ch}}_{*\mathrm{T}}=Q^{\mathrm{ch}}_{*\mathrm{P}}=\frac{0.9924}{\delta}-\frac{1.3284}{\delta^2}, \tag{3.90}$$

$$Q^{\mathrm{ch}}_{*\mathrm{T}}=\frac{3.7839}{\delta}-\frac{3.5508}{\delta^2}. \tag{3.91}$$

They also provide the asymptotic formulas of these coefficients for the diffuse-specular scattering at $\alpha=0.5$ and 0.1. Comparing (3.88) and (3.89) one can see that the coefficients of the asymptotic formulas essentially depend on the kinetic model equation.

The asymptotic formula ($\delta\to\infty$) of the cylindrical Poiseuille flow $G^{\mathrm{tb}}_{*\mathrm{P}}$ for the diffuse scattering (2.22) was obtained by Lang and Loyalka[74] applying the BGK equation

$$G^{\mathrm{tb}}_{*\mathrm{P}}=\frac{\delta}{4}+1.0162+\frac{0.5490}{\delta}-\frac{0.607}{\delta^2}. \tag{3.92}$$

Chernyak *et al.*[13] applying the S model obtained the following expressions of the coefficients $G^{\mathrm{tb}}_{*\mathrm{P}}$, $G^{\mathrm{tb}}_{*\mathrm{T}}$, $Q^{\mathrm{tb}}_{*\mathrm{P}}$ and $Q^{\mathrm{tb}}_{*\mathrm{T}}$ for the diffuse scattering:

$$G^{\mathrm{tb}}_{*\mathrm{P}}=\frac{\delta}{4}+1.0073+\frac{0.6712}{\delta}-\frac{0.8657}{\delta^2}, \tag{3.93}$$

$$G^{\mathrm{tb}}_{*\mathrm{T}}=Q^{\mathrm{tb}}_{*\mathrm{P}}=\frac{1.125}{\delta}-\frac{1.4687}{\delta^2}+\frac{0.6704}{\delta^3}-\frac{2.3424}{\delta^4}, \tag{3.94}$$

$$Q^{\mathrm{tb}}_{*\mathrm{T}}=\frac{3.75}{\delta}-\frac{3.8085}{\delta^2}+\frac{1.8518}{\delta^3}-\frac{2.3593}{\delta^4}. \tag{3.95}$$

3.10. Arbitrary Drops of the Pressure and Temperature

3.10.1. Main Relations

In this section, we realize the second stage of the problem formulated in Sec. 3.1, viz. we obtain the mass flow rate as a function of the pressures P_{I} and P_{II} and the temperatures T_{I} and T_{II}. For this purpose it is better to introduce two rarefaction parameters:

$$\delta_{\mathrm{I}}=\frac{\sqrt{\pi}}{2}\frac{a}{\lambda_{\mathrm{I}}}=\frac{aP_{\mathrm{I}}}{\mu(T_{\mathrm{I}})}\left(\frac{m}{2k_{\mathrm{B}}T_{\mathrm{I}}}\right)^{1/2},$$

$$\delta_{\mathrm{II}}=\frac{\sqrt{\pi}}{2}\frac{a}{\lambda_{\mathrm{II}}}=\frac{aP_{\mathrm{II}}}{\mu(T_{\mathrm{II}})}\left(\frac{m}{2k_{\mathrm{B}}T_{\mathrm{II}}}\right)^{1/2}, \tag{3.96}$$

where λ_{I} and λ_{II} are the mean free paths in the left and right containers, respectively. Here, Eq. (2.3) has been used. These rarefaction parameters can be related each with other if the intermolecular interaction law is given. Assuming the molecules to be hard spheres, from (2.40) we obtain $\lambda\propto 1/n \propto T/P$. Then, it is easily obtained

$$\delta_{\mathrm{I}}=\frac{P_{\mathrm{I}}}{P_{\mathrm{II}}}\frac{T_{\mathrm{II}}}{T_{\mathrm{I}}}\delta_{\mathrm{II}}. \tag{3.97}$$

Under the supposition of the small drops,

$$\Delta P/P_{\mathrm{I}}\ll 1, \quad \Delta T/T_{\mathrm{I}}\ll 1, \tag{3.98}$$

the variation of the rarefaction parameter δ along the capillary is negligible small and we may assume

$$\delta_{\mathrm{I}}=\delta_{\mathrm{II}}=\delta. \tag{3.99}$$

In this case the mass flow rates and the heat fluxes are easily calculated via the coefficients G_* and Q_* using their representations (3.31).

Under the condition (3.98) the TPD exponent γ can be calculated assuming $G_*=0$ in (3.31), where the gradients are calculated as

$$\xi_{\mathrm{P}}=\frac{(P_{\mathrm{II}}-P_{\mathrm{I}})}{LP_{\mathrm{I}}}, \quad \xi_{\mathrm{T}}=\frac{(T_{\mathrm{II}}-T_{\mathrm{I}})}{LT_{\mathrm{I}}}. \tag{3.100}$$

Then, the coefficient γ is easily obtained

$$\gamma=\frac{G_{*\mathrm{T}}}{G_{*\mathrm{P}}}. \tag{3.101}$$

If the differences $\Delta P/P_{\mathrm{I}}$ and $\Delta T/T_{\mathrm{I}}$ are large, the values of δ_{I} and δ_{II} may be different so significantly that the regime of the gas flow can vary from the hydrodynamic to free-molecular one along the capillary. In this case the rarefaction parameter δ varies along the capillary from the value δ_{I} to the value δ_{II}. *A priori* we do not know the function $\delta(\tilde{x})$. Below a differential equation for this function will be obtained. Since numerical data are available only for the tube flow we will not consider the channel flow here.

Let us introduce the new reduced flow rate as

$$G^{\mathrm{tb}}=\frac{L}{\pi a^2 P_{\mathrm{I}}}\left(\frac{2k_{\mathrm{B}}T_{\mathrm{I}}}{m}\right)^{1/2}\dot{M}^{\mathrm{tb}}. \tag{3.102}$$

TABLE 23. Reduced flow rate $G^{th}_{\Delta P}$ vs δ_I and δ_{II} by Sharipov and Seleznev (Ref. 145): diffuse scattering

	$G^{th}_{\Delta P}$														
δ_I	$\delta_{II}=0.01$	$\delta_{II}=0.02$	$\delta_{II}=0.04$	$\delta_{II}=0.08$	$\delta_{II}=0.1$	$\delta_{II}=0.2$	$\delta_{II}=0.4$	$\delta_{II}=0.8$	$\delta_{II}=1.0$	$\delta_{II}=2.0$	$\delta_{II}=4.0$	$\delta_{II}=8.0$	$\delta_{II}=10.0$	$\delta_{II}=20.0$	$\delta_{II}=40.0$	$\delta_{II}=80.0$	$\delta_{II}=100.0$
0.0	1.4884	1.4776	1.4628	1.4431	1.4360	1.4126	1.3952	1.3971	1.4060	1.4811	1.6812	2.1355	2.3722	3.5867	6.0606	11.043	13.539
0.01		1.4679	1.4545	1.4366	1.4300	1.4101	1.3931	1.3961	1.4053	1.4808	1.6817	2.1363	2.3730	3.5877	6.0617	11.044	13.540
0.02			1.4480	1.4316	1.4256	1.4054	1.3909	1.3951	1.4045	1.4811	1.6822	2.1371	2.3740	3.5888	6.0629	11.046	13.541
0.04				1.4234	1.4181	1.4000	1.3877	1.3937	1.4036	1.4814	1.6834	2.1389	2.3759	3.5910	6.0652	11.048	13.544
0.08					1.4070	1.3946	1.3836	1.3922	1.4029	1.4825	1.6861	2.1425	2.3796	3.5953	6.0698	11.053	13.549
0.1						1.3921	1.3820	1.3918	1.4028	1.4833	1.6875	2.1443	2.3816	3.5975	6.0722	11.055	13.551
0.2							1.3779	1.3920	1.4043	1.4887	1.6953	2.1540	2.3918	3.6087	6.0839	11.067	13.563
0.4								1.3990	1.4132	1.5025	1.7130	2.1745	2.4129	3.6314	6.1077	11.092	13.588
0.8									1.4414	1.5370	1.7522	2.2175	2.4570	3.6779	6.1558	11.141	13.637
1.0										1.5561	1.7729	2.2397	2.4796	3.7015	6.1799	11.165	13.662
2.0											1.8815	2.3537	2.5950	3.8207	6.3016	11.288	13.785
4.0												2.5897	2.8328	4.0631	6.5472	11.536	14.033
8.0													3.3188	4.5541	7.0418	12.033	14.531
10.0														4.8012	7.2900	12.282	14.780
20.0															8.5345	13.529	16.027
40.0																16.026	18.524
80.0																	23.522

TABLE 24. Reduced flow rate $G^{tb}_{\Delta T}$ vs δ_I and α at $T_{II}/T_I=3.8$ by Sharipov (Ref. 141)

	$G^{tb}_{\Delta T}$				$G^{tb}_{\Delta T}$		
δ_I	$\alpha=1$	$\alpha=0.8$	$\alpha=0.6$	δ_I	$\alpha=1$	$\alpha=0.8$	$\alpha=0.6$
0.01	0.9489	1.392	2.107	0.8	0.6054	0.7244	0.8813
0.02	0.9299	1.347	2.008	0.9	0.5877	0.6963	0.8381
0.03	0.9139	1.310	1.932	1.0	0.5716	0.6712	0.8001
0.04	0.9001	1.280	1.869	2.0	0.4582	0.5070	0.5662
0.05	0.8878	1.253	1.816	3.0	0.3884	0.4158	0.4476
0.06	0.8768	1.229	1.769	4.0	0.3389	0.3549	0.3728
0.07	0.8667	1.208	1.727	5.0	0.3013	0.3104	0.3204
0.08	0.8573	1.188	1.689	6.0	0.2714	0.2763	0.2814
0.09	0.8487	1.170	1.654	7.0	0.2471	0.2492	0.2511
0.1	0.8405	1.153	1.622	8.0	0.2268	0.2270	0.2268
0.2	0.7788	1.031	1.395	9.0	0.2096	0.2084	0.2067
0.3	0.7351	0.9480	1.249	10.0	0.1948	0.1926	0.1899
0.4	0.7006	0.8854	1.142	20.0	0.1139	0.1096	0.1048
0.5	0.6717	0.8348	1.058	30.0	0.08022	0.07637	0.07217
0.6	0.6468	0.7923	0.9885	40.0	0.06181	0.05852	0.05495
0.7	0.6249	0.7560	0.9307	50.0	0.05017	0.04735	0.04423

Note that unlike G^{tb}_*, this flow rate G^{tb} does not vary along the capillary, but it is constant. If we express $\dot{M}^{tb}$ from (3.26) and substitute it into (3.102), we obtain

$$G^{tb}=\frac{L\mathscr{P}}{\mathscr{T}^{1/2}}G^{tb}_*(\delta(\tilde{x})),\quad \mathscr{P}(\tilde{x})=\frac{P(\tilde{x})}{P_I},\quad \mathscr{T}(\tilde{x})=\frac{T(\tilde{x})}{T_I}. \tag{3.103}$$

In Sec. 3.1. it was shown that under the condition $L\gg 1$ the pressure and temperature gradients are small at any ratios P_I/P_{II} and T_I/T_{II}. So, G^{tb}_* can be split into two parts as (3.31). Taking into account (3.3), (3.10) and the definitions of $\mathscr{P}$ and $\mathscr{T}$ (3.103) we have

$$G^{tb}=\frac{L\mathscr{P}}{\mathscr{T}^{1/2}}\left[G^{tb}_{*T}(\delta)\frac{1}{\mathscr{T}}\frac{d\mathscr{T}}{d\tilde{x}}-G^{tb}_{*P}(\delta)\frac{1}{\mathscr{P}}\frac{d\mathscr{P}}{d\tilde{x}}\right]. \tag{3.104}$$

With the help of (2.39) and (3.37) we may relate $\delta(\tilde{x})$ with $\mathscr{P}$ and $\mathscr{T}$ as

$$\delta(\tilde{x})=\delta_I\frac{\mathscr{P}(\tilde{x})}{\mathscr{T}(\tilde{x})}. \tag{3.105}$$

This implies the use of the hard sphere model for the molecules. Using this relation the differential equation is easily obtained for the function $\delta(\tilde{x})$

$$\frac{d\delta}{d\tilde{x}}=\delta\left[\frac{G_{*T}(\delta)}{G_{*P}(\delta)}-1\right]\frac{1}{\mathscr{T}}\frac{d\mathscr{T}}{d\tilde{x}}-\frac{\delta_I}{L\mathscr{T}^{1/2}}\frac{G^{tb}}{G^{tb}_{*P}(\delta)} \tag{3.106}$$

with the boundary condition as: $\delta(-L/2)=\delta_I$. In this equation G^{tb} is a parameter and we have to fit G^{tb} so as δ would be equal to δ_{II} at $\tilde{x}=L/2$.

To solve the differential equation (3.106) we need to know the temperature distribution $\mathscr{T}(\tilde{x})$ along the capillary. Since the thermal conductivity of the capillary wall is significantly larger than the conductivity of the gas, the temperature distribution is determined by the thermal property of the capillary and must be calculated independently of the gas flow problem. Below some particular temperature distributions will be considered.

3.10.2. Isothermal Flow

First, let us consider the isothermal flow, i.e., $T_I=T_{II}$ and $\mathscr{T}(\tilde{x})=1$. In this case Eq. (3.106) is reduced to

$$G^{tb}_{*P}(\delta)d\delta=-\frac{\delta_I}{L}G^{tb}d\tilde{x}, \tag{3.107}$$

which is easily integrated

$$G^{tb}=-\frac{1}{\delta_I}\int_{\delta_I}^{\delta_{II}}G^{tb}_{*P}(\delta)d\delta. \tag{3.108}$$

Sharipov and Seleznev[145] performed this integration using the data of Table 17. Their results are presented in Table 23 where the following coefficient is introduced

$$G^{tb}_{\Delta P}(\delta_I,\delta_{II})=-\frac{P_I G^{tb}}{(P_{II}-P_I)}, \tag{3.109}$$

which satisfies the condition

$$\lim_{\delta_{II}\to\delta_I}G^{tb}_{\Delta P}(\delta_I,\delta_{II})=G^{tb}_{*P}(\delta_I). \tag{3.110}$$

Analyzing the data of Table 23 we conclude that the formula

$$G^{tb}_{\Delta P}(\delta_I,\delta_{II})=G^{tb}_{*P}\left(\frac{\delta_I+\delta_{II}}{2}\right) \tag{3.111}$$

can be successfully used to calculate the mass flow rate $G^{tb}_{\Delta P}$ at any pressure difference if and only if $T_I=T_{II}$.

TABLE 25. TPD exponent γ vs δ_1 and α at $T_{II}/T_I=3.8$ by Sharipov (Ref. 141)

	γ				γ		
δ_1	$\alpha=1$	$\alpha=0.8$	$\alpha=0.6$	δ_1	$\alpha=1$	$\alpha=0.8$	$\alpha=0.6$
0.01	0.4921	0.4862	0.4789	0.8	0.3381	0.2967	0.2525
0.02	0.4857	0.4764	0.4653	0.9	0.3276	0.2860	0.2416
0.03	0.4802	0.4684	0.4544	1.0	0.3179	0.2761	0.2317
0.04	0.4754	0.4615	0.4452	2.0	0.2454	0.2067	0.1664
0.05	0.4710	0.4554	0.4371	3.0	0.1986	0.1650	0.1301
0.06	0.4670	0.4498	0.4298	4.0	0.1652	0.1362	0.1063
0.07	0.4633	0.4447	0.4232	5.0	0.1401	0.1151	0.08927
0.08	0.4598	0.4399	0.4171	6.0	0.1205	0.09892	0.07649
0.09	0.4564	0.4355	0.4114	7.0	0.1050	0.08612	0.06653
0.1	0.4532	0.4312	0.4061	8.0	0.09225	0.07573	0.05852
0.2	0.4273	0.3981	0.3653	9.0	0.08173	0.06716	0.05194
0.3	0.4071	0.3734	0.3362	10.0	0.07295	0.06003	0.04649
0.4	0.3899	0.3533	0.3133	20.0	0.03039	0.02551	0.02023
0.5	0.3749	0.3364	0.2945	30.0	0.01653	0.01411	0.01145
0.6	0.3615	0.3216	0.2786	40.0	0.01035	0.008950	0.007383
0.7	0.3493	0.3085	0.2648	50.0	0.007066	0.006176	0.005162

3.10.3. Isobaric Flow

Let us consider the isobaric flow, i.e., when $P_I=P_{II}$. The gas flow is caused only by the temperature drop. In this case the differential equation (3.106) cannot be reduced. Sharipov[141] solved the differential equation (3.106) using the data of Tables 7, 10 and 17. The temperature ratio was taken as $T_{II}/T_I=293/77.2=3.8$. These values usually are met in practice and correspond to the room temperature and to the temperature of liquid nitrogen, respectively.

The calculations were carried out with two temperature distribution $\mathscr{T}(\tilde{x})$. It was found that the mass flow G^{tb} essentially depends on this distribution. This means that Eq. (3.106) must be solved anew for every given function $\mathscr{T}(\tilde{x})$. If the thermal conductivity does not vary along the capillary, the temperature distribution is linear, i.e.,

$$\mathscr{T}(\tilde{x})=1+\left(\frac{T_{II}}{T_I}-1\right)\frac{\tilde{x}}{L}. \tag{3.112}$$

The numerical data for this distribution are presented in Table 24 where the coefficient $G^{tb}_{\Delta T}$ is introduced:

$$G^{tb}_{\Delta T}=\frac{T_I G^{tb}}{(T_{II}-T_I)}, \tag{3.113}$$

which satisfies the condition

$$\lim_{\delta_{II}\to\delta_I} G^{tb}_{\Delta T}(\delta_I,\delta_{II})=G^{tb}_{*T}(\delta_I). \tag{3.114}$$

Here, it is impossible to offer some simple formula like (3.111).

It should be note that one cannot calculate the mass flow rate G^{tb} as the linear combination of $G^{tb}_{\Delta P}$ and $G^{tb}_{\Delta T}$

$$G^{tb}=-G^{tb}_{\Delta P}\frac{P_{II}-P_I}{P_I}+G^{tb}_{\Delta T}\frac{T_{II}-T_I}{T_I}. \tag{3.115}$$

This is valid only at the small pressure and temperature drops.

3.10.4. Thermomolecular Pressure Difference

To calculate the TPD exponent γ we assume that the mass flow rate through the tube vanishes, i.e., $G^{tb}=0$. Then from (3.104) for every cross section we have

$$G^{tb}_{*P}(\delta)\frac{1}{\mathscr{P}}\frac{d\mathscr{P}}{d\tilde{x}}=G^{tb}_{*T}(\delta)\frac{1}{\mathscr{T}}\frac{d\mathscr{T}}{d\tilde{x}}. \tag{3.116}$$

With the help of (3.105) the last equation is reduced to

$$\frac{d\mathscr{P}}{d\mathscr{T}}=\frac{\mathscr{P}G^{tb}_{*T}(\delta_1\mathscr{P}/\mathscr{T})}{\mathscr{T}G^{tb}_{*P}(\delta_1\mathscr{P}/\mathscr{T})}. \tag{3.117}$$

To obtain the TPD exponent γ we have to solve this differential equation considering $\mathscr{P}$ as a function of $\mathscr{T}$ with the boundary condition: $\mathscr{P}=1$ at $\mathscr{T}=1$. When the function $\mathscr{P}(\mathscr{T})$ is known, the pressure ratio, which is established in the stationary state, is calculated as $P_{II}/P_I=\mathscr{P}(T_{II}/T_I)$. Then the exponent γ is found from (1.5) as

$$\gamma=\frac{\ln(P_{II}/P_I)}{\ln(T_{II}/T_I)}. \tag{3.118}$$

It should be noted that the function $\mathscr{P}(\mathscr{T})$ is not determined by the temperature distribution $\mathscr{T}(\tilde{x})$ along the tube. Therefore, the exponent γ depends only on the temperature ratio and on the rarefaction parameter δ_1.

Equation (3.117) was solved by Sharipov[141] using the data of Tables 7, 10 and 17 for the temperature ratio $T_{II}/T_I=3.8$. The numerical results are given in Table 25. Here it is also impossible to offer some simple formula like (3.111). The exponent γ must be calculated anew for every given ratio T_{II}/T_I.

3.11. Applicability to Polyatomic Gases

Numerical results on the capillary flow of polyatomic gases can be found in the literature.[40,41,80,103,104] Comparing these results with the data presented here we conclude that

only the Poiseuille flow, i.e., the coefficient G_{*P} is very slightly affected by the internal structure of molecules. All other coefficients G_{*T}, Q_{*P} and Q_{*T} for polyatomic gases essentially differ from those for monatomic gas. So, the numerical data presented in Tables 1–10, 21, and 23 can be successfully applied to any gas including a polyatomic one. The data given in Tables 11–20, 22, 24, and 25 can be applied to monatomic gases only.

4. Gas Flow Through Slits and Orifices

4.1. Remarks

In the present section we consider the gas flow through a capillary with the length equal to zero, $l=0$. This means that the containers are separated by an infinitesimally thin partition having a slit or an orifice. The sketch of the flow and the coordinates are given in Fig. 2. This type of rarefied gas flows is very difficult for numerical calculations. According to the general statement of the problem the containers are very large, therefore a numerical grid must cover a sufficiently large region in the containers. An estimate shows that to reach a reasonable precision of the calculations, the region size must be many times (about 40) larger than the mean free path, while the increment of the numerical grid must be smaller than the mean free path. Thus, unlike the one-dimensional flow considered in the previous section, the numerical scheme for the slit/orifice flows always has a large number of grid points. That is why there are very few rigorous results on the gas flow through slits and orifices.

Unfortunately, the majority of papers[48,75,77,131,161,162] on this topic present the experimental and theoretical results only in figures. This form of the result presentation gives only a qualitative behavior of the flow rates, which is usually known.

A number of papers[75,82,111,129,152,171] offered asymptotic formulas for the mass flow rate near the free-molecular regime ($\delta \ll 1$). But there is no agreement between them. Moreover, these formulas work for very small values of the rarefaction parameter. Therefore, they also give only qualitative behavior of the flow rate and are useless in practice.

Here we consider only papers providing the tabulated numerical data on the slit/orifice gas flow in the large range of the Knudsen number. The mass flow rate will be given as a function of the two rarefaction parameters δ_I and δ_{II} defined by (3.96). The heat flux will not be considered here. The reader interested in the heat flux through a slit can find the corresponding data in Ref. 142.

4.2. Free-Molecular Regime

In the free-molecular regime ($\delta_I=\delta_{II}=0$) the mass flow rate can be easily calculated because the distribution function is Maxwellian (2.30) with the different number densities and temperatures in the two velocity semi-spaces: $v_x<0$ and $v_x>0$.

4.2.1. Outflow to Vacuum

If the pressure ratio is very large, i.e., $P_I/P_{II}\to\infty$, we may consider that there is only the gas flow from the left container to the right one. The bulk velocity in the orifice/slit section can be calculated directly by (2.5). Regarding that in the orifice/slit section $n=n_I/2$ and for $v_x<0$ the distribution function is zero, we have

$$u_x=\frac{1}{(n_I/2)}\int_{v_x>0} f^M(n_I,T_I,0)v_x d\mathbf{v}$$
$$=2\left(\frac{m}{2\pi k_B T_I}\right)^{3/2}\int_{v_x>0}\exp\left(-\frac{mv^2}{2k_B T_I}\right)v_x d\mathbf{v}$$
$$=\sqrt{\frac{2k_B T_I}{\pi m}}=\frac{1}{2}\langle v\rangle_I, \tag{4.1}$$

where $\langle v\rangle_I$ is the mean thermal molecular velocity (2.42) in the left container. The mass flow rate takes the form

for slit

$$\dot{M}^{sl}_{fm}=\frac{n_I}{2}\,m\,a\,u_x=\frac{1}{4}n_I\,m\,a\langle v\rangle_I=aP_I\left(\frac{m}{2\pi k_B T_I}\right)^{1/2}, \tag{4.2}$$

for orifice

$$\dot{M}^{or}_{fm}=\frac{n_I}{2}m\pi a^2 u_x=\frac{1}{4}n_I\,m\,\pi a^2\langle v\rangle_I=a^2P_I\left(\frac{\pi m}{2k_B T_I}\right)^{1/2}. \tag{4.3}$$

4.2.2. Arbitrary Drop of the Pressure

If the pressure in the right container is not so small as to neglect it, we may consider that there are two contrary flows of gas which do not interact each with other. So, the total mass flow rate can be calculated as the difference of the two contrary ones:

for slit

$$\dot{M}^{sl}_{fm}=a\left(\frac{m}{2\pi k_B}\right)^{1/2}\left(\frac{P_I}{\sqrt{T_I}}-\frac{P_{II}}{\sqrt{T_{II}}}\right), \tag{4.4}$$

for orifice

$$\dot{M}^{or}_{fm}=a^2\left(\frac{\pi m}{2k_B}\right)^{1/2}\left(\frac{P_I}{\sqrt{T_I}}-\frac{P_{II}}{\sqrt{T_{II}}}\right). \tag{4.5}$$

In the case of small pressure and temperature drops

$$\frac{\Delta P}{P_I}\ll 1,\quad \frac{\Delta T}{T_I}\ll 1, \tag{4.6}$$

we have

$$\dot{M}^{sl}_{fm}=-aP_I\left(\frac{m}{2\pi k_B T_I}\right)^{1/2}\left(\frac{\Delta P}{P_I}-\frac{1}{2}\frac{\Delta T}{T_I}\right), \tag{4.7}$$

$$\dot{M}^{or}_{fm}=-a^2P_I\left(\frac{\pi m}{2k_B T_I}\right)^{1/2}\left(\frac{\Delta P}{P_I}-\frac{1}{2}\frac{\Delta T}{T_I}\right). \tag{4.8}$$

TABLE 26. Reduced flow rate $\mathcal{G}_P^{sl}$ vs δ_I and α

	$\mathcal{G}_P^{sl}$					
	a			b		c
δ_I	$\alpha=0$	$\alpha=0.5$	$\alpha=1$	$\alpha=0.5$	$\alpha=1$	$\alpha=1$
0.01	1.009	1.009	1.009	...	...	...
0.02	1.017	1.017	1.017	...	...	...
0.04	1.029	1.030	1.030	1.036	1.036	...
0.08	1.052	1.054	1.055	1.061	1.062	...
0.1	1.061	1.064	1.066	1.072	1.074	...
0.25	1.126	1.134	1.138	...	...	1.1370
0.4	1.183	1.196	1.203	1.212	1.219	...
0.5	1.220	1.237	1.244	...	...	1.2474
0.8	1.328	1.351	1.361	1.371	1.383	...
1.0	1.398	1.426	1.438	1.449	1.462	1.4396
2.0	1.753	1.786	1.801	1.811	1.831	1.8002
4.0	2.445	2.484	2.500	2.504	2.533	2.4814
8.0	3.819	3.858	3.872	...	...	3.7827
10.0	4.506	4.546	4.556	4.556	4.590	...
15.0	6.218	6.248	6.255	...	...	...
20.0	7.934	7.950	7.955	7.957	7.988	...
30.0	11.31	11.31	11.30	...	...	...
40.0	14.65	14.66	14.66	...	...	...

[a]Sharipov (Ref. 140), BGK, discrete velocity method.
[b]Sharipov (Ref. 142), S model, discrete velocity method.
[c]Hasegawa and Sone (Ref. 61), BGK, integro-moment method.

4.3. Transition Regime

4.3.1. Reduced Flow Rates

Numerical data on the slit/orifice flow in the transition regime will be presented in terms of the reduced flow rate defined as

$$\mathcal{G}^{sl}=\frac{\dot{M}^{sl}}{aP_I}\left(\frac{2\pi k_B T_I}{m}\right)^{1/2}, \quad \mathcal{G}^{or}=\frac{\dot{M}^{or}}{a^2 P_I}\left(\frac{2k_B T_I}{\pi m}\right)^{1/2} \tag{4.9}$$

for slit and orifice, respectively. In the case of the small pressure and temperature difference (4.6) the reduced flow rate $\mathcal{G}$ can be decomposed as[c]

$$\mathcal{G}=-\mathcal{G}_P\frac{\Delta P}{P_I}+\mathcal{G}_T\frac{\Delta T}{2T_I}. \tag{4.10}$$

From (4.7)–(4.9) one can see that in the free molecular regime ($\delta_I=\delta_{II}=0$) the introduced coefficients $\mathcal{G}_P$ and $\mathcal{G}_T$ are equal to unity. It should be noted that these coefficients have been introduced so as their relation with the rarefaction parameters δ_I and δ_{II} does not contain any specific characteristic of gas. So, representing theoretical data on $\mathcal{G}_P$ and $\mathcal{G}_T$ it is not necessary to specify the gas.

4.3.2. Isothermal Flow Through a Slit

Numerical calculations of the isothermal ($T_{II}=T_I$) gas flow through a slit caused by the small pressure drop ($\Delta P/P_I\ll 1$), i.e., the coefficient $\mathcal{G}_P^{sl}$, was carried out by Hasegawa and Sone.[61] They applied the integro-moment method to the linearized BGK model (2.67) and assumed the diffuse scattering (2.22) on the surface. Sharipov[140,142] calculated the same coefficient $\mathcal{G}_P^{sl}$ applying the optimized discrete velocity method to the linearized BGK model (2.67) and to the linearized S model (2.68) assuming the diffuse-specular (2.23) gas–surface interaction.

The data from the papers[61,140,142] are presented in Table 26 where the coefficient $\mathcal{G}_P^{sl}$ is given as a function of the parameter δ_I. The values of the other parameter δ_{II} are not indicated, because under the conditions $\Delta P/P_I\ll 1$ and $T_{II}=T_I$ we have $\delta_{II}=\delta_I$. One can see that at $\alpha=1$ (diffuse scattering) there is good agreement between the results obtained from the different equations and by the different methods. A comparison of the flow rate for $\alpha=1$ with that for $\alpha=0$ shows that the difference of $\mathcal{G}_P^{sl}$ does not exceed 3%. Regarding that in practice the coefficient α is close to unity and rarely reaches the value 0.5, we may consider that the coefficient $\mathcal{G}_P^{sl}$ does not depend on α.

The following formulas interpolating the numerical data on $\mathcal{G}_P^{sl}$ were offered by Sharipov:[140]

$$\mathcal{G}_P^{sl}=1-(0.2439\lg\delta_I-0.3833)\delta_I - (0.0338\lg\delta_I-0.055)\delta_I^2, \quad \delta_I\leqslant 8, \tag{4.11}$$

$$\mathcal{G}_P^{sl}=\frac{\pi^{3/2}}{16}\delta_I-\frac{4.449-25.17\lg\delta_I}{\delta_I} + \frac{138.7-238.3\lg\delta_I}{\delta_I^2}, \quad \delta_I\geqslant 8. \tag{4.12}$$

The formulas cover the entire range of the rarefaction parameter δ_I and can be used for any α.

[c]If the superscripts sl and or are omitted the corresponding expression is valid for both slit and orifice.

4.3.3. Isothermal Flow Through an Orifice

There is no theoretical data on the coefficient $\mathscr{G}_P^{or}$ in the transition regime. Below its empirical formulas are given.

Small pressure drop: Borisov *et al.*[18] carried out a set of experiments with various gases (He, Ne, Ar, Kr, Xe, H_2 and N_2) measuring the flow rate caused by the small pressure drop ($\Delta P/P_I \ll 1$ and $T_{II}=T_I$). As is known the light gases such as He and Ne have the gas–surface interaction parameter α less than unity even for a contaminated surface, while the heavy gases such as Kr and Xe are perfectly accommodated on the surface. However, the difference between the flow rates of these gases was within 0.3%. This is one more confirmation that the mass flow rate through a slit/orifice caused by the pressure drop does not depend on the gas–surface interaction law.

By the least-square method Borisov *et al.*[18] obtained the following empirical formula:

$$\mathscr{G}_P^{or}=1+0.342\,\delta_I, \tag{4.13}$$

which is valid for $\delta_I<50$. In the range $\delta_I>50$ the results based on the Stokes equation (see Sec. 4.4.1) can be used.

Large pressure drop: Fujimoto and Usami[59] measured the mass flow rate through a short tube at the large pressure drop ($P_I \gg P_{II}$). Under this condition we assume that $\delta_{II}=0$. The gas used by them was air. The length-to-radius ratio varied in the range from 0.05 to 25.4. If we extrapolate the empirical formula offered by them to the zero length, we obtain

$$\mathscr{G}^{or}=1+\frac{0.4733+0.6005/\sqrt{\delta_I}}{1+4.559/\delta_I+3.094/\delta_I^2}. \tag{4.14}$$

This formula is valid in the range $\delta_I<11$.

4.3.4. Nonisothermal Flow Through a Slit

The gas flow caused by the small temperature drop ($\Delta T/T_I \ll 1$ and $P_I=P_{II}$), i.e., the coefficient $\mathscr{G}_T^{sl}$, was calculated by Sharipov[142] using the S model (2.68), which was solved by the discrete velocity method. The results are presented in Table 27 where the coefficient $\mathscr{G}_T^{sl}$ is given as a function of δ_I. Since at the small temperature difference we have $\delta_{II}=\delta_I$, the values of the second parameter δ_{II} are not indicated. One can see that unlike $\mathscr{G}_P^{sl}$, the coefficient $\mathscr{G}_T^{sl}$ depends on the gas–surface interaction parameter α.

4.3.5. Thermomolecular Pressure Difference

If a small temperature difference between the containers is maintained, a small pressure difference will be established. In this case the TPD exponent γ can be expressed in terms of the coefficients $\mathscr{G}_P$ and $\mathscr{G}_T$. Assuming the total mass flow $\mathscr{G}$ in Eq. (4.10) is equal to zero and regarding the smallness of the pressure and temperature drops we obtain

$$\gamma=\frac{\mathscr{G}_T}{2\mathscr{G}_P}. \tag{4.15}$$

Thus, with the help of Tables 26 and 27 one can easily calculate the exponent γ.

TABLE 27. Reduced flow rate $\mathscr{G}_T^{sl}$ vs δ_I and α by Sharipov (Ref. 142)

	$\mathscr{G}_T^{sl}$	
δ_I	$\alpha=0.5$	$\alpha=1$
0.04	0.9940	0.9968
0.08	0.9819	0.9883
0.1	0.9756	0.9841
0.2	0.9458	0.9642
0.4	0.8976	0.9309
0.8	0.8238	0.8756
1.0	0.8011	0.8586
2.0	0.6991	0.7728
4.0	0.5727	0.6535
10.0	0.3914	0.4621
20.0	0.2814	0.3384

Since in the free-molecular regime both coefficients $\mathscr{G}_P$ and $\mathscr{G}_T$ are equal to unity, the exponent $\gamma=1/2$ at $\delta_I=\delta_{II}=0$. This is the well known result of the kinetic theory of gases.

4.4. Hydrodynamic Regime

4.4.1. Small Pressure Drop

A rigorous analytical solution in the hydrodynamic regime ($\delta_I \gg 1$ and $\delta_{II} \gg 1$) is available only for the isothermal gas flow ($T_I=T_{II}$) caused by the small pressure drop ($\Delta P/P_I \ll 1$). Under these suppositions the inertial terms in the Navier–Stokes equation (2.44) can be omitted. Moreover, the gas can be considered as incompressible. Finally, we obtain the so-called Stokes equations

$$\mu\Delta\mathbf{u}=\nabla P, \quad \nabla\cdot\mathbf{u}=0. \tag{4.16}$$

This equation system was solved by Roscoe[128] for the flow through an elliptic aperture. Then, the solution was repeated by Hasimoto.[62]

Slit flow: For the slit flow the solution of the system (4.16) reads

$$u_x=-\left(\frac{\Delta P\,a}{8\mu}\right)\frac{\xi\sqrt{(1-\eta^2)^3}}{\xi^2-\eta^2}, \tag{4.17}$$

$$u_y=-\operatorname{sign}(x)\operatorname{sign}(y)\left(\frac{\Delta P\,a}{8\mu}\right)\frac{\eta\sqrt{(\xi^2-1)(1-\eta^2)}}{\xi^2-\eta^2}, \tag{4.18}$$

$$P=P_I+\frac{\Delta P}{2}\left[1+\operatorname{sign}(x)\frac{\xi\sqrt{\xi^2-1}}{\xi^2-\eta^2}\right], \tag{4.19}$$

where the curvilinear coordinates (ξ,η) are related with the Cartesian (x,y) as

$$\frac{x^2}{\xi^2-1}+\frac{y^2}{\xi^2}=\frac{a^2}{4}, \quad \frac{x^2}{\eta^2-1}+\frac{y^2}{\eta^2}=\frac{a^2}{4}, \quad 0\le\eta\le 1\le\xi. \tag{4.20}$$

The mass flow rates M^{sl} is easily obtained

$$\dot{M}^{sl}|_{\delta\to\infty}=n_l m\int_{-a/2}^{a/2}u_x(0,y)\mathrm{d}y=-\frac{\pi n_l m a^2\Delta P}{32\mu}. \tag{4.21}$$

With the help of (3.96), (4.9) and (4.10) the dimensionless flow rate $\mathscr{G}_P^{sl}$ is obtained as

$$\mathscr{G}_P^{sl}=\frac{\pi^{3/2}}{16}\delta_l=0.348\ \delta_l. \tag{4.22}$$

Orifice flow: For the stationary axisymmetric gas flow the solution of the system (4.16) reads

$$u_x=-\left(\frac{\Delta P\ a}{2\mu\pi}\right)\frac{\sqrt{(1-\eta^2)^3}}{\xi^2-\eta^2}, \tag{4.23}$$

$$u_r=-\mathrm{sign}(x)\left(\frac{\Delta P\ a}{2\mu\pi}\right)\frac{\eta(1-\eta^2)\sqrt{\xi^2-1}}{\xi^2-\eta^2}, \tag{4.24}$$

$$P=P_l+\Delta P\left[\frac{1}{2}+\mathrm{sign}(x)\frac{1}{\pi}\left(\frac{\sqrt{\xi^2-1}}{\xi^2-\eta^2}+\arctan\sqrt{\xi^2-1}\right)\right]. \tag{4.25}$$

Here, the curvilinear coordinates (ξ,η) are related with the coordinates (x,r) as

$$\frac{x^2}{\xi^2-1}+\frac{r^2}{\xi^2}=a^2,\quad \frac{x^2}{\eta^2-1}+\frac{r^2}{\eta^2}=a^2\quad 0\leqslant\eta\leqslant 1\leqslant\xi. \tag{4.26}$$

The mass flow rate $\dot{M}^{or}$ is easily obtained

$$\dot{M}^{or}|_{\delta_l\to\infty}=n_l m\int_0^a u_x(x,r)r\mathrm{d}r=-\frac{n_l m a^3\Delta P}{3\mu}. \tag{4.27}$$

With the help of (3.96), (4.9) and (4.10) the dimensionless flow rate $\mathscr{G}_P^{or}$ is obtained as

$$\mathscr{G}_P^{or}=\frac{2}{3\sqrt{\pi}}\delta_l=0.376\ \delta_l. \tag{4.28}$$

4.4.2. Large Pressure Drop

The mass flow through an orifice caused by a large pressure drop ($P_I\gg P_{II}$) in the hydrodynamic regime ($\delta_I\gg 1$ and $\delta_{II}\gg 1$) was estimated by Liepmann.[75] Considering the orifice as a nozzle, to which one can apply the Euler equation, Liepmann obtained

$$\mathscr{G}^{or}=A(\zeta)\sqrt{2\pi\zeta}\left(\frac{2}{\zeta+1}\right)^{(\zeta+1)/2(\zeta-1)}, \tag{4.29}$$

where ζ is the ratio of the specific heats and A is a coefficient to be obtained from an experiment. In Table 28 the dependence of A and $\mathscr{G}^{or}$ on ζ is presented.

TABLE 28. Dependence of A and $\mathscr{G}^{or}$ on ζ by Liepmann (Ref. 75)

Gas	ζ	A	$\mathscr{G}^{or}$
Ar	1.66	0.812	1.476
N_2	1.40	0.824	1.414
CO_2	1.30	0.830	1.388

4.5. Applicability to Polyatomic Gases

The conclusions on the applicability of the data presented in this section can be based on the experimental data by Borisov *et al.*[18] They measured the mass flow rate through an orifice under the small pressure drop for both monatomic and polyatomic gases. As it was pointed out in Sec. 4.3.3 the difference of the flow rate for different gases was within 0.3%. There are no analogous data on the slit flow, but the conclusion will very likely be the same. So, the results given in the present section on the coefficient $\mathscr{G}_P$, i.e., the data presented in Table 26 and Eqs. (4.11)–(4.13), (4.22), (4.28) can be successfully applied to any gas including a polyatomic one.

Since the thermal creep through a long capillary is very affected by the internal structure of molecules, it would be logical to conclude that the coefficient $\mathscr{G}_T$ for a polyatomic gas differs significantly from that for a monatomic one. So, the data presented in Table 27 can be applied to monatomic gases only.

In the case of the large pressure drop the free molecular mass flow (4.4) and (4.5) does not depend on the internal structure of molecules, while the hydrodynamic flow rate (4.29) depends on the ratio of the specific heats and hence, on the molecular structure. The variation of $\mathscr{G}^{or}$ for different gases is within 6% (see Table 28).

It is obvious that with the decreasing rarefaction parameter δ_l the influence of the internal molecular structure will decrease. It will vanish at $\delta_l=0$ for any pressure drop. From Sec. 4.3.3 one can see that this influence vanishes at the small pressure drop for any rarefaction parameter. So, we may conclude that the influence of the internal molecular structure on the isothermal mass flow rate is largest in the hydrodynamic regime ($\delta_{II}\gg 1$) at the large pressure drop ($P_I\gg P_{II}$). From Table 28 one can see that for gases with the specific heat ratio being in the range $1.3<\zeta<1.66$ the influence of the internal structure on the mass flow rate does not exceed 6%.

5. Gas Flow Through Capillaries of Finite Length

5.1. Remarks

In this section, we consider the gas flow through a capillary with a finite length-to-diameter ratio. The sketch of the gas flow and the coordinates are given in Fig. 1. Like the slit/orifice flow here the main difficulty is the calculation of the flow field in the containers near the capillary entrances. To overcome this difficulty, usually it is assumed[4,32,113,114,127,174] that the molecules come to the capillary with the Maxwellian distribution function, i.e., there is no variation of the distribution function in the containers. This supposition can be justified only in the free-molecular

regime. However, in the transition and hydrodynamic regimes the distribution function of the molecules entering into the capillary from the containers significantly differs from the Maxwellian. That is why the above mentioned supposition gives a great error in the calculation.

Here we consider only papers providing numerical data on the mass flow rate without this supposition. The definitions of the rarefaction parameters $\delta_{\rm I}$ and $\delta_{\rm II}$ (3.96) will be used in this section. Since the heat flux through finite capillaries is investigated very poorly, it will not be considered here. The reader interested in the heat flux can find the corresponding data in Refs. 144, 146.

5.2. Free-Molecular Regime

5.2.1. Transmission Probability

Let us consider the collisionless regime ($\delta_{\rm I}=\delta_{\rm II}=0$). In this case the mass flow rate can be calculated in terms of the transmission probability. Let $W_{\rm I\to II}$ be a probability that a particle entering into capillary from the left container will go out to the right one. The quantity $W_{\rm I\to II}$ is called the transmission probability. Let $W_{\rm II\to I}$ be a transmission probability from the right container to the left one. Then, the mass flow rate can be calculated as

for channel

$$\dot{M}^{\rm ch}_{\rm fm}=W^{\rm ch}_{\rm I\to II}\dot{M}^{\rm sl}_{\rm fm,I}-W^{\rm ch}_{\rm II\to I}\dot{M}^{\rm sl}_{\rm fm,II}, \tag{5.1}$$

for tube

$$\dot{M}^{\rm tb}_{\rm fm}=W^{\rm tb}_{\rm I\to II}\dot{M}^{\rm or}_{\rm fm,I}-W^{\rm tb}_{\rm II\to I}\dot{M}^{\rm or}_{\rm fm,II}, \tag{5.2}$$

where $\dot{M}_{\rm fm,I}$ and $\dot{M}_{\rm fm,II}$ are mass flows into the capillary from the left and right container, respectively. Calculating them with the help of (4.2) and (4.3) we have

$$\dot{M}^{\rm ch}_{\rm fm}=a\left(\frac{m}{2\pi k_{\rm B}}\right)^{1/2}\left(W^{\rm ch}_{\rm I\to II}\frac{P_{\rm I}}{\sqrt{T_{\rm I}}}-W^{\rm ch}_{\rm II\to I}\frac{P_{\rm II}}{\sqrt{T_{\rm II}}}\right), \tag{5.3}$$

$$\dot{M}^{\rm tb}_{\rm fm}=a^2\left(\frac{\pi m}{2k_{\rm B}}\right)^{1/2}\left(W^{\rm tb}_{\rm I\to II}\frac{P_{\rm I}}{\sqrt{T_{\rm I}}}-W^{\rm tb}_{\rm II\to I}\frac{P_{\rm II}}{\sqrt{T_{\rm II}}}\right). \tag{5.4}$$

In the case of isotropic capillary when

$$W_{\rm I\to II}=W_{\rm II\to I}=W, \tag{5.5}$$

we have

$$\dot{M}^{\rm ch}_{\rm fm}=a\left(\frac{m}{2\pi k_{\rm B}}\right)^{1/2}W^{\rm ch}\left(\frac{P_{\rm I}}{\sqrt{T_{\rm I}}}-\frac{P_{\rm II}}{\sqrt{T_{\rm II}}}\right), \tag{5.6}$$

$$\dot{M}^{\rm tb}_{\rm fm}=a^2\left(\frac{\pi m}{2k_{\rm B}}\right)^{1/2}W^{\rm tb}\left(\frac{P_{\rm I}}{\sqrt{T_{\rm I}}}-\frac{P_{\rm II}}{\sqrt{T_{\rm II}}}\right). \tag{5.7}$$

Thus, if one knows the transmission probability W, one easily calculates the mass flow rate in the free molecular regime.

TABLE 29. Transmission probability $W^{\rm ch}$ vs L: diffuse scattering

	$W^{\rm ch}$		
L	a	b	c
0.1	0.9525	0.9525	···
0.2	0.9096	0.9096	···
0.4	0.8362	0.8362	···
0.5	0.8047	0.8048	0.8047
1.0	0.6844	0.6848	0.6844
2.0	0.5421	0.5417	0.5421
4.0	0.3992	0.3999	···
5.0	0.3565	0.3582	0.3565
10.0	0.2408	0.2457	···

[a]Equation (5.8).
[b]Clausing (Ref. 49).
[c]Yamamoto and Asai (Ref. 174).

5.2.2. Diffuse Scattering

In the case of the perfect accommodation of the gas on the surface, i.e., the diffuse scattering (2.22), the transmission probabilities satisfy Eq. (5.5) and can be calculated by two methods: using Clausing's equation (2.93) or by the test particle Monte Carlo (MC) method described in Sec. 2.11.2.

Clausing[49] was the first to derive the integral equation (2.93) and solve it. De Marcus and Hopper[52,53] performed a more accurate solution of the integral equation by the variational method. Berman[8] offered the following analytical expressions for W based on the variational solution

for channel

$$W^{\rm ch}=\frac{1}{2}[1+(1+L^2)^{1/2}-L]-\frac{\frac{3}{2}\{L-\ln[L+(L^2+1)^{1/2}]\}^2}{L^3+3L^2+4-(L^2+4)(1+L^2)^{1/2}}, \tag{5.8}$$

TABLE 30. Transmission probability $W^{\rm tb}$ vs L: diffuse scattering

	$W^{\rm tb}$			
L	a	b	c	d
0.1	0.9524	0.9524	···	0.9535
0.2	0.9092	0.9092	···	0.9109
0.4	0.8341	0.8341	···	0.8332
0.5	0.8013	0.8013	···	0.8007
1.0	0.6720	0.6720	···	0.6716
2.0	0.5142	0.5136	0.5142	0.5135
4.0	0.3566	0.3589	···	0.3548
5.0	0.3105	0.3146	···	0.3090
10.0	0.1910	0.1973	···	0.1919
20.0	0.1094	0.1135	0.1093	0.1098
40.0	0.05949	0.0613	0.05946	0.05977
80.0	0.03127	0.0319	0.03125	0.03119

[a]Equation (5.9).
[b]Clausing (Ref. 49).
[c]Neudachin *et al.* (Ref. 112).
[d]MC method.

TABLE 31. Transmission probability W^{tb} vs L and α by de Marcus (Ref. 53): variational method

	W^{tb}		
L	$\alpha=0.4$	$\alpha=0.6$	$\alpha=0.8$
2	0.74693	0.65890	0.58247
100	...	0.054743	0.036744

for tube

$$W^{tb}=1+\frac{L^2}{4}-\frac{L}{4}(L^2+4)^{1/2}-\frac{[(8-L^2)(L^2+4)^{1/2}+L^3-16]^2}{72L(L^2+4)^{1/2}-288\ \ln[L/2+(L^2/4+1)^{1/2}]}. \tag{5.9}$$

A direct numerical solution of the Clausing equation (2.93) for the channel was obtained by Yamamoto and Asai.[174] In Table 29 the values of the transmission probability W^{ch} calculated with the help of Eq. (5.8) (second column), the results by Clausing[49] (third column) and data by Yamamoto and Asai[174] (fourth column) are presented. One can see that at the larger values of L the results by Clausing are slightly overstated. There is an excellent agreement (to four significant figures) between the direct numerical solution[174] and Eq. (5.8).

Neudachin *et al.*[112] obtained the variational solution of the integral equation (2.93) for the tube. In the book by Bird[10] the simple program to calculate the transmission probability W^{tb} by the test particle MC method is given. Using this program one can easily calculate the transmission probability W^{tb} for any L. In Table 30 the values of W^{tb} calculated with the help of Eq. (5.9) (second column), the results of Clausing[49] (third column), the data by Neudachin *et al.*[112] (fourth column) and the results obtained with the help of the program by Bird[10] (fifth column) are presented. Here, we may also conclude that Eq. (5.9) is in excellent agreement with the results of the work[112] and with the data obtained by the MC method. The results by Clausing are overstated for large L.

TABLE 32. Transmission probability W^{tb} vs L and α: MC method

	W^{tb}		
L	$\alpha=0.4$	$\alpha=0.6$	$\alpha=0.8$
0.1	0.9808	0.9707	0.9626
0.2	0.9625	0.9440	0.9263
0.4	0.9274	0.8971	0.8641
0.5	0.9136	0.8732	0.8357
1.0	0.8485	0.7847	0.7280
2.0	0.7476	0.6568	0.5818
4.0	0.6181	0.5093	0.4248
5.0	0.5728	0.4634	0.3796
10.0	0.4240	0.3212	0.2476
20.0	0.2880	0.2040	0.1485
40.0	0.1803	0.1191	0.08373
50.0	0.1526	0.09970	0.06877
100.0	0.08722	0.05457	0.03668

5.2.3. Diffuse-Specular Scattering

The Clausing equation (2.93) for the diffuse-specular gas–surface interaction (2.23) was solved by De Marcus[53] only for the tube. The results are presented in Table 31.

To apply the MC method to the diffuse-specular scattering a small modification of the program by Bird[10] is necessary. In Table 32 the results obtained with the help of the modified program are presented. One can see that the results based on the variational method[53] and the MC results are in good agreement.

No data on W^{ch} are available in the literature for the diffuse-specular reflection. But it can be easily obtained by the test particle MC method described by Bird.[10]

5.2.4. Surface Roughness

The influence of the wall roughness on the transmission probability was investigated by Davis *et al.*[50] and by Porodnov *et al.*[121] The roughness can be characterized by two quantities: the ratio of the roughness height to the capillary diameter h/a, and the angle of the roughness inclination. Generally it is necessary to define the distribution function of both quantities. It is difficult to give some quantitative dependence of the transmission probability on the roughness. From the results of Refs. 50, 121 we can say only that: (i) the influence approaches its maximum value if the capillary diameter is comparable with its own length provided that the roughness has a "saw" form with an inclination of about 45°. In this case the decrease of the transmission probability exceed 10% even for $h/a=0.05$. It should be noted that a nonsymmetric "saw" can make the capillary nonisotropic, i.e., the condition (5.5) can be violated.

5.2.5. Thermomolecular Pressure Difference

To relate the TPD exponent γ with the transmission probability we assume that the total mass flow through a tube is zero. Then, from (5.3) or (5.4) we have

$$W_{I-II}\frac{P_I}{\sqrt{T_I}}=W_{II-I}\frac{P_{II}}{\sqrt{T_{II}}}. \tag{5.10}$$

If one rewrites this equation in the form (1.5) one obtains the following expression for the exponent γ:

$$\gamma=\frac{1}{2}-\frac{\ln(W_{I-II}/W_{II-I})}{\ln(T_I/T_{II})}. \tag{5.11}$$

It can be seen that under the condition (5.5) the exponent $\gamma=1/2$ for both channel and tube. Thus, the diffuse-specular gas–surface interaction always gives $\gamma=1/2$ in the free-molecular regime.

Experimental data on the exponent γ are available in the literature.[55,64] The experiment with a smooth Pyrex tube[55] gave $\gamma=0.4$. This means that the transmission probability

from the "hot" container to the "cold" one $W_{I\to II}$ is larger than the transmission probability in the opposite direction $W_{II\to I}$. Since the diffuse-specular scattering leads to $\gamma=1/2$ at any value of the parameter α, it cannot correctly describe this experimental result. It would be more correct to use another gas–surface interaction law, i.e., the Cercignani–Lampis kernel (2.24).

The experiments with a leached Pyrex tube, which provides the diffuse scattering, gave $\gamma=1/2$ as the theory predicts.

5.3. Reduced Flow Rates

To present the mass flow rates through a tube we will use the notation (3.102). Let us introduce an analogous notation for the channel flow as

$$G^{ch}=\frac{L}{aP_I}\left(\frac{2k_BT_I}{m}\right)^{1/2}\dot{M}^{ch}. \tag{5.12}$$

If the pressure and the temperature drops are small, i.e., $\Delta P/P_I\ll 1$ and $\Delta T/T_I\ll 1$, both flow rates G^{ch} and G^{tb} can be decomposed as

$$G=-G_P\frac{\Delta P}{P_I}+G_T\frac{\Delta T}{T_I}. \tag{5.13}$$

One must not confuse the coefficients G_{*P} and G_{*T} introduced in Sec. 3.2. with those introduced here. The matter is that G_{*P} and G_{*T} are used only for long capillaries but for any pressure and temperature drops, while G_P and G_T are used only for small pressure and temperature drops but for any capillary length. The coefficients coincide if the capillary is long and at the same time the pressure and temperature drops are small. Note that the coefficients G_P and G_T have been introduced so as their relation with the rarefaction parameters δ_I and δ_{II} does not contain any specific characteristic of gas. So, representing theoretical data on these coefficients it is not necessary to specify the gas.

5.4. Hydrodynamic Regime

The mass flow rate through a capillary of finite length first was obtained in the hydrodynamic regime under the supposition of the small pressure drop $\Delta P/P_I\ll 1$. Under this condition we may consider $\delta_I=\delta_{II}$. The capillary can be considered as a resistor to the gas flow: when the capillary is longer, the mass flow rate is smaller at the same pressure difference. So, the capillary resistance is proportional to the capillary length. Since the capillary ends create an additional resistance for the flow, the idea was to substitute the real length by some effective length. Mathematically this means

$$G_P^{ch}=\frac{\delta_I}{6}\frac{L}{L+\Delta L^{ch}},\quad G_P^{tb}=\frac{\delta_I}{4}\frac{L}{L+\Delta L^{tb}}. \tag{5.14}$$

The additional lengths ΔL would not depend on the real capillary length L. This representation of G_P provides the expressions (3.65) in the limit of the infinite length.

TABLE 33. Reduced flow rate G_P^{ch} vs L in the hydrodynamic regime

	G_P^{ch}/δ_I	
L	a	b
1	0.0908	0.0901
5	0.1427	0.1425
10	0.1538	0.1536
30	0.1622	0.1621

[a]Akinshin *et al.* (Ref. 5).
[b]Equation (5.18).

The additional length ΔL^{tb} for the tube flow was calculated by Weissberg[164] based on the solution of the Navier–Stokes equation by the variational method. It was found that the upper limit as: $\Delta L^{tb}\leqslant 3.47\pi/8$. If one calculates ΔL^{tb} from the hydrodynamic solution of the orifice flow (4.28) taking into account the relation

$$\mathscr{G}_P^{or}=\sqrt{\pi}\lim_{L\to 0}\frac{G_P^{tb}}{L}=\frac{\sqrt{\pi}}{4}\frac{\delta_I}{\Delta L^{tb}}, \tag{5.15}$$

one obtains $\Delta L^{tb}=3\pi/8$, which is close to the upper limit. Thus, we may assume that the formula

$$G_P^{tb}=\frac{\delta_I}{4}\frac{L}{(L+3\pi/8)} \tag{5.16}$$

is valid for any tube length in the hydrodynamic regime.

The same formula can be obtained for the channel flow. Taking into account the relation

$$\mathscr{G}_P^{ch}=\sqrt{\pi}\lim_{L\to 0}\frac{G_P^{ch}}{L}=\frac{\sqrt{\pi}}{6}\frac{\delta_I}{\Delta L^{ch}} \tag{5.17}$$

and the hydrodynamic solution (4.22), we obtain $\Delta L^{ch}=8/(3\pi)$. For the mass flow rate through a channel we have

$$G_P^{ch}=\frac{\delta_I}{6}\frac{L}{[L+8/(3\pi)]}, \tag{5.18}$$

which gives the correct value of the mass flow rate in both limits $L=0$ and $L\to\infty$.

TABLE 34. Reduced flow rate G_P^{ch} vs L and δ_I by Sharipov (Ref. 132): diffuse scattering

	G_P^{ch}			
δ_I	$L=1$	$L=5$	$L=10$	$L=30$
0.0	0.386	1.00	1.35	1.97
0.02	0.391	1.00	1.35	1.88
0.04	0.396	1.00	1.34	1.81
0.1	0.406	1.01	1.32	1.68
0.2	0.421	1.02	1.28	1.57
0.4	0.447	1.03	1.26	1.49
1.0	0.512	1.10	1.27	1.43
2.0	0.601	1.19	1.36	1.50
4.0	0.762	1.43	1.61	1.76
8.0	1.00	1.89	2.13	2.32
10.0	1.18	2.18	2.44	2.65

TABLE 35. Additional length ΔL^{ch} vs δ_l: diffuse scattering

δ_l	0.2	0.4	1.0	2.0	4.0	8.0	10.0	∞
ΔL^{ch}	3.52	2.67	2.02	1.63	1.43	1.44	1.33	0.84

Exact numerical calculations of the Stokes equation (4.16) for the viscous flow through a finite channel was carried out by Akinshin *et al.*[5] The results of the calculations are presented in Table 33. The comparison of these numerical results with the formula (5.18) shows that there is perfect agreement between them.

Thus, the formulas (5.16) and (5.18) can be successfully used in the hydrodynamic regime for a capillary of arbitrary length if the pressure drop is small $\Delta P/P_1 \ll 1$.

5.5. Transition Regime

5.5.1. Isothermal Flow Through a Channel

Exact numerical results of the gas flow through a channel caused by the small pressure drop ($\Delta P/P_1 \ll 1$) were obtained by Sharipov[132,144,146] applying the integro-moment method to the BGK model and to the S model. The results based on the BGK model are presented in Table 34. The values of the coefficient G_P^{ch} obtained from the S model coincide with those obtained from the BGK model.

An analysis of the data shows that in the transition regime we also may utilize the idea of the effective length, i.e, the flow rate through the finite channel G_P^{ch} can be related with the flow rate through the infinite channel G_{*P}^{ch} as

$$G_P^{ch}(L,\delta_l)=\frac{L}{L+\Delta L^{ch}}G_{*P}^{ch}(\delta_l), \tag{5.19}$$

where the additional length ΔL^{ch} depends only on the rarefaction parameter δ_l. Unfortunately, for an intermediate δ_l we cannot apply Eq. (5.19) in the whole range of the length L. The range of the application depends on the precision that one needs. If the precision is 2% the application of Eq. (5.19) is restricted by the following condition

$$\delta_l L \geq 20. \tag{5.20}$$

In Table 35 the quantity ΔL^{ch} as a function of δ_l is presented. These data and those given in Table 3 can be used to calculate the flow rate G_P^{ch} if the dimensionless length satisfies the condition (5.20).

5.5.2. Isothermal Flow Through a Tube

There are not any rigorous theoretical data for the gas flow through a tube of finite length. Below, some empirical formulas are given.

Small pressure drop: Lund and Berman[106] obtained a semiempirical formula for the coefficient G_P^{tb}, which coincides with all limit solutions known by 1966: (i) $L=0$ and $\delta_l \to \infty$, (ii) $L \to \infty$ and $\delta_l \to \infty$, (iii) L is arbitrary and $\delta_l=0$. A lot of empirical coefficients were introduced which depend on the type of the gas, type of capillary material and the length-to-radius ratio l/a. Finally, the semiempirical formula was very complicated. An analysis of the formula shows that: (i) the empirical coefficients E and C (notations of Lund and Berman) are close to unity; the coefficient σ is close to 1.6, and the coefficient A^* is close to 1.1. Here, we give the simplified formula assuming $E=C=1$, $\sigma=1.6$, $A^*=1.1$ for all types of the gas and for all types of the capillary

$$G_P^{tb}=G_d+\frac{G_0 G_t}{G_0+G_t}, \tag{5.21}$$

where

$$G_d=\frac{1.50}{1+1.14\delta_l}\left[1+\frac{0.0547\delta_l L(0.793\delta_l-1)/(1+0.042L)}{1+17.7\delta_l+4.64\delta_l^2+5.02\delta_l^3}\right] \times\left[1+\frac{2.53\delta_l+2.67/W^{tb}-L}{(1+1.61\delta_l)L}\right]^{-1}, \tag{5.22}$$

$$G_0=\frac{2\delta_l L}{3\pi}\left[1+\frac{1.35}{1+0.557\delta_l}\right], \tag{5.23}$$

$$G_t=\frac{\delta_l}{4}\left[1+\frac{3.79}{1+0.954\delta_l}\right]. \tag{5.24}$$

This formula can be serve for an estimate of the mass flow rate through a tube of arbitrary length.

Large pressure drop: Fujimoto and Usami[59] performed experiments on the gas flow through a short tube ($0.05 \leq L \leq 25.2$) at different pressure ratios P_I/P_{II}. For the large pressure drop $P_I/P_{II}>100$ (it is practically outflow into vacuum, $\delta_{II}=0$) they offered the following empirical formula for the coefficient G^{tb} defined by (3.102)

$$G^{tb}=\frac{L}{\sqrt{\pi}}\left[W^{tb}+\frac{0.4733+0.907\sqrt{1/(\delta_l \mathscr{W})}}{1+10.4/(\delta_l \mathscr{W})+16.1/(\delta_l \mathscr{W})^2}\right], \tag{5.25}$$

where

$$\mathscr{W}=\frac{4}{\sqrt{\pi}}\left\{W^{tb}+0.125\exp\left[-\frac{(12W^{tb}-11.2)^2}{2}\right] +0.18\exp(-14.7W^{tb})-0.08\right\}, \tag{5.26}$$

W^{tb} is the transmission probability. It is implied that the gas–surface interaction is diffuse and the data on W^{tb} can be calculated by (5.9). This formula is valid for $\delta_l<11$ and $L \leq 25.2$.

5.5.3. Nonisothermal Flow Through a Channel

The nonisothermal gas flow through a capillary of finite length is the least investigated problem considered in the review. To our knowledge, only numerical results on the gas flow through a channel at the small pressure and temperature drops obtained by Sharipov *et al.*[132,144,146] are available. The linearized S model (2.68) was applied as an input equation, which was solved by the integro-moment method. Two temperature distributions (1.1) were considered:

(i) linear distribution

TABLE 36. Reduced flow rates G_T^{ch} vs L and δ_I by Sharipov and Seleznev (Ref. 144): diffuse scattering

	G_T^{ch}			
	distr. (5.27)		distr. (5.28)	
δ_I	$L=1$	$L=5$	$L=1$	$L=5$
0.02	0.192	0.491	0.191	0.491
0.04	0.190	0.480	0.190	0.480
0.1	0.186	0.452	0.186	0.453
0.2	0.180	0.416	0.180	0.417
0.4	0.169	0.367	0.169	0.366
1.0	0.146	0.285	0.146	0.280
2.0	0.118	0.217	0.118	0.211

$$\tau_w(\tilde{x}) = \frac{1}{2} + \frac{\tilde{x}}{L}, \tag{5.27}$$

(ii) step distribution

$$\tau_w(\tilde{x}) = \begin{cases} 0 & \text{for} \quad -L/2 \leq \tilde{x} \leq 0, \\ 1 & \text{for} \quad 0 \leq \tilde{x} \leq L/2. \end{cases} \tag{5.28}$$

In Table 36 the reduced flow rates G_T^{ch} are presented as the function of δ_I and L. One can see that the coefficient G_T^{ch} very slightly depends on the temperature distribution $\tau_w(\tilde{x})$.

5.5.4. Thermomolecular Pressure Difference

Using the data on G_T^{ch} (Table 36) and G_P^{ch} (Table 34) one can easily calculate the TPD exponent γ for the small temperature drop. To find γ one has to assume $G=0$ in (5.13). Using the smallness of ΔP and ΔT one obtains

$$\gamma = \frac{G_T^{ch}}{G_P^{ch}}. \tag{5.29}$$

5.6. Applicability to Polyatomic Gases

Since in the free-molecular regime there is no influence of the molecular structure to the mass flow all results on the transmission probability, i.e., the data given in Tables 29–33 can be applied to any gas including a polyatomic one.

There are no theoretical data on the polyatomic gas flows through a capillary of finite length in the transition regime. Regarding that the coefficient G_P is intermediate between the coefficients G_{*P} and ∞_P, we may conclude that G_P is very slightly dependent on the molecular structure. So the data given in Tables 34, 35 and Eqs. (5.16), (5.18), (5.19), (5.21) can be applied to any gas including a polyatomic one.

Since the thermal creep through a long capillary G_{*T} essentially depends on the molecular structure, it is logical to conclude that the coefficient G_T for a polyatomic gas differs significantly from that for a monatomic one. This means that the data given in Table 36 are applied to monatomic gases only.

6. Concluding Remarks

Numerical and analytical results on the rarefied gas flows through capillaries of different length are analyzed in the review. The numerical data and analytical formulas presented here can be used to calculate the mass flow rate and the heat flux caused by both pressure and temperature drops on the capillary ends.

In Sec. 1 geometrical parameters of capillaries and main assumptions on the gas flow were described. Two types of the capillary cross section were considered: the round cross section (tube) and the cross section composed by two infinite planes (channel). The first type of the capillary is very important in practical calculations. The second type is an example of the degenerated geometry, which is not met in practice but it is very important for theoretical investigations and serves to test new numerical methods and new kinetic models.

In Sec. 2 three regimes of the gas flows were regarded: (i) the free-molecular regime, when every molecule moves without collision with each other; (ii) the transition regime, when the molecular mean free path has the same order as the capillary diameter; (iii) the hydrodynamic regime, when the mean free path is so small that the gas can be considered as continuous medium. The main methods of calculation of rarefied gas flows in every regime were given.

In Sec. 3 long capillaries were considered. This means that the capillary length is so large that the end effects can be neglected. This supposition significantly simplifies numerical calculations because the gas flow becomes one dimensional. That is why there is a lot of calculation data on this type of flow. The numerical results on the flow rate and the heat flux in the transition regime were tabulated. Analytical formulas were offered for the near free-molecular and near hydrodynamic regimes.

It is obvious that the most reliable results should be obtained applying the Boltzmann equation or using the direct simulation Monte Carlo method. However, to reduce the computational efforts two recommendations, based on the data presented in Sec. 3, can be given:

(i) The BGK model can be successfully applied for numerical calculations of isothermal rarefied gas flows. It is valid for both monatomic and polyatomic gases;

(ii) Since the BGK model gives the incorrect Prandtl number, the S model is recommended for calculations of nonisothermal flows of monatomic gases. In the case of nonisothermal flows of polyatomic gases some special model equations should be applied.

In Sec. 4 the rarefied gas flows through an infinitesimal slit and orifice were analyzed. Because of the complexity for numerical calculations there is little information on this type of two-dimensional gas flows. Analytical solutions of the gas flow through a slit and orifice are available only in the free-molecular and hydrodynamic regimes. The reliable numerical data on the mass flow rate in the transition regime are available only for the slit flow caused by the small pressure and temperature drops. There are some empirical formulas

[115] T. Ohwada, Y. Sone, and K. Aoki, Phys. Fluids A **1**, 1588 (1989).
[116] T. Ohwada, Y. Sone, and K. Aoki, Phys. Fluids A **1**, 2042 (1989).
[117] Y. Onishi, Trans. Jpn. Soc. Aeronout. Space Sci. **15**, 117 (1972).
[118] L. Onsager, Phys. Rev. **37**, 405 (1931); **38** 2265 (1931).
[119] B. T. Porodnov and P. E. Suetin, Izv. Akad. Nauk SSSR, Mekh. Zhidkosti Gaza N6, 93 (1967).
[120] B. T. Porodnov and P. E. Suetin, Zh. Tekhn. Fiz. **39**, 748 (1969).
[121] B. T. Porodnov, P. E. Suetin, S. F. Borisov, and M. B. Nevolin, Izv. Vyssh. Uchebn. Zaved. Fiz. N10, 150 (1972).
[122] B. T. Porodnov, V. D. Akinshin, V. I. Kichaev, S. F. Borisov, and P. E. Suetin, Zh. Tekhn. Fiz. **44**, 818 (1974).
[123] B. T. Porodnov and F. T. Tukhvetov, Izv. Akad. Nauk SSSR. Mekh. Zhid. Gaza N6, 143 (1978).
[124] B. T. Porodnov and F. T. Tukhvetov, J. Eng. Phys. **36**, 61 (1979).
[125] B. T. Porodnov, A. N. Kulev, and F. T. Tukhvetov, J. Fluid Mech. **88**, 609 (1978).
[126] B. T. Porodnov, P. E. Suetin, S. F. Borisov, and V. D. Akinshin, J. Fluid Mech. **64**, 417 (1974).
[127] P. Raghuraman and D. R. Willis, Phys. Fluids **20**, 895 (1977).
[128] P. D. Roscoe, Philos. Mag. **40**, 338 (1949).
[129] A. Rotenberg and H. Weitzner, Phys. Fluids **12**, 1573 (1969).
[130] E. M. Shakhov, *Method of Investigation of Rarefied Gas Flows* (Nauka, Moscow, 1974) (in Russian).
[131] E. M. Shakhov, Zh. Vychisl. Mat. Mat. Fiz. **14**, 970 (1974).
[132] F. M. Sharipov, Ph.D. dissertation, Ural Polytechnical Institute, Ekaterinburg, 1987 (in Russian).
[133] F. M. Sharipov, Zh. Vychisl. Mat. Mat. Fiz. **30**, 310 (1990).
[134] F. M. Sharipov, Izv. Akad. Nauk SSSR. Mekh. Zhid. Gaza N1, 163 (1991).
[135] F. M. Sharipov, "Onsager reciprocity relations in rarefied molecular gas flows," in *Rarefied Gas Dynamics*, Proceedings of the 17th International Symposium, Germany, 1990, edited by A. E. Beylich (VCH, Weinheim, 1991), pp. 75–82.
[136] F. Sharipov, Physica A **203**, 437 (1994).
[137] F. Sharipov, Physica A **203**, 457 (1994).
[138] F. Sharipov, Physica A **209**, 457 (1994).
[139] F. Sharipov, J. Stat. Phys. **78**, 413 (1995).
[140] F. Sharipov, Phys. Fluids **8**, 262 (1996).
[141] F. Sharipov, J. Vac. Sci. Technol. A **14**, 2627 (1996).
[142] F. Sharipov, Phys. Fluids **9**, 1804 (1997).
[143] F. M. Sharipov, V. D. Akinshin, and V. D. Seleznev, Dokl. Akad. Nauk SSSR **305**, 558 (1989); Sov. Phys. Dokl. **34** 224 (1989).
[144] F. M. Sharipov and V. D. Seleznev, "Rarefied gas flow through short channels under pressure and temperature drops," in *Rarefied Gas Dynamics*, Proceedings of the 17th International Symposium, Germany, 1990, edited by A. E. Beylich (VCH, Weinheim, 1991), pp. 605–611.
[145] F. M. Sharipov and V. D. Seleznev, J. Vac. Sci. Technol. A **12**, 2933 (1994).
[146] F. M. Sharipov, V. D. Seleznev, and A. M. Makarov, Inzh.-Fiz. Zh. **59**, 70 (1990).
[147] F. M. Sharipov and E. A. Subbotin, J. Appl. Math. Phys. (ZAMP) **44**, 572 (1993).
[148] C. E. Siewert, R. D. M. Garcia, and P. Grandjean, J. Math. Phys. **21**, 2760 (1980).
[149] J. C. Slattery, *Momentum, Energy and Mass Transfer in Continua* (McGraw-Hill, New York, 1972), Chap. IV, Sec. 3.2.
[150] Y. Sone, J. Phys. Soc. Jpn. **21**, 1836 (1966).
[151] Y. Sone and K. Yamamoto, Phys. Fluids **11**, 1672 (1968).
[152] J. D. Stewart, J. Fluid Mech. **35**, 599 (1969).
[153] P. E. Suetin and B. T. Porodnov, Zh. Tekhn. Fiz. **37**, 171 (1967).
[154] P. E. Suetin, B. T. Porodnov, V. G. Chernyak, and S. F. Borisov, J. Fluid Mech. **60**, 581 (1973).
[155] P. E. Suetin and V. G. Chernyak, Izv. Akad. Nauk SSSR. Mekh. Zhidkosti Gaza N6, 107 (1977).
[156] P. E. Suetin, S. G. Skakun, and V. G. Chernyak, Zh. Tekhn. Fiz. **42**, 642 (1972).
[157] K. Takao, Trans. Jpn. Soc. Aerospace Sci. **4**, 82 (1961).
[158] K. Takao, "Rarefied gas flow between two parallel plates," in *Rarefied Gas Dynamics*, Proceedings of the 2nd International Symposium (Academic, New York, 1961), pp. 465–473.
[159] B. I. M. Ten Bosch, J. J. M. Beenakker, and I. Kuščer, Physica A **123**, 443 (1984).
[160] D. Valougeorgis and J. R. Thomas, Phys. Fluids **29**, 423 (1986).
[161] D. S. Wadsworth and D. A. Erwin, Numerical analysis of rarefied slit flows.-Part II: Navier-Stokes Simulations, AIAA Paper 91-1748.
[162] D. S. Wadsworth and D. A. Erwin, Phys. Fluids A **5**, 235 (1993).
[163] M. Wakabayashi, T. Ohwada, and F. Golse, Eur. J. Mech. B/Fluids **15**, 175 (1996).
[164] H. L. Weissberg, Phys. Fluids **5**, 1033 (1962).
[165] P. Welander, Ark. Fys. **7**, 507 (1954).
[166] M. M. R. Williams, Proc. Cambridge Philos. Soc. **66**, 189 (1969).
[167] M. M. R. Williams, J. Fluid Mech. **36**, 145 (1969).
[168] M. M. R. Williams, in *Rarefied Gas Dynamics*, Proceedings of the 7th International Symposium, edited by C. Cercignani, D. Dini, and S. Nocilla (1970).
[169] M. M. R. Williams, J. Fluid. Mech. **45**, 759 (1971).
[170] D. R. Willis, Phys. Fluids **5**, 127 (1962).
[171] D. R. Willis, J. Fluid Mech. **21**, 21 (1965).
[172] Yu. I. Yalamov, I. N. Ivchenko, and B. V. Deryagin, Dokl. Akad. Nauk SSSR **177**, 74 (1967); Sov. Phys. Dokl. **12**, 1044 (1968).
[173] Yu. I. Yalamov, I. N. Ivchenko, and B. V. Deryagin, Dokl. Akad. Nauk SSSR **175**, 549 (1967); Sov. Phys. Dokl. **12**, 714 (1968).
[174] K. Yamamoto and M. Asai, "Nearly free molecular flow through a two-dimensional channel of finite length," in *Rarefied Gas Dynamics*, Proceedings of the 11th International Symposium, edited by R. Campargue (Commissariat a l'Energie Atomique, Paris, 1979), Vol. 1, pp. 219–228.
[175] V. M. Zhdanov and R. V. Smirnova, Zh. Prikl. Mat. Tekhn. Fiz. N5, 103 (1978).
[176] V. M. Zhdanov and V. A. Zaznoba, Inzh.-Fiz. Zh. **44**, 772 (1983).
[177] S. Ziering, Phys. Fluids **3**, 503 (1960).
[178] S. Ziering, "Plane Poiseuille flow," in *Rarefied Gas Dynamics*, Proceedings of the 2nd International Symposium, edited by L. Talbot (Academic, New York, 1961), pp. 451–464.